2010

Oxygen and Hydrogen Diffusion In Minerals

John Richard Farver
Bowling Green State University - Main Campus, jfarver@bgsu.edu

Reviews in Mineralogy & Geochemistry
Vol. 72 pp. 447-507, 2010

Oxygen and Hydrogen Diffusion in Minerals

John R. Farver

Department of Geology
Bowling Green State University
Bowling Green, Ohio 43403, U.S.A.

jfarver@bgsu.edu

INTRODUCTION

This chapter provides a summary and review of experimentally determined oxygen and hydrogen volume diffusion in minerals. A very extensive and detailed review of stable isotope exchange processes including oxygen and hydrogen volume diffusion can be found in Cole and Chakraborty (2001) and a detailed review of hydrogen diffusion in minerals, especially nominally anhydrous minerals, can be found in Ingrin and Blanchard (2006). In addition, a detailed review of oxygen and hydrogen diffusion in silicate melts is provided by Zhang and Ni (2010), and oxygen and hydrogen diffusion rates can also be found in the chapters, in this volume, on specific minerals and mineral groups (e.g., Van Orman and Crispin 2010; Cherniak 2010). Interested readers are encouraged to refer to these reviews for additional information on oxygen and hydrogen diffusion in geological materials.

In this chapter only volume diffusion through the crystal lattice will be considered. The majority of the experiments employed isotope tracers (e.g., ^{18}O, ^{2}H). The isotope diffusion of hydrogen in the nominally anhydrous minerals is regarded as an impurity tracer diffusion mechanism, and the effective diffusion coefficients obtained from the hydrogen uptake or extraction experiments correspond to chemical interdiffusion of different species. The relationship between the measured effective diffusivity and the hydrogen diffusivity is governed by the specific reaction involved (e.g., see Kohlstedt and Mackwell 1998).

EXPERIMENTAL METHODS

Elsewhere in this volume, a detailed outline and discussion of the experimental methods employed in diffusion studies is presented by Watson and Dohmen (2010). Therefore, only a brief overview of methods commonly employed for oxygen and hydrogen diffusion studies is presented below.

Bulk exchange experiments

Hydrothermal bulk exchange. Carefully sized powders of either natural or synthetic crystals of the mineral of interest are loaded into a sealed tube with a known amount of ^{18}O and/or ^{2}H- enriched water. Most hydrothermal experiments are conducted at elevated confining pressures using cold-seal reaction vessels. After the diffusion anneal, the fractional approach to equilibrium is calculated by comparing the $^{18}O/^{16}O$ or $^{2}H/H$ ratio of the sample material before and after the experiment as determined by conventional mass spectrometry. For oxygen isotope analysis, the samples are typically prepared by conventional BrF_5 extraction of total oxygen, converted to CO_2 (Clayton and Mayeda 1963), and analyzed using a gas source mass spectrometer.

1529-6466/10/0072-0010$10.00 DOI: 10.2138/rmg.2010.72.10

Values for the fractional approach to equilibrium, *f*, are calculated for the run products using the appropriate equilibrium fractionation equations (e.g., Chacko et al. 2001). The fractional approach to equilibrium is used to determine the value of $(Dt/a^2)^{1/2}$ by using the solution to the diffusion equation for uptake from a well-stirred solution of limited volume by a sphere (Crank 1975, p. 95, Fig. 6.4) or by an infinite cylinder (Crank 1975, p. 79, Fig. 5.7), depending upon the symmetry of the sample. *D* is the diffusion coefficient, *t* is the run duration, and *a* is the radius of the sample grains. The diffusion coefficient can also be obtained from uptake by a sample with a plane sheet symmetry using the equation $(Dt/l^2)^{1/2}$ where *l* is the half thickness of the sheet (Crank 1975, p. 59, Fig. 4.6).

Dry bulk exchange. Dry (water absent) oxygen bulk exchange experiments using carefully sized powders of natural or synthetic minerals have also been performed. These experiments are typically run at ambient pressures (0.1 MPa) by exposing the sample to flowing CO_2 or O_2 gas that has a measurably different $^{18}O/^{16}O$ ratio than the sample. By using a flowing stream the isotope composition of the gas remains constant throughout the diffusion anneal and only the isotope change in the mineral grains need be considered. The diffusion coefficients can be calculated from these so-called partial exchange experiments (Muehlenbachs and Kushiro 1974; Connolly and Muehlenbachs 1988) using the diffusion equation for the boundary conditions of a gas of isotopically constant composition and a spherical grain geometry:

$$\frac{\delta^{18}O_f - \delta^{18}O_{eq}}{\delta^{18}O_i - \delta^{18}O_{eq}} = \frac{6}{\pi^2}\sum_{n=1}^{n=\infty}\frac{1}{n^2}\left(\exp\left[-n^2 t/\tau\right]\right)$$

where $\delta^{18}O$ refers to the final, f, initial, i, or equilibrium, eq, value of the oxygen isotope ratio of the sample, *t* is the duration of the experiment, and $\tau = (r^2/\pi^2 D)$, where *r* is the grain radius and *D* is the diffusion coefficient (Muehlenbachs and Kushiro 1974).

The oxygen isotope analysis of the run products is typically obtained using the BrF_5 method (Clayton and Mayeda 1963). This equation assumes a spherical symmetry for the grains, and the validity of the equation can be assessed using a range of run durations and/or grain sizes.

Single crystal experiments

The use of single crystals and spatially resolved analysis of diffusion gradients overcomes most of the potential problems associated with the bulk exchange methods (Zhang 2008, p. 288-292). Details of the single crystal method can be found in several previous papers and reviews (e.g., Brady 1995; Cole and Chakraborty 2001; Watson and Dohmen 2010) and only a brief overview of the method will be presented here. In the single crystal method, samples consist of cut and polished or cleaved pieces of single crystals, typically with a specific crystallographic orientation. It is common to thermally anneal the samples ("pre-anneal") to remove any surface defects acquired during the mechanical polishing and/or to equilibrate the point defect chemistry with the conditions of the diffusion anneal (e.g., at specific buffered pO_2 or f_{H_2O} conditions, see Ryerson et al. 1989). The diffusion tracer sources may be in a surrounding solution or gas phase, or as a thin-film coating the surface or fine-grained source surrounding the sample. The experiments can be done at ambient pressure (0.1 MPa) in a range of gas compositions, or at elevated pressures using cold-seal pressure vessels, internally-heated vessels, or solid-medium, such as a piston cylinder or multianvil apparatus. The pO_2 and f_{H_2O} of the experiments can be buffered using gas-mixing (at 0.1 MPa) or a variety of solid oxide pairs or mineral breakdown reactions (e.g., see Huebner 1971).

After the diffusion anneal, the tracer concentration profile (e.g., ^{18}O, ^{2}H) is measured as a function of distance from the surface exposed to the tracer. The concentration profile is typically measured by Secondary Ion Mass Spectrometry (SIMS), Nuclear Reaction Analysis (NRA), or Fourier Transform Infrared Spectrometry (FTIR)—a brief description of these methods is provided below.

The single crystal experiments are typically designed such that the measured concentration profile can be modeled by the constant surface concentration (infinite, well-stirred reservoir) solution to the diffusion equation for a semi-infinite medium:

$$\frac{C_{(x,t)} - C_0}{C_1 - C_0} = \text{erfc}\left(\frac{x}{2\sqrt{Dt}}\right)$$

where $C_{x,t}$ is the concentration at some distance x from the surface, C_0 is the initial concentration in the sample, C_1 is the concentration at the sample surface, D is the diffusion coefficient, t is the duration of the anneal, and erfc is the complementary error function. The value of D is often obtained by taking the inverse error function of the concentration ratio and plotting it against the distance from the source. The slope of a straight line fit to the erf^{-1} values versus distances plot is $1/[2(Dt)^{1/2}]$, from which D can be evaluated knowing the duration, t, of the experiment.

In the case where the sample geometry corresponds to a solid with homogeneous initial concentration bounded by two infinite parallel planes of thickness $2L$ in contact with an infinite reservoir, the solution to the diffusion equation takes the form of:

$$\frac{C_{(x,t)} - C_0}{C_1 - C_0} = 1 - \frac{4}{\pi}\sum_{n=0}^{\infty}\frac{(-1)^n}{2n+1}\exp\left(\frac{-D(2n+1)^2\pi^2 t}{4L^2}\right)\cos\left(\frac{(2n+1)\pi x}{2L}\right)$$

where the origin is located at the mid-point of the slab. Appropriate solutions to the diffusion equation for other geometries and boundary conditions can be derived as well (see Crank 1975; Ingrin and Blanchard 2006; Zhang 2010).

The use of single crystals followed by microbeam (e.g., SIMS) or macrobeam (e.g., NRA) analysis for diffusion experiments has the decided advantage over bulk experiments in that the effects of surface reactions like dissolution-precipitation on the tracer uptake can be easily evaluated. In addition, anisotropy of the diffusion can be directly measured using oriented crystals.

ANALYTICAL METHODS

A detailed outline and discussion of the analytical methods employed in diffusion studies is presented by Cherniak et al. (2010) and only a brief overview of analytical methods commonly employed for oxygen and hydrogen diffusion studies is presented below.

Mass Spectrometry

The majority of the run products from bulk exchange diffusion experiments have been analyzed using conventional gas source mass spectrometers. Secondary ion mass spectrometry (SIMS) has been used extensively for the analysis of single crystal oxygen diffusion experiments (see Giletti et al. 1978; Valley et al. 1998) and occasionally for H-^{2}H exchange experiments (Vennemann et al. 1996; Suman et al. 2000). SIMS analysis involves bombarding the sample surface with an ion beam (typically O^-, Cs^+, or Ar^+) and the secondary ions emitted from the sample are measured with a mass spectrometer. As the primary beam sputters away the sample it provides an average concentration as a function of distance from the sample surface in the form of a depth profile that is the diffusion profile. By controlling the sputter rate, diffusion profiles <1 μm can be easily resolved. For longer, (>10 μm), diffusion profiles, the sample can be sliced in half in a direction normal to the diffusion interface and a step-scan profile can be collected with sample spot sizes down to ~10 μm (e.g., see Farver and Yund 1999). SIMS analysis provides a direct determination of the isotopic concentration versus depth and allows simultaneous determination of multiple isotopes/elements during depth profiling to ensure chemical homogeneity.

Nuclear Reaction Analysis

Nuclear Reaction Analysis (NRA) has also been widely employed for determining diffusion profiles for oxygen (see Ryerson et al. 1989; Watson and Cherniak 1997) and hydrogen or deuterium (Dersch et al. 1997). The technique involves using a particle accelerator to direct a beam of monoenergetic particles at the surface of the sample. For ^{18}O analysis, the sample is irradiated with monoenergetic protons inducing the reaction $^{18}O(p,\alpha)^{15}N$ which produces α particles. The energy of the α particles as they exit the sample is dependent upon the depth within the sample at which they were generated, and the intensity of the α particle signal at a given energy is dependent on the ^{18}O concentration at a particular depth. As the α particles leave the sample surface their energy is solely a function of their depth of origin. The α particle energy spectrum observed is a convolution of the ^{18}O depth profile and spreading factors due to beam energy spread and straggling of protons and α particles as they travel through the sample. Hence the ^{18}O depth profile is obtained by deconvolution of these effects (see Robin et al. 1973; Ryerson et al. 1989).

To determine a hydrogen diffusion profile the sample surface is irradiated with ^{15}N with variable energies producing the nuclear reaction $^{15}N + {}^{1}H \rightarrow {}^{12}C + \alpha + \gamma$. Depth profiling is performed by varying the incident beam energy to sample H at depth, with depth in the sample determined by the energy loss rate of the ^{15}N in the sample. The number of γ-rays emitted at a given incident energy is proportional to the hydrogen concentration at the respective depth and the hydrogen diffusion profile is obtained by measuring the yield of the characteristic reaction γ-rays as a function of beam energy (Lanford 1992, 1995; Dersch et al. 1997). To determine deuterium diffusion profiles a ^{3}He beam of fixed energy is used. The reaction is $^{3}He + {}^{2}H \rightarrow {}^{4}He + p$ and in like fashion to collecting the ^{18}O diffusion profile, the deuterium concentration as a function of depth is obtained from the proton energy spectrum (Dersch and Rauch 1999). The primary advantage of these techniques is the very high depth resolution of a few nanometers to tens of nanometers.

Fourier Transform Infrared Spectroscopy

The most frequently used method for measuring hydrogen (and water) diffusion is Fourier Transform Infrared (FTIR) spectroscopy. The vibrational modes of the OH dipoles have strong distinct bands in the IR region. The wavenumber of the absorption band is dependent on the strength of the hydrogen (or deuterium) bond, bond geometry, and neighbor interactions. As such, polarized IR spectra can provide information about the structure of the OH as well as its concentration (see Libowitzky and Beran 2006). FTIR provides high sensitivity (<1 ppm H_2O) and the ability to distinguish between adsorbed OH and intrinsic water molecules as well as between OH in inclusions and OH structurally bound in the mineral. Instruments equipped with a microscope have the added advantage that spectra can be collected from areas less than 50 μm in diameter and instruments equipped with a heating/cooling stage allow for *in situ* analysis of hydrogen uptake or loss. The combination of high sensitivity and spatial resolution has made FTIR the method of choice for collecting bulk $H\text{-}^{2}H$ exchange and $H\text{-}^{2}H$ diffusion profiles (see also Rossman 2006 and references therein).

Other methods

Radioactive tritium is sometimes used as a tracer for hydrogen diffusion (e.g., Shaffer et al. 1974). The tritium concentration in the run products can be determined using autoradiography (e.g., Caskey 1974) or liquid scintillation counting (e.g., Cathcart et al. 1979) but requires serial sectioning (i.e., successive grinding and polishing) to obtain the diffusion profile.

The mass difference between hydrogen and deuterium is great enough to potentially monitor the weight change due to $H\text{-}^{2}H$ exchange using a thermobalance. This thermogravimetric method has been employed for hydrous minerals like lawsonite (Marion et al. 2001) but appears to not be sensitive enough for applications to nominally anhydrous minerals.

RESULTS

The available published experimental hydrogen and oxygen volume diffusion data for minerals are compiled in the Appendix. In the Appendix, the data are grouped by mineralogy into different silicates and nonsilicates. The data are further grouped by diffusing species and mechanism into oxygen self-diffusion (^{18}O tracer), hydrogen self-diffusion (^{3}H, ^{2}H, or H tracer), and hydrogen chemical diffusion (^{3}H, ^{2}H, or H tracer). The temperature and pressure ranges of the experiments are noted as well as the nature of the samples (natural or synthetic, and powdered or single crystal). When possible, the Arrhenius parameters of activation energy, E_a, and pre-exponential factor, D_0, are noted or the diffusion coefficient, D, is reported in the case of individual experiments. Experiments where the pO_2 or f_{H_2O} were expressly buffered are noted, and the analytical method employed is provided.

Quartz

Oxygen. The earliest reported oxygen diffusion study in quartz was by Haul and Dumbgen (1962) using powdered natural quartz samples. The experiments were run at 1010-1220 °C and at a near ambient oxygen fugacity (0.21 MPa) in dry O_2 gas. Haul and Dumbgen (1962) monitored the change in isotopic composition of the gas during the diffusion anneal (bulk exchange) and assumed a plate geometry diffusion model using the specific surface area as determined by gas adsorption as a measure of sample geometry. The Arrhenius relation obtained has the activation energy of 230 kJ/mol (Fig. 1).

The first hydrothermal oxygen diffusion studies in quartz were reported by Choudhury et al. (1965) who used a combination of nuclear reaction analysis using the $^{18}O(p,\alpha)^{15}N$ reaction with micro-sectioning to determine tracer diffusion profiles for natural single crystal quartz. The experiment was run at 667 °C and 82 MPa. They noted a significant anisotropy, with the value of D_{ox} parallel to c about a factor of 50 greater than perpendicular to c. Their D_{ox} value parallel to c is more than 8 orders of magnitude greater than the dry D_{ox} value predicted by extrapolation of the Haul and Dumbgen (1962) data to 667 °C.

The next reported oxygen diffusion study was by Schachtner and Sockel (1977) who monitored the bulk exchange of ^{18}O in single crystals of natural quartz annealed in dry O_2 gas using nuclear reaction analysis. Their experiments were run at 870-1180 °C and the Arrhenius relation obtained is in reasonable agreement with the data of Haul and Dumbgen (1962), especially given the large potential systematic errors inherent in the bulk exchange technique (see Dennis 1984).

The first published data for oxygen diffusion in quartz single crystals obtained by SIMS analysis were from Freer and Dennis (1982). Their experiments were run under hydrothermal conditions at 600-700 °C and 100 MPa water pressure using high quality natural Brazil quartz samples. They analyzed oxygen transport only along the c-axis and their results are plotted on Figure 1. Freer and Dennis (1982) noted, based on the somewhat limited data available at that time, there was a significant difference in activation energies for dry experiments compared to wet in various minerals with the activation energy for the dry experiments significantly greater than for the wet experiments. Based on this observation, they suggested that the dry experiments may represent volume diffusion predominantly, but there might be some additional water-mineral interaction in the wet experiments such as hydrolysis, surface exchange and/or solution-precipitation.

To address the possibility of water-mineral interactions in hydrothermal experiments, and to minimize their effects, Freer and Dennis (1982) focused on sample preparation techniques. In the case of quartz, they found that by annealing the cut and polished samples in distilled water at conditions similar to the diffusion experiments prior to the diffusion experiments, this "pre-anneal" acted like a chemical polish, dissolving the quartz and producing a flat damage-free surface. In addition, they used a high solid:fluid weight ratio (2.5 to 5:1) for the diffusion

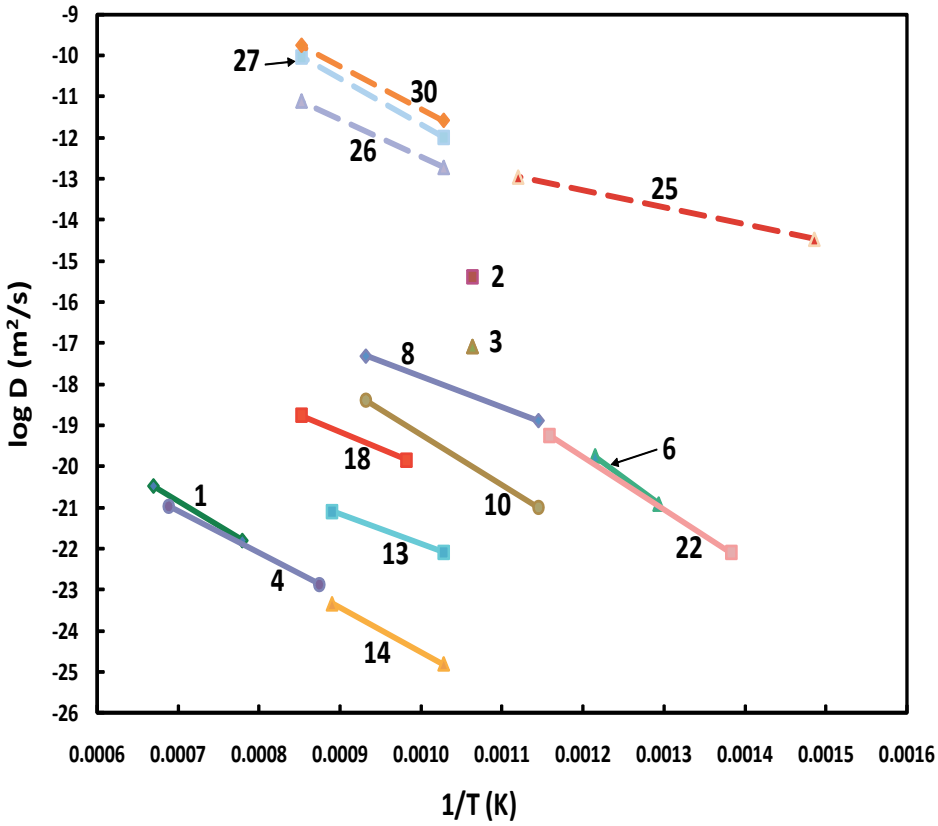

Figure 1. Arrhenius plot of select oxygen (solid) and hydrogen (dashed) diffusion coefficients and Arrhenius relations reported for quartz. The numbers next to the points and lines correspond to the data source as presented in the Appendix. Sources: 1 = Haul and Dumbgen (1962); 2 = Choudhury et al. (1965); 3 = Choudhury et al. (1965); 4 = Schachtner and Sockel (1977); 6 = Giletti and Yund (1984); 8 = Giletti and Yund (1984); 10 = Giletti and Yund (1984); 13 = Dennis (1984); 14 = Dennis (1984); 18 = Sharp et al. (1991); 22 = Farver and Yund (1991a); 25 = Kats et al. (1962); 26 = Kats et al. (1962); 27 = Kronenberg et al. (1986); and 30 = Kronenberg et al. (1986).

experiments. The ^{18}O depth profiles obtained after the diffusion experiments show no indication of sample surface exchange or solution-precipitation and yield an excellent fit to the diffusion equation consistent with a diffusional exchange mechanism alone.

Giletti and Yund (1984) reported results of hydrothermal oxygen diffusion experiments in quartz samples measured using SIMS analysis of single crystals. They found a strong anisotropy with diffusion parallel to *c* about 2 orders of magnitude greater than perpendicular to *c* at 700 °C and 100 MPa water pressure. They noted that measured diffusivities from experiments using natural growth faces were the same as those using cut and polished faces with no evidence for chemical reactions at the surface. Most of their experiments were on a natural Brazil quartz with 7 OH/10^6Si but they also used synthetic crystals with up to 4000 OH/10^6Si and reported no difference in the oxygen diffusion rates between the natural and synthetic crystals. Their experiments ranged from 500° to 800 °C—across the α to β quartz polymorphic transition—and they reported a decrease in the activation energy going from α-quartz (284 kJ/mol) to β-quartz (142 kJ/mol) as measured along the *c*-axis at 100 MPa. In addition, Giletti and Yund (1984) observed an apparent marked dependence of oxygen diffusion on water pressure, with an increase in oxygen diffusivity of a factor of 10 for an increase from 25 to 350 MPa water pressure at 700 °C and transport parallel to *c*.

Simultaneous with the Giletti and Yund (1984) paper (same issue of JGR), Dennis (1984) also reported the results of hydrothermal oxygen diffusion experiments in natural quartz single

crystals measured using SIMS. The diffusion experiments were run at 515-850 °C and 100 MPa confining pressure (Dennis 1984). Consistent with the results of Giletti and Yund (1984), Dennis (1984) found a strong anisotropy, with transport parallel to *c* about a factor of 100 greater than perpendicular to $(10\bar{1}0)$ over the temperature range of the experiments. However, in stark contrast to the results of Giletti and Yund (1984), Dennis (1984) reported that at a constant temperature of 700 °C, over a total confining pressure range of 11.5-100 MPa there was no apparent dependency of D_{ox} on f_{H_2O}.

Over similar conditions of T, P, crystal orientation, and f_{H_2O}, the data from Dennis (1984) and Giletti and Yund (1984) are in very good agreement (see Fig. 1). A comparison to the earlier study of Freer and Dennis (1982) for oxygen diffusion determined under identical condition to Dennis (1984) shows a good correlation of the activation energies (138 kJ/mol) but the pre-exponential factor is a factor of 10^4 less in the Freer and Dennis (1982) study. Dennis (1984) stated that no attempt was made to duplicate the experiments and the [earlier] results should be treated with caution. A comparison of the results of Dennis (1984) and Giletti and Yund (1984) to the results of Choudhury et al. (1965) for experiments run at 667 °C and 82 MPa show the absolute values of D_{ox} are between 10^3 to $10^4\times$ greater for the Choudhury et al. (1965) study. Giletti and Yund (1984) indicated potential systematic errors in the nuclear activation method might account for the discrepancy and Dennis (1984) noted that significant solution-reprecipitation in the charges used by Choudhury et al. (1965) could not be ruled out.

As noted by Dennis (1984) with regard to the apparent absence of a dependence of D_{ox} on f_{H_2O} in his experiments versus the apparent nearly linear dependence ($D_{ox} \propto (f_{H_2O})^{1.1}$) reported by Giletti and Yund (1984), "both studies have examined too restricted a range of f_{H_2O} conditions with only a limited number of results. Consequently, the slopes of the isotherms in a plot of log D_{ox} vs. f_{H_2O} cannot be determined with any degree of precision."

In order to evaluate the dependence of oxygen diffusion on f_{H_2O} over a much greater range of f_{H_2O} conditions, Farver and Yund (1991a) employed a range of hydrogen/oxygen buffers (FeO-Fe_3O_4, Ni-NiO, Mn_3O_4-Mn_2O_3) corresponding to a range in f_{H_2O} of 2.5 to 239 MPa (Chou 1987) at a constant temperature and confining pressure of 700 °C and 100 MPa. In addition, in consideration of the Elphick and Graham (1988) fast proton transient model for enhanced oxygen diffusion in quartz and feldspars, Farver and Yund (1991a) conducted two experiments using the Ag-AgCl hydrogen buffer (Frantz and Eugster 1973) to evaluate the effect of a_{H+} on oxygen diffusion in quartz. The results of their study yielded a strong dependence of D_{ox} on f_{H_2O} with $D_{ox} \propto (f_{H_2O})^{0.78}$, but there was no measurable dependence on f_{H_2}, f_{O_2}, or a_{H+} (Fig. 2). From this strong, nearly linear dependence of D_{ox} on log f_{H_2O}, Farver and Yund (1991a) suggested that molecular water was the dominant oxygen-bearing transport species in quartz under hydrothermal conditions and that if protons play a role in the oxygen diffusion mechanism the critical concentration of protons is low. Zhang et al. (1991) derived the theoretical basis for demonstrating that molecular water is the dominant oxygen-transporting species in quartz and feldspars in hydrothermal diffusion experiments (see discussion section below). Also, the results of *ab initio* calculations reported by McConnell (1995) support the predominant role of molecular water in oxygen diffusion in quartz under hydrothermal conditions. The fast transient protons model of Graham and Elphick (1991) has not proven useful for quantitative predictions of oxygen diffusion, and the results of the experimental and theoretical studies cited above have found much greater acceptance.

Oxygen diffusion rates in natural quartz single crystals were reported by Sharp et al. (1991) from a series of experiments with ^{18}O-enriched CO_2. The experiments were run at 745-900 °C and 0.06 to 720 MPa and the diffusion profiles were measured using SIMS. The diffusion coefficients obtained at $p(CO_2) = p(\text{total}) = 10$ MPa for diffusion parallel to the *c*-axis are approximately 100× less than the D values reported from hydrothermal experiments (Giletti and Yund 1984; Dennis 1984) and 100× greater than the D values reported from previous 0.1

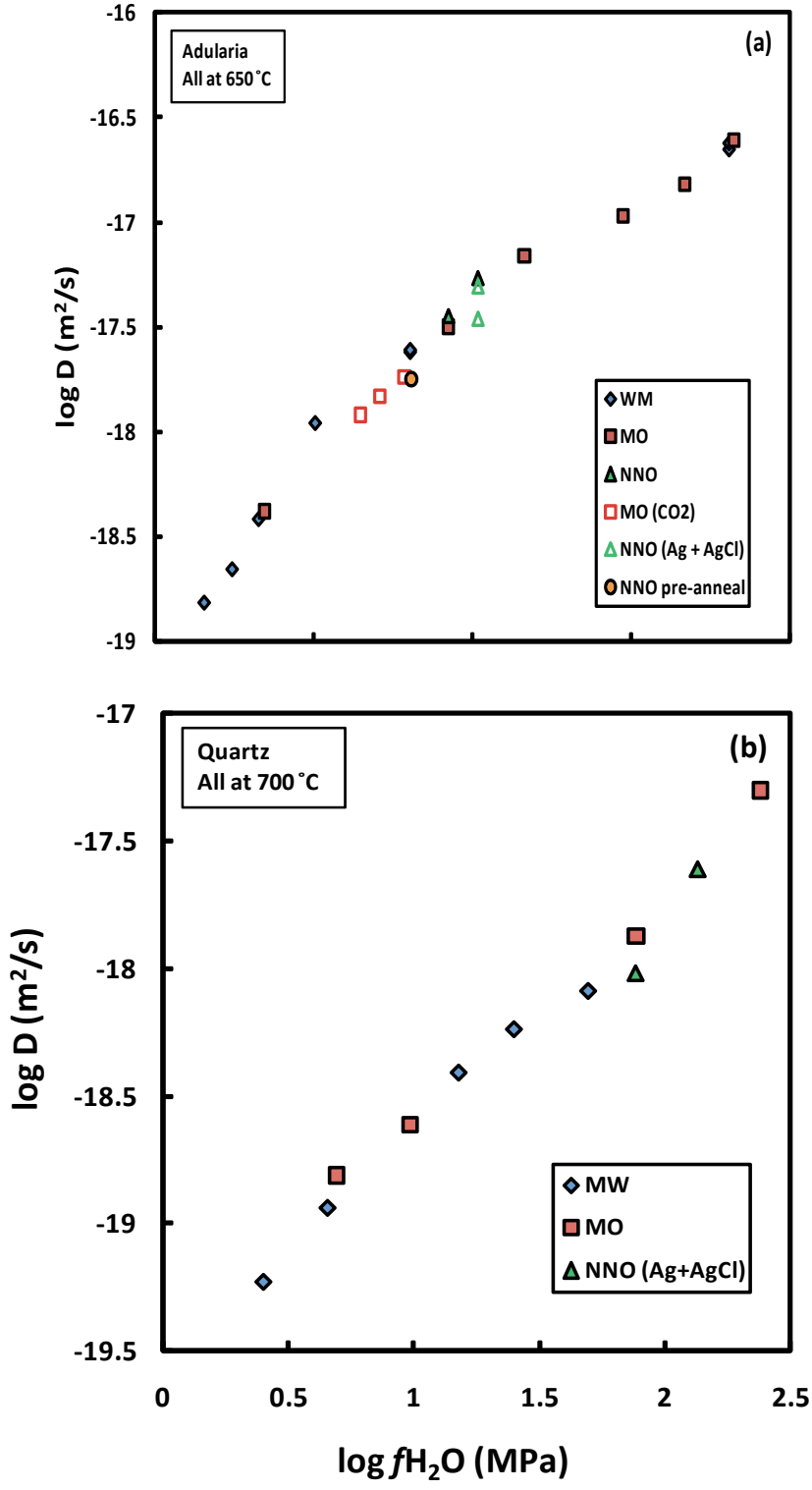

Figure 2. Oxygen diffusion coefficients as a function of log f_{H_2O} for (a) adularia hydrothermal experiments at 650 °C and (b) quartz hydrothermal experiments at 700 °C (after Farver and Yund 1990, 1991a).

MPa quartz-O_2 experiments (Dennis 1984). The oxygen diffusion coefficient measured at 0.06 MPa and in vacuum agreed with the previously reported values from experiments at 0.1 MPa in O_2 gas (see Fig. 1). Sharp et al. (1991) called upon a diffusing species other than oxygen that enhances the oxygen diffusion rate in the quartz-CO_2 system relative to that occurring at very low pressures or in vacuum.

Hydrogen. In efforts to explain the hydrostatic weakening of quartz (Griggs 1967) there have been numerous studies focused on water in quartz (see Kroenenberg 1994 for review). However, most studies have been dedicated to determining the nature of the defects and concentrations of various hydrous components, and there are few actual isotope diffusion experiments. The three studies of note are Kats et al. (1962), Shaffer et al. (1974), and Kronenberg et al. (1986).

The earliest reported hydrogen diffusion study in quartz was by Kats et al. (1962) who used a ^2H_2O tracer source at 2.5 MPa. The diffusion profiles were measured using IR spectroscopy, and the experiments were run at 400-620 °C in the α-quartz field and at 700-900 °C in the β-quartz field. A major contribution of the Kats et al. (1962) study was the successful assigning of absorption bands found between ~3600 and ~3200 cm^{-1} wavenumbers to specific hydrogen defects and constraining their nearby structural and chemical environments. The *D* values for the H-^{2}H exchange experiments yield different Arrhenius relations for α and β-quartz, with a significantly greater activation energy of 175.5 kJ/mol for the β-quartz compared to 79 kJ/mol for the α-quartz. The activation energy of 175.5 kJ/mol for hydrogen self-diffusion in the β-quartz is similar to activation energies reported by Haul and Dumbgen (1962) of 230 kJ/mol and Schachtner and Sockel (1977) of 195 kJ/mol for oxygen diffusion experiments run in O_2 gas. However their diffusion coefficients reported for oxygen diffusion are about 10 orders of magnitude less than the diffusion coefficient reported for hydrogen diffusion at 900 °C (Fig. 1).

Shaffer et al. (1974) measured hydrogen diffusion in single crystals of synthetic quartz under low pressure (0.06 MPa) hydrothermal conditions at 720-850 °C using a tritium (radioactive) tracer. The tritium diffusion profiles were measured using a combination of serial sectioning and liquid scintillation counting. At constant tritium composition, the diffusion coefficients yielded an Arrhenius relation as shown on Figure 1. However, the activation energies were found to increase with increasing water concentration. The diffusion was measured only along the *c*-axis and hence anisotropy could not be evaluated. Compared to the study of Kats et al. (1962), the Shaffer et al. (1974) data yield a much lower activation energy and *D* values about 3 orders of magnitude less than reported by Kats et al. (1962) over the temperature range of the experiments.

In an extensive study of the role of hydrogen uptake on the observed hydrolytic weakening behavior of quartz, Kronenberg et al. (1986) annealed single crystals of natural Brazil and Swiss quartz hydrostatically over the temperature range 700-900 °C and water pressures of 400-1500 MPa. The hydrogen uptake and H-^{2}H exchange profiles were determined using FTIR. The rate of interstitial hydrogen diffusion (uptake) yielded an Arrhenius relation in close agreement with the hydrogen diffusivities reported by Kats et al. (1962) at much lower pressure of 2.5 MPa. The results of Kronenberg et al. (1986) did not compare well with the data from Shaffer et al. (1974). In addition to investigating the hydrogen uptake in quartz, Kronenberg et al. (1986) studied H-^{2}H exchange in quartz. The diffusion coefficients for H-^{2}H exchange compare favorably with those determined for hydrogen uptake (Fig. 1). In contrast to the strong anisotropy observed for diffusion of oxygen (Giletti and Yund 1984; Dennis 1984) and alkalis (Freer 1981) in quartz, hydrogen diffusion is isotropic within uncertainty limits.

Feldspars

Oxygen. The first oxygen isotope exchange data for feldspars were reported by Merigoux (1968) from experiments conducted at 440-805 °C and 25 to 60 MPa, using bulk exchange between adularia ($Or_{86.5}$) or albite (Ab_{99}) and distilled water. Assuming an isotropic diffusion

model, the data defined an Arrhenius relation with activation energies of 134 kJ/mol for adularia and 154.8 kJ/mol for albite. Merigoux (1968) also reported that oxygen exchange proceeded much faster when the feldspar and fluid were far from chemical equilibrium with respect to their Na/K ratios.

In part to address the potential influence of fine-scale recrystallization in Merigoux's (1968) experiments, Yund and Anderson (1974) determined oxygen bulk exchange between K-feldspars and a 2M KCl solution. The Yund and Anderson (1974) experiments were run at 400-900 °C and 200 MPa using samples of microcline (Or_{100}) and adularia (Or_{100}) that were exchanged twice with molten KCl at 900 °C to produce the essentially pure compositions, and diffusion was assumed isotropic. The reported Arrhenius relations are E_a = 123.9±4 kJ/mol and $D_0 = 2.80\times10^{-10}$ m^2/s for the microcline and E_a = 123.9±5 kJ/mol and $D_0 = 5.3\times10^{-11}$ m^2/s for the adularia (Fig. 3). Yund and Anderson (1974) interpreted the apparently greater diffusion rate in the microcline to be due to the presence of microcracks along twin boundaries and noted that a similar difference was observed for potassium diffusion in the same microcline (Lin and Yund 1972) and an orthoclase (Foland 1974). The results of Yund and Anderson (1974) compared favorably with the results of Merigoux (1968) over the temperature range of the experiments with their *D*-values being about a factor of 3 to 4 greater than Merigoux's (1968).

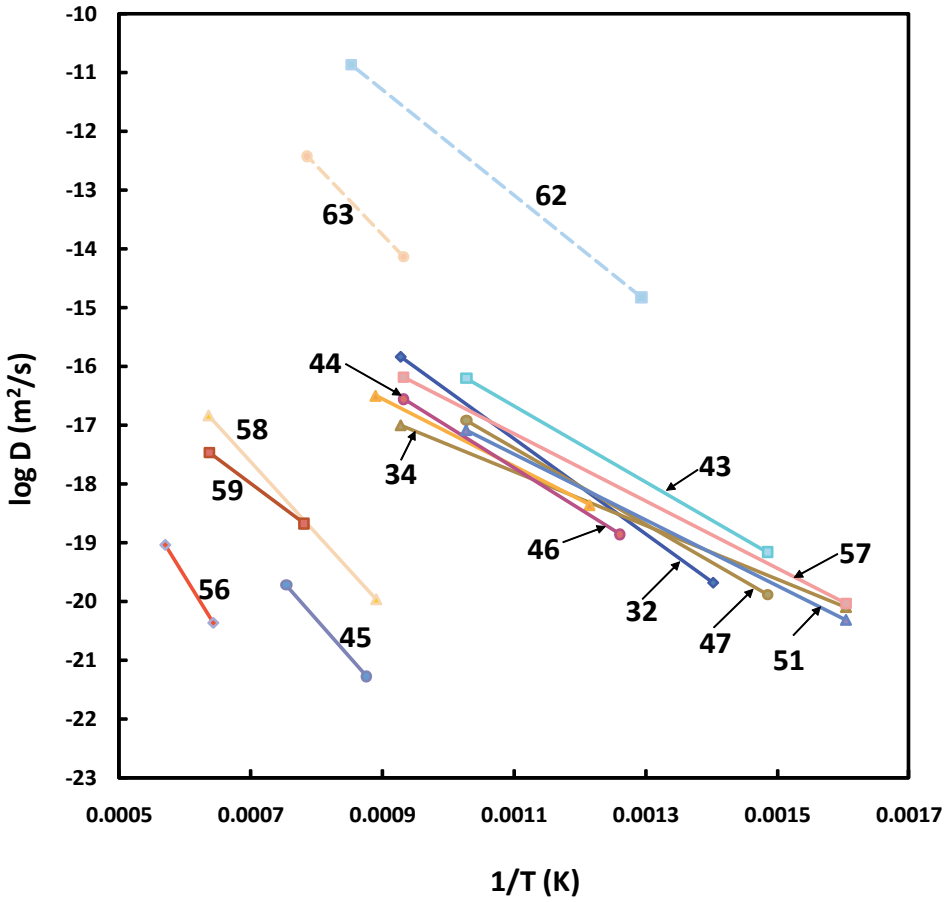

Figure 3. Arrhenius plot of select oxygen (solid) and hydrogen (dashed) diffusion coefficients and Arrhenius relations reported for feldspars. The numbers next to the points and lines correspond to the data source as presented in the Appendix. Sources: 32 = Merigoux (1968); 34 = Giletti et al. (1978); 43 = Yund and Anderson (1974); 44 = Freer et al. (1997); 45 = Derdau et al. (1998); 46 = Merigoux (1968); 47 = Yund and Anderson (1974); 51 = Giletti et al. (1978); 56 = Muehlenbachs and Kushiro (1974); 57 = Giletti et al. (1978); 58 = Elphick et al. (1988); 59 = Ryerson and McKeegan (1984); 62 = Kronenberg et al. (1996); and 63 = Johnson (2003).

In addition to the hydrothermal experiments at 200 MPa, Yund and Anderson (1974) ran several experiments using CO_2, unpurified air, or dried air as the isotope exchange medium. Because of low exchange rate and the small differences in isotope composition between the exchange media and the feldspar samples, the *D* values calculated from these experiments were only very approximate. For the CO_2 exchange experiments at 712-843 °C, *D* values of the order of 10^{-20} m^2/s were obtained, which are to 3 to 4 orders of magnitude lower than the *D* values from the hydrothermal exchange experiments over the same temperature range.

Muehlenbachs and Kushiro (1974) reported oxygen isotope bulk exchange data for a synthetic anorthite and an intermediate composition plagioclase. They used dry O_2 or CO_2 as the exchange medium, and ran their experiments at 1280-1480 °C and 0.1 MPa. The Arrhenius parameters obtained yield a much greater activation energy (344 kJ/mol) than had been reported previously for feldspars from hydrothermal experiments and much slower diffusion rates when extrapolated to the lower temperatures at which the hydrothermal experiments were run (Fig. 3).

The apparently greater oxygen diffusion coefficients reported by Yund and Anderson (1974) compared to the results of Merigoux (1968) were resolved by the results of Yund and Anderson (1978). In the Yund and Anderson (1978) study, oxygen isotope bulk exchange experiments between adularia and a 2 M KCl solution were conducted at a constant temperature of 650 °C and at pressures ranging from 12.5 to 400 MPa. Their results showed a strong positive dependence of the oxygen diffusion coefficients in adularia on water pressure (or f_{H_2O}). The observed pressure dependence on *D* would account for most of the difference between Merigoux's (1968) data for adularia at 32.5 to 60 MPa compared to Yund and Anderson's (1974) data from experiments run at 200 MPa. Yund and Anderson (1978) noted that the observed increase in the oxygen diffusion coefficient with increased water pressure suggested "water" in the form of molecular H_2O, OH^- or H^+, plays some special role in the mechanism of oxygen isotope exchange between feldspars and water.

Employing the emerging technology of the ion microprobe (SIMS), Giletti et al. (1978) measured oxygen isotope exchange between ^{18}O-enriched water and single crystals of feldspars. The feldspar samples ranged in composition from adularia (Or_{98}) to albite (Ab_{97}, Ab_{99}) to anorthite (An_{96}) and two intermediate plagioclase feldspars ($Ab_{82.5}$ and $Ab_{35.7}$). The experiments were run at 350-800 °C and 100 or 200 MPa confining pressure. By using crystallographically oriented crystals and SIMS depth profiling analysis, Giletti et al. (1978) were able to measure the oxygen diffusion coefficients normal to the (001), (010), ($\bar{1}11$), and (130) faces, and found them to be the same within a factor of four. Their results indicated all of the different feldspar compositions have similar oxygen exchange behavior and taken together yield the Arrhenius parameters E_a = 100 kJ/mol and $D_0 = 2.0\times10^{-12}$ m^2/s (Fig. 3).

A comparison of Giletti et al.'s (1978) results with the previous results for oxygen diffusion in adularia from Yund and Anderson (1974) showed excellent agreement between the single crystal/SIMS method and the bulk exchange method. For albite, the results of Giletti et al. (1978) compared well with the results from the earlier bulk exchange experiments of Merigoux (1968) and Anderson and Kasper (1975) at 600 °C, but differ at other temperatures due to the significantly lower activation energy of 87.5 kJ/mol reported by Giletti et al. (1978) compared to 154.8 kJ/mol reported by Merigoux (1968). The oxygen diffusion coefficients determined in the anorthite yield an activation energy of 110 kJ/mol. Giletti et al. (1978) noted the oxygen diffusion coefficient reported by Muehlenbachs and Kushiro (1974) for a natural plagioclase exchanged with CO_2 at 1280 °C falls on an extrapolation of their data for anorthite but would deviate greatly at lower temperatures due to the much greater activation energy of 344 kJ/mol reported by Meuhlenbachs and Kushiro (1974).

All of the early oxygen diffusion studies in feldspars employed essentially perfect crystals (except for twinning) and Yund et al. (1981) noted that in order to truly understand metamorphic processes it seemed especially important to evaluate the effect of dislocations on ionic diffusion

in silicates. They accomplished this by measuring oxygen diffusion in an undeformed albite sample with a low dislocation density of $<10^6$ cm^{-2} and in a sample deformed at high temperature and pressure to produce a uniform dislocation density of 5×10^9 cm^{-2}. The experiments were run using the bulk exchange method under hydrothermal conditions at 450-700 °C and 200 MPa. Their results for the undeformed albite agreed well with the previous results of Anderson and Kasper (1975) and Giletti et al. (1978) with an activation energy of 139.8±3 kJ/mol. The results for the deformed sample yielded a measurably greater oxygen diffusivity (about a factor of 4) than the undeformed sample but with similar activation energy of 129.3±5 kJ/mol. Yund et al. (1981) interpreted their results to indicate, in the case of the deformed sample, the measured oxygen diffusivity was a combination of lattice and dislocation-assisted or pipe diffusion along static dislocation cores. Using the simple model of Hart (1957), Yund et al. (1981) determined the effective oxygen diffusion coefficient for a dislocation core or pipe was about five orders of magnitude greater than for oxygen lattice diffusion in albite.

Out of concern that hydrothermal experimental methods might cause surface changes deeper than induced isotope exchange profiles, Elphick et al. (1986) developed a technique involving hydrothermal deposition of labeled materials (the overgrowth technique). The results of their experiments using Amelia albite at 400-600 °C and 200 MPa for isotope exchange perpendicular to (001) were in excellent agreement with the results of Giletti et al. (1978).

Elphick et al. (1986) noted that the dry oxygen diffusion data available for feldspars (Muehlenbachs and Kushiro 1974) were determined over a necessarily limited temperature range, implying there may be large uncertainties in the reported activation energy of 375 kJ/mol. To address these concerns, Elphick et al. (1988) re-determined oxygen diffusivities in anorthite (An_{97}-Ab_{03}) under dry conditions using $^{18}O_2$ gas and analysis of the diffusion profiles by SIMS. The experiments were run at 850-1300 °C and 0.1 MPa. Their results indicated a much lower activation energy of 236±8 kJ/mol compared to the value of 375 kJ/mol reported by Muehlenbachs and Kushiro (1974). In addition, they confirmed that the activation energy under dry conditions was much greater than the activation energy of 110 kJ/mol reported for hydrothermal conditions (Giletti et al. 1978), and the oxygen diffusion coefficient obtained at 800 °C under dry conditions is about four orders of magnitude less than under hydrothermal conditions, with the difference between the dry and wet oxygen diffusivities becoming even greater at lower temperatures due to the difference in activation energies (Fig. 3).

In response to lingering questions as to water's effect on oxygen diffusion in feldspars, and specifically to address Ewald's (1985) interpretation that the apparent dependence of ^{18}O exchange in feldspars was due to a two-stage process with a relatively rapid water pressure dependent surface reaction followed by a pressure independent rate-limiting diffusion process, Farver and Yund (1990) conducted a set of oxygen diffusion experiments using single crystals of adularia and albite under rigorously buffered conditions. They measured the oxygen isotope profiles using SIMS, paying particular attention to whether any surface reactions had influenced the isotope exchange. The feldspar samples were prepared by cleaving along the (001) face in order to avoid the possibility of enhanced dissolution or surface reactions due to damage to the surface by mechanical polishing. The resulting isotope depth profiles show no evidence of surface reactions and there is an excellent fit of the data to the error function, which is the solution to the diffusion equations for the boundary conditions of the experiments. In addition, consistent with a diffusion mechanism, there was no time dependency observed for experiments run at similar experimental condition but different durations.

The oxygen diffusion experiments of Farver and Yund (1990) were conducted under hydrothermal conditions at 650 °C from 5 to 1500 MPa confining pressure using a combination of hydrogen/oxygen buffers (FeO-Fe_3O_4, Ni-NiO, and Mn_2O_3-Mn_3O_4), a hydrogen ion buffer (Ag-AgCl), and variable mole fractions of water (dilution with CO_2 by addition of $Ag_2C_2O_4$). By independently varying the hydrogen, oxygen, and water fugacities, confining pressure and

hydrogen ion activity, the effect of each parameter on the oxygen diffusion rate was evaluated. Their results indicated the oxygen diffusion rates correlated strongly with the water fugacity but were independent of f_{H_2}, f_{O_2}, a_{H+}, a_{OH^-}, and confining pressure in so much as these parameters could be varied independent of the water fugacity (Fig. 2). For example, the apparent correlation of D with a_{H+} and confining pressure is due to the dependence of these parameters on the water fugacity in the pure water system.

Farver and Yund (1990) proposed that consistent with size and charge consideration of the possible species, the dependence of oxygen diffusion on water fugacity indicates that the dominant oxygen-bearing transport species in "wet" experiments is molecular water. They noted that regardless of what the oxygen-bearing transport species is, it must also exchange ^{18}O atoms with the ^{16}O atoms in the feldspar structure and this exchange may be greatly enhanced if protons are present to hydrolyze and thereby weaken the Si-O and Al-O bonds as suggested by Elphick and Graham's (1988) fast transient protons model. In addition, they noted the lack of correlation of oxygen diffusion with the a_{H+} over the range of their experimental conditions does not preclude the possibility that there is some lower critical hydrogen ion concentration required to enhance the oxygen exchange process. Hence, the substantial difference in oxygen diffusion rates in feldspars in dry versus wet conditions may be due to water's ability to supply protons, by dissociation, as well as being the dominant oxygen-bearing transport species. However, as noted above, the fast transient protons model of Graham and Elphick (1991) has not proven useful for quantitative predictions of oxygen diffusion, and the results of the experimental (Farver and Yund 1990, 1991a) and theoretical studies (Zhang et al. 1991; McConnell 1995) have gained broad acceptance.

As part of a study of oxygen diffusion at controlled oxygen fugacity in several minerals including diopside, akermanite and spinel, Ryerson and McKeegan (1994) reported oxygen diffusion data for anorthite (An_{96}). The experiments were run using a gas-solid isotope exchange with 99% ^{18}O-enriched CO-CO_2 gas mixtures to control the oxygen fugacity. The diffusion profiles were measured by depth profiling with SIMS. The anorthite experiments were run at 1008-1295 °C and 0.1 MPa, and yielded an activation energy of 162±36 kJ/mol for diffusion in the (010) direction. Their activation energy is substantially less than the ~375 kJ/mol reported by Muehlenbachs and Kushiro (1974) from bulk exchange experiments using a synthetic powdered anorthite sample. A comparison of Ryerson and McKeegan's (1994) results to the results of Elphick et al. (1988) obtained from experiments with O_2 gas followed by SIMS analysis for diffusion along the (001) direction shows good agreement of the diffusion coefficients over the temperature range of the experiments, with an overlap at ~1000 °C. However, the activation energy reported by Elphick et al. (1988) is 236 kJ/mol, which is significantly greater than the 162 kJ/mol reported by Ryerson and McKeegan (1994), and hence extrapolations of the two data sets deviates at higher or lower temperatures. Ryerson and McKeegan (1994) noted that the overlap of the two data sets suggests that any f_{O_2}-dependence of oxygen diffusion in nearly pure anorthite is not strong, and they presented an Arrhenius relation for the combined results of the two studies with E_a = 217 kJ/mol and $D_0 = 1.5\times10^{-10}$ m^2/s (Fig. 3).

As part of an experimental study of the equilibrium fractionation of oxygen isotopes between albite and CO_2, Matthews et al. (1994) also determined oxygen diffusion rates by bulk exchange. The diffusion coefficients were calculated from experiments run at 750 °C and 850 °C and 0.1 MPa in CO_2 gas. The resulting diffusion coefficients compare well with those reported by Yund and Anderson (1974) for orthoclase. A linear fit to the three data points reported by Matthews et al. (1994) yields an activation energy of 90 kJ/mol, but the limited number of data points and temperature range implies large uncertainties on the calculated activation energy.

Although a significant amount of experimental data existed for oxygen diffusion in feldspars, Freer et al. (1997) suggested there was almost no direct information about the actual mechanism (e.g., vacancy or interstitial) of oxygen diffusion under hydrothermal conditions.

As a means to determine the mechanism of oxygen diffusion in feldspars, Freer et al. (1997) conducted experiments involving simultaneous diffusion of two isotopes of different mass (^{17}O and ^{18}O) in order to determine the isotope-mass-effect from which the diffusion mechanism can be deduced. The isotope-mass-effect method has been successfully employed to identify diffusion mechanisms in high symmetry metals and oxides (see Peterson 1975), but had not been applied to monoclinic minerals before.

To test the application of the isotope-mass-effect method in feldspars, Freer et al. (1997) conducted hydrothermal oxygen diffusion experiments using sanidine single crystals and ^{17}O and ^{18}O-enriched water. The experiments were run at 550-850 °C and 100 MPa, and the oxygen isotope depth profiles for transport perpendicular to the (001) cleavage plane were determined with an ion microprobe. The diffusion data for both isotopes followed a single Arrhenius relationship with activation energy of 109.7±4 kJ/mol (Fig. 3). Their results were strikingly similar to the data reported for other feldspar compositions, under similar experimental conditions (Yund and Anderson 1974; Anderson and Kasper 1975; Giletti et al. 1978).

In their assessment of whether the isotope-mass-effect data could be employed to determine the mechanism for oxygen diffusion in feldspars, Freer et al. (1997) noted that correlation factors had not been calculated for monoclinic lattices, but Sherwood (1981) had adopted a value of 0.66 for vacancy diffusion in a monoclinic lattice. For their analysis, Freer et al. (1997) assumed for monoclinic feldspars that a correlation factor of 1 indicates diffusion by an interstitial mechanism and a value ≤0.78 indicates a vacancy mechanism (see Freer et al. 1997 for details).

Freer et al. (1997) reported that the diffusion coefficients from the 750 °C and 850 °C experiments were not consistent enough to provide reliable estimates of the D_{17}/D_{18} ratio but the 550 °C and 650 °C experiments yielded an isotope-mass-effect of 0.49 to 1.10. Of these, they considered the 650 °C data to be most reliable, giving an isotope-mass-effect of 0.83 to 1.03. By their criteria, these values would imply an interstitial mechanism provided the ΔK value is close to 1. The ΔK value is a measure of how much any coupling between the diffusing atom and the lattice will reduce the isotope-mass-effect, where $0 < K < 1$, and a value of $\Delta K = 1$ corresponds to the extreme case that only the migrating atom is moving (see Freer et al. 1997 for details). They noted that an interstitial mechanism for oxygen diffusion in feldspars is consistent with their modeling results (Wright et al. 1996) for albite. The computer simulations reported by Wright et al. (1996) predict that the transport of OH is energetically easier by an interstitial mechanism than by a vacancy mechanism but oxygen transport in the form of molecular water is not precluded by the simulations, and the presence of hydrogen bearing species enables oxygen diffusion to proceed more easily.

In a complementary study to Freer et al.'s (1997) investigation of oxygen diffusion in sanidine under hydrothermal conditions, Derdau et al. (1998) determined oxygen diffusion in sanidine under anhydrous conditions. The Derdau et al. (1998) experiments were conducted at 869-1053 °C and 0.1 MPa using single crystals of sanidine cleaved along the (001) face and annealed in an ^{18}O-enriched O_2 gas. The oxygen diffusion profiles in the (001) direction were measured using SIMS. The measured diffusion coefficients define an Arrhenius relation with the activation energy of 245±15 kJ/mol. Their activation energy for dry oxygen diffusion in sanidine is identical within uncertainty to the activation energy for dry oxygen diffusion in anorthite (Elphick et al. 1988). Consistent with the results of previous studies of oxygen diffusion in feldspars, the oxygen diffusion in sanidine is faster under wet conditions, with significantly lower activation energy (Freer et al. 1997).

As noted in Freer et al. (1997) and Derdau et al. (1998), Wright et al. (1996) used computer simulations to investigate the energetics of defect formation in albite and to calculate O and OH migration activation energies. Wright et al.'s (1996) results indicate that water can be accommodated in the albite structure as both OH groups and as H_2O molecules. Their

calculations suggest that in pure albite, molecular water interstitials will be the lowest energy water defect, consistent with the results of Beran's (1986) model of water allocation in sanidine based on detailed FTIR analysis that suggested most of the water will be present as molecular water, with the OH defect being minor. An important outcome of Wright et al.'s (1996) computer simulation study is a predicted diffusional anisotropy for both O and OH in albite. However, Giletti et al. (1978) reported that oxygen diffusion coefficients in albite at 800 °C for transport measured perpendicular to (001), ($\bar{1}$11), (130), and (010) ranged from 1.4×10^{-17} to 2.4×10^{-17} m^2/s, and Freer et al. (1997) noted that there was no direct experimental evidence for anisotropy for oxygen diffusion in any feldspar.

Oxygen diffusion rates have also been reported for the feldspathoid nepheline by Connolly and Muehlenbachs (1988). The experiments were run at 1000-1300 °C and 0.1 MPa, employing the bulk exchange between powdered natural nepheline and an ^{18}O-enriched CO_2 gas. The oxygen diffusion in nepheline can be described by an Arrhenius relation with an activation energy of 105±10 kJ/mol. Connolly and Muehlenbachs (1988) noted that the relatively low activation energy for oxygen diffusion in nepheline was consistent with consideration of its relatively open structure (i.e., high ionic porosity).

Hydrogen. Hydrogen extraction experiments in adularia were reported by Kronenberg et al. (1996). Their experiments were run in air at 500-900 °C and they monitored the decrease in the H_2O structural defect concentration using FTIR. While there was a debate over whether the mobile defect in their study was hydrogen atoms or molecular water (Doremus 1998a; Kronenberg et al. 1998), the results indicate that the diffusion rates are rapid, and are similar to the H-^{2}H exchange rates in quartz reported by Kats et al. (1962), with an activation energy of 172±15 kJ/mol (Fig. 3).

Olivine

Oxygen. Oxygen diffusion rates in olivine were first reported by Muehlenbachs and Kushiro (1974) for bulk exchange of powdered synthetic forsterite with O_2 gas at 0.1 MPa and 1280 °C. The first hydrothermal determination of oxygen diffusion in forsterite was reported by Giletti et al. (1979) for single crystals run at 1000 °C and 400 MPa confining pressure for transport perpendicular to (110). These first two experimental studies were at singular temperatures and, as such, Arrhenius parameters are not available.

The first experimental study of oxygen diffusion in forsterite over a range of temperature was reported by Reddy et al. (1980). Their experiments were run at 1275-1625 °C and 0.1 MPa in O_2 gas. The single crystal samples were analyzed using nuclear reaction analysis by measuring the alpha particle spectrum from the induced nuclear reaction $^{18}O(p,\alpha)^{15}N$. Analysis of the crystallographically oriented crystals indicated that oxygen diffusion in the *b*-direction was consistently greater than in the *a*- or *c*-directions. The results for oxygen diffusion along the *b*-direction yielded an Arrhenius relation with activation energy of 364 kJ/mol.

The Reddy et al. (1980) study was followed soon after by Jaoul et al. (1980), who measured oxygen diffusion in single crystals of synthetic forsterite at 1150-1600 °C. Two different ^{18}O exchange reservoirs were employed. One was a solid layer of MgO or Mg_2SiO_4 enriched to 20-40% ^{18}O, sputtered onto the forsterite surface. The second was an ^{18}O-enriched atmosphere composed of argon containing saturated $H_2{}^{18}O$ vapor with a specific amount of hydrogen. By selecting appropriate ratios of the gases, Jaoul et al. (1980) were able to buffer the experiments at $pO_2 = 10^{-4.4}$ to $10^{-9.2}$ atm. The isotope exchange profiles were obtained for transport along the [100], [010], and [001] directions using either an ion microprobe (SIMS) or nuclear microanalysis using the $^{18}O(p,\alpha)^{15}N$ nuclear reaction. Jaoul et al. (1980) found the accuracy of their measurements was not sufficient to establish a directional anisotropy for oxygen diffusion in forsterite. In addition, a comparison to the results of Reddy et al. (1980) from experiments run at $pO_2 = 0.1$ MPa and analyzed in a similar fashion showed that the oxygen diffusivity is

independent of pO_2 within stated uncertainties. The slope of a linear fit through all of their data yields an activation energy of 328±42 kJ/mol, which is similar, within uncertainties, to the activation energy of 364 kJ/mol reported by Reddy et al. (1980).

Jaoul et al. (1983) reported oxygen diffusion data for forsterite measured using an improved nuclear reaction analysis method employing the $^{18}O(p,\alpha)^{15}N$ nuclear reaction. The experimental samples and design were similar to their previous study (Jaoul et al. 1980). The experiments were conducted using single crystals of synthetic forsterite isotopically exchanged with an ^{18}O-enriched atmosphere consisting of $H_2/H_2{}^{18}O$ mixtures in proportions adjusted to yield a range of pO_2 from 10^{-3} to $10^{-8.2}$ MPa. The experiments were conducted at 1300-1600 °C in the three principal crystallographic directions. Their results at 1600 °C showed the oxygen diffusion coefficient in the [001] direction was less than in the [100] and [010] directions, although values overlap within the stated standard errors. The results obtained at 1600 °C for the [001] direction over a five orders of magnitude range in pO_2 confirmed their earlier findings (Jaoul et al. 1980) that within experimental uncertainties there is no pO_2 dependence on the oxygen diffusion coefficient in forsterite. For the [001] direction, the variation in D as a function of temperature defines an Arrhenius relation with an activation energy of 293 kJ/mol. Within uncertainties, this activation energy is similar in magnitude to the values previously reported by Jaoul et al. (1980) and Reddy et al. (1980). However, the major finding of the Jaoul et al. (1983) study was their diffusion coefficients were systematically 5-10× less than the previously reported values (Fig. 4). They suggested this may be due to improvements in the nuclear activation analysis method, refinements in sample preparation, and/or differences in point defect chemistry when the oxygen partial pressure is maintained so low.

In order to evaluate the potential influence of iron on oxygen diffusion in olivine, Houlier et al. (1988) measured oxygen diffusion in single crystals of natural San Carlos olivine [$(Mg_{0.89}Fe_{0.11})_2SiO_4$]. The experiments were conducted at 1300 °C in controlled oxygen partial pressures in the range of 10^{-7} to $10^{-8.3}$ MPa using a $H_2/H_2{}^{18}O$ gas mixture. The oxygen diffusion profiles were measured using the $^{18}O(p,\alpha)^{15}N$ nuclear reaction. The mean value of D_{Ox} from five experiments run at 1300 °C and different crystallographic directions and pO_2 values, is $D_{Ox} \sim 10^{-18.0\pm0.6}$ m^2/s. The oxygen diffusion coefficient is a factor of 30 greater than the values previously reported for synthetic forsterite determined under similar conditions (Jaoul et al. 1980, 1983).

In two complementary studies published simultaneously, Ryerson et al. (1989) and Gerard and Jaoul (1989) reported oxygen diffusion data measured in single crystals of natural San Carlos olivine ($Fo_{\sim 92}$). Both of these studies used the $^{18}O(p,\alpha)^{15}N$ nuclear reaction analysis method to determine the oxygen isotope diffusion profiles, and both used an olivine-orthopyroxene-silica buffer. The Ryerson et al. (1989) study used a $CO+CO_2$ gas source and buffered the f_{O_2} of the experiments at the Ni-NiO and Fe-FeO buffers. The Gerard and Jaoul (1989) study used an $Ar+H_2/Ar+H_2O$ gas source to buffer the pO_2 of their experiments at 7×10^{-7} to 5×10^{-2} Pa. Ryerson et al. (1989) also investigated the effects of different sample preparation techniques including polishing, polishing followed by chemical etching, and polishing followed by chemical etching followed by Ar ion milling, and found no measurable difference in the diffusion coefficients obtained. In addition, Ryerson et al. (1989) investigated diffusion rates along the [010] and [100] directions and found that the rates along the [010] direction were slightly faster but within the overlap of uncertainties. Gerard and Jaoul (1989) investigated transport only along the [001] direction. The Ryerson et al. (1989) experiments were run at 1200-1400 °C, from which they obtained an activation energy for the [100] direction of 266±11 kJ/mol, and the Gerard and Jaoul (1989) experiments were run at 1190-1500 °C, from which they obtained an activation energy of 318±17 kJ/mol (Fig. 4). While statistically different, these activation energies are similar to the activation energies reported for oxygen diffusion under similar experimental conditions in synthetic forsterite samples (see Jaoul et al. 1980, 1983).

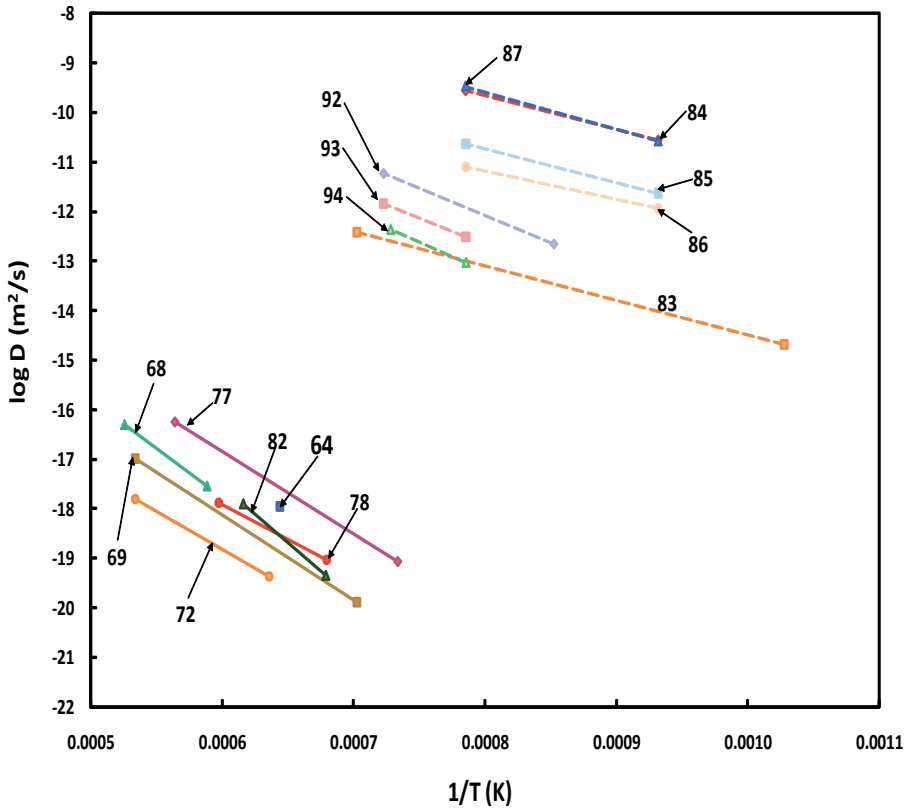

Figure 4. Arrhenius plot of select oxygen and hydrogen diffusion coefficients and Arrhenius relations reported for olivine. The numbers next to the points and lines correspond to the data source as presented in the Appendix. Sources: 64 = Muehlenbachs and Kushiro (1974); 68 = Reddy et al. (1980); 69 = Jaoul et al. (1980); 72 = Jaoul et al. (1983); 77 = Gerard and Jaoul (1989); 78 = Ryerson et al. (1989); 82 = Costa and Chakraborty (2008); 83 = Ingrin and Blanchard (2006); 84 = Mackwell and Kohlstedt (1990); 85 = Mackwell and Kohlstedt (1990); 86 = Kohlstedt and Mackwell (1998); 87 = Kohlstedt and Mackwell (1998); 92 = Demouchy and Mackwell (2003); 93 = Demouchy and Mackwell (2003); and 94 = Demouchy and Mackwell (2003).

The major finding of both the Ryerson et al. (1989) and Gerard and Jaoul (1989) studies was, unlike the case of pure forsterite (see Jaoul et al. 1980, 1983), the oxygen diffusion in the natural olivine shows a positive dependence on the pO_2 of the experiment. In Ryerson et al.'s (1989) experiments they found that the diffusion coefficient was dependent on pO_2 to the 0.21±0.03 power and in the Gerard and Jaoul (1989) experiments they found that the diffusion coefficient was dependent on pO_2 to the 0.34 power. The positive dependence on pO_2 led both authors to conclude that the point defect responsible for oxygen diffusion in olivine is an oxygen interstitial not an oxygen vacancy. The only difference between the two studies is the exact nature of the oxygen interstitial point defect. In the case of Ryerson et al. (1989), they called upon a doubly charged oxygen interstitial, noting that the predicted $[O_I''] \propto p(O_2)^{1/6}$ relation is similar to the dependence obtained from their experiments of $D_{ox} \propto p(O_2)^{0.21}$. Whereas, Gerard and Jaoul (1989) called upon a singly charged oxygen interstitial point defect, noting that the predicted $[O_I'] \propto p(O_2)^{1/3}$ relation is similar to the dependence obtained from their experiments of $D_{ox} \propto p(O_2)^{0.34}$.

In their study of oxygen diffusion along high diffusivity paths in forsterite, Yurimoto et al. (1992) measured oxygen lattice diffusion rates as well. Their samples were synthetic single crystals of forsterite polished and pre-annealed at 1200 °C in air for 10 hours to remove any residual polishing damage. The crystals were annealed in an ^{18}O-enriched CO_2 atmosphere at

1100 °C and 1200 °C and 6.4 kPa. Oxygen diffusion profiles were measured along the *c*-axis direction by depth profiling with an ion microprobe (SIMS). The resulting oxygen isotope concentration profiles showed two distinct regions with depth, first a region that fit the error function relation for diffusion into a semi-infinite medium with a constant concentration source, and the second a "tailing" region. The error function fit to the first region was interpreted to represent the lattice diffusion while the tail was modeled as a fast-path diffusion along dislocations. The oxygen diffusion coefficients obtained for lattice diffusion correspond well with previously reported values (e.g., Jaoul et al. 1983) and the dislocation diffusion coefficients calculated from the depth profile tail regions are about $10^4\times$ faster than the lattice diffusion.

Oxygen and silicon diffusion rates in olivine have been reported by Dohmen et al. (2002) to evaluate the relationship between diffusion of individual species and creep rate. Their experiments consisted of gem quality olivine (Fo_{93}) crystals from Nanga Parbat, Pakistan. The samples were polished on surfaces perpendicular to [001], on which a thin film (200-500 nm) of ^{18}O and ^{29}Si enriched olivine was deposited using Pulsed Laser Deposition. The thin-film coated samples were pre-annealed at 900 °C and $f_{O_2} = 10^{-14}$ bars for 40 hours. Diffusion anneals were at 1100-1500 °C and $f_{O_2} = 10^{-9}$ bars in a continuously flowing CO/CO_2 gas. The silica activity in the olivine was buffered using enstatite powder. The oxygen diffusion rates obtained agree within an order of magnitude to the values reported by Gerard and Jaoul (1989) and Ryerson et al. (1989), with a similar activation energy of 338±14 kJ/mol.

Costa and Chakraborty (2008) investigated the effect of water on oxygen and silicon diffusion in olivine. Their experiments were performed at 1200-1350 °C and 2 GPa under water undersaturated (45 ppm H_2O in olivine, f_{H_2O} ~1 GPa, f_{O_2} ~IW buffer) and close to water saturated (~370 ppm H_2O in olivine, f_{H_2O} ~9 GPa, f_{O_2} ~QFM buffer) conditions. The samples were natural San Carlos olivine coated with a thin film of ^{18}O and ^{29}Si enriched olivine. The isotope concentration profiles were measured using SIMS. The results indicate at 1200 °C the oxygen diffusion coefficient at 2 GPa and f_{H_2O} ~0.97 GPa is a factor of 10-70 greater than at 1 atm, dry. In addition, activation energies for oxygen diffusion under dry and wet conditions are similar indicating there is no change in the diffusion mechanism, consistent with computer simulations of oxygen diffusion in pure forsterite (Walker et al. 2003). Unlike the findings under dry conditions, diffusion rates for oxygen and silicon are similar under water-present conditions and the diffusion anisotropy is weak to absent. Finally, Costa and Chakraborty (2008) noted the change in behavior from dry to wet conditions occurs at low H concentration (<10 ppm H_2O in olivine at 2 GPa and 1200 °C).

Hydrogen. The first detailed study of hydrogen uptake in olivine was reported by Mackwell and Kohlstedt (1990), who presented the results of a more comprehensive follow-up study of hydrogen uptake in natural olivine and syntetic forsterite in Kohlstedt and Mackwell (1998). In their earlier study, Mackwell and Kohlstedt (1990) demonstrated that protons diffuse rapidly in olivine and the diffusion is charge compensated by a counter flux of polarons that is related to the excess charge on ferric iron in an octahedral cation site and/or a flux of electrons. In their follow-up study, Kohlstedt and Mackwell (1998) found that the hydrogen uptake in olivine occurred by two distinctly different mechanisms. The first is relatively rapid diffusion compensated by a counter flux of polarons or electrons, as noted in their earlier study. The hydrogen diffusion by this mechanism yields an Arrhenius relation for transport parallel to (100) over the temperature range 800-1000 °C with an activation energy of 110±50 kJ/mol (Fig. 4). The second, slower diffusion rates correspond to an exchange mechanism controlled by the mobility of metal vacancy point defects. In addition, Kohlstedt and Mackwell (1998) found that the hydrogen diffusion in olivine is anisotropic, with transport parallel to [100] more than one order of magnitude greater than parallel to [010] or [001] over the temperature range of their experiments. The rapid hydrogen diffusion rates are several orders of magnitude greater than the diffusivities of other ionic species in olivine, indicating that hydrogen diffuses through the lattice as protons not coupled to other ionic species.

In order to better constrain the speciation and transport rates of the mobile water-derived defects in olivine in the absence of polarons, Demouchy and Mackwell (2003) studied hydrogen diffusion in iron-free synthetic forsterite. Their experiments involved hydrogenation of dry synthetic forsterite single crystals at 1000 °C and 1.5 GPa and at 900-1110 °C at 0.2 GPa. The oxygen fugacity was buffered using Fe-FeO or Ni-NiO powders. The hydrogenation rates were determined by FTIR analysis of water content for transport along the three principal crystallographic axes. They found that the very rapid hydrogenation reported by Mackwell and Kohlstedt (1990) for iron-bearing olivine does not occur in iron-free forsterite, supporting the model of proton-polaron exchange for this process. In addition, the results of the hydrogenation for forsterite are consistent with the incorporation of water-derived species being rate-limited by the diffusivity of metal vacancies, and indicate that the transport of the water-derived species is not strongly coupled to the iron concentration.

Pyroxene

Oxygen. The earliest experimental determinations of oxygen diffusion in pyroxene were bulk exchange experiments reported by Muehlenbachs and Kushiro (1974). Their experiments were done using powdered synthetic enstatite or diopside exchanged with an O_2 or CO_2 gas reservoir at 1280 °C and 0.1 MPa. The oxygen diffusion coefficients were calculated from the bulk isotope exchange assuming a spherical geometry, and yield D_{Ox} values of 1.8 to 6.0×10^{-16} m^2/s. These experiments were conducted at a single temperature and as such, no Arrhenius parameters could be determined.

The first oxygen diffusion experiments in a pyroxene over a range of temperatures were reported by Connolly and Muehlenbachs (1988) using powdered synthetic diopside exchanged with CO_2 gas at 0.1 MPa and 1150-1350 °C. The bulk isotope exchange was determined, and diffusion coefficients calculated assuming spherical geometries. A linear fit to the diffusion coefficients yields an Arrhenius relation with the activation energy of ~405 kJ/mol. Connolly and Muehlenbachs (1988) noted that the relatively high activation energy for oxygen diffusion in diopside was consistent with its high packing density (i.e., low ionic porosity).

Oxygen diffusion rates in single crystals of natural diopside were determined by Farver (1989) under hydrothermal conditions at 700-1250 °C and 100 MPa. The isotope concentration profiles were measured by SIMS depth profiling of samples oriented parallel and perpendicular to the *c*-axis. The results indicate that the oxygen diffusion coefficients for transport parallel to the *c*-axis are nearly two orders of magnitude greater than those perpendicular to *c*. The Arrhenius relation obtained for diffusion parallel to *c* yields an activation energy of 226±21 kJ/mol, and the data perpendicular to *c* yield a similar activation energy, although over a much smaller temperature range of 1000-1200 °C. The Arrhenius relations of Farver (1989) cross the Arrhenius relation of the dry 0.1 MPa data of Connolly and Muehlenbachs (1988) at ~1150 °C but due to the large difference in activation energies between the wet and dry experiments, oxygen diffusion coefficients are orders of magnitude less at dry conditions compared to wet at geologically relevant temperatures of <1000 °C (Fig. 5). This marked difference in activation energies for oxygen diffusion under dry compared to wet conditions has been noted for other silicate minerals (see Brady 1995; Brady and Cherniak 2010), and Farver (1989) suggested that the difference was due to a change in the mechanism of oxygen diffusion due to the presence of some hydrogen-related species in the hydrothermal experiments. Also, Farver (1989) noted oxygen diffusion rates in diopside are significantly less than other silicate minerals at similar experimental conditions.

Oxygen diffusion rates for three natural diopsidic clinopyroxenes containing 0.71 to 2.56 mol% FeO, were reported by Ryerson and McKeegan (1994). The samples were polished and etched single crystals pre-annealed at the same temperature and pO_2 conditions of the diffusion experiments. An ^{18}O-enriched CO-CO_2 gas mixture was used as both the tracer source and the

means to fix the oxygen fugacity of the experiments. The experiments were run at 1104-1251 °C and total pressure of 0.1 MPa. Three different CO-CO_2 gas mixtures were used to buffer the oxygen fugacities at just slightly above Ni-NiO, QFM, and Fe-FeO oxide buffers. The isotope exchange profiles along the [001] direction were measured by SIMS analysis. The diffusion profiles obtained for all of the clinopyroxene samples were in good agreement with a solution to the diffusion equation for constant diffusion coefficient and constant surface concentration. At a given temperature, the diffusion coefficients for the three different diopside compositions are in good agreement, and Ryerson and McKeegan (1994) reported a single Arrhenius relation fit to all of the data with an activation energy of 457±26 kJ/mol (Fig. 5).

A comparison of Ryerson and McKeegan's (1994) results to those of Connolly and Muehlenbachs (1988) shows a comparable activation energy, but at a given temperature, the oxygen diffusion coefficients determined by Connolly and Muehlenbachs (1988) are ~2 orders of magnitude greater than those reported by Ryerson and McKeegan (1994). The Connolly and Muehlenbachs (1988) study employed grain-size sorted samples of powdered synthetic diopside partially equilibrated with an anhydrous ^{18}O-enriched gas. Ryerson and McKeegan (1994) noted that diffusion coefficients determined by the bulk exchange method typically yield activation energies comparable to those determined by depth profiling, but with a greater pre-exponential factor (e.g., Ryerson 1987). This may be due to underestimation of the surface

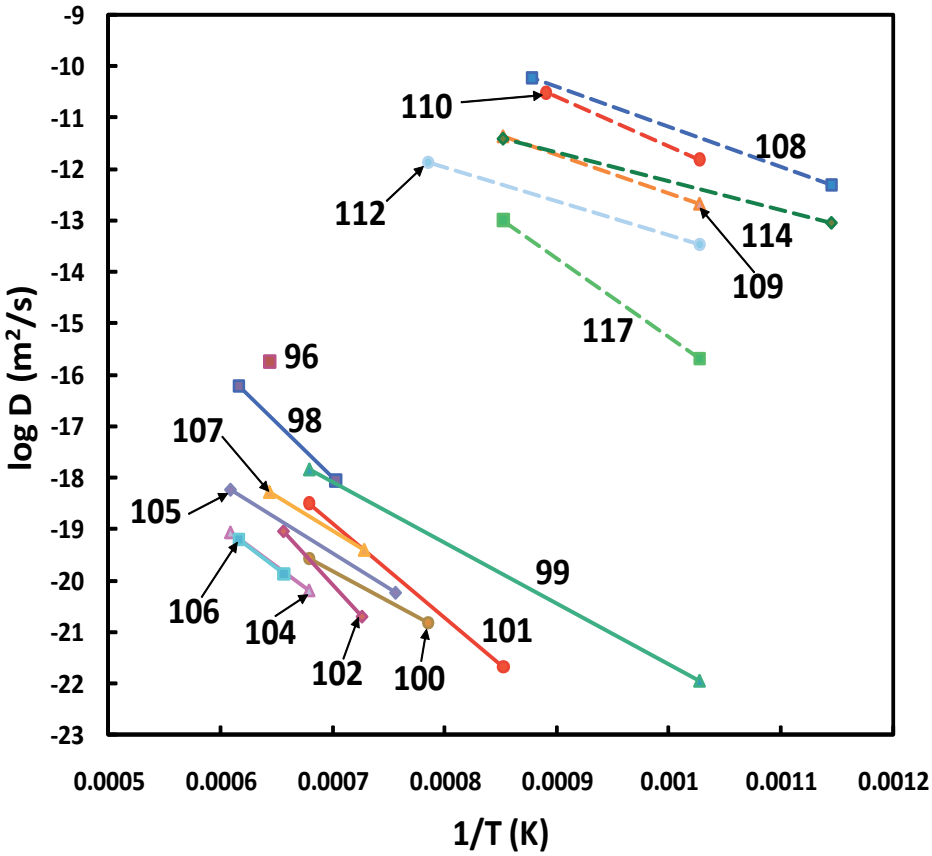

Figure 5. Arrhenius plot of select oxygen (solid) and hydrogen (dashed) diffusion coefficients and Arrhenius relations reported for pyroxenes. The numbers next to the points and lines correspond to the data source as presented in the Appendix. Sources: 96 = Muehlenbachs and Kushiro (1974); 98 = Connolly and Muehlenbachs (1988); 99 = Farver (1989); 100 = Farver (1989); 101 = Elphick and Graham (1990); 102 = Ryerson and McKeegan (1994); 104 = Pacaud et al. (1999); 105 = Ingrin et al. (2001); 106 = Ingrin et al. (2001); 107 = Ingrin et al. (2001); 108 = Hercule and Ingrin (1999); 109 = Hercule and Ingrin (1999); 110 = Carpenter-Woods et al. (2000); 112 = Ingrin et al. (1995); 114 = Hercule (1996); and 117 = Stalder and Skogby (2003).

to volume ratios of crushed particles, and for unaccounted-for variations in the effective diffusion in powder (see Ando and Oishi 1983). Comparison to the oxygen diffusion in single crystals of diopside under hydrothermal conditions as reported by Farver (1989) shows significantly greater diffusion coefficients than those measured by Ryerson and McKeegan (1994) and a much lower activation energy (~225 kJ/mol compared to ~457 kJ/mol). Ryerson and McKeegan (1994) noted that diffusion coefficients obtained for oxygen in other silicate minerals under wet versus dry conditions display similar relationships. The increased oxygen diffusion coefficients and decreased activation energies in the wet experiments reflect that the dominant oxygen transport is by hydrous species, particularly molecular water, which is rapid compared to dry oxygen (see Zhang et al. 1991).

A high temperature oxygen diffusion study in synthetic diopside was reported by Pacaud et al. (1999). The experiments were conducted at 1200-1400 °C under controlled oxygen partial pressures of 10^{-11} to 10^{-2} bars. An ^{18}O-enriched Ar-H_2-H_2O gas mixture was employed and the resulting isotope exchange profiles along the *b*-axis were measured using NRA and the $^{18}O(p,\alpha)^{15}N$ reaction. The diffusion coefficients define an Arrhenius relation with activation energy of 310±30 kJ/mol.

The results of Pacaud et al.'s (1999) study are in good agreement with Ryerson and McKeegan's (1994) data, taking into account the uncertainties of the diffusion coefficients. Pacaud et al. (1999) suggested that the slightly higher diffusivities reported by Ryerson and McKeegan (1994) might be due to the presence of Fe, albeit at relatively low amounts of < 3 mol% FeO, compared to their Fe-free synthetic samples, or it may reflect anisotropy, as the Ryerson and McKeegan (1994) data were for diffusion along the *c*-axis while their data were for diffusion along the *b*-axis. Consistent with the observations of Ryerson and McKeegan (1994), but over a much greater range of pO_2, Pacaud et al. (1999) concluded that the oxygen diffusion coefficients in diopside are independent of pO_2.

Comparison of Pacaud et al.'s (1999) data to Farver's (1989) data from hydrothermal experiments at 100 MPa show that the diffusion coefficient reported by Farver (1989) at 1250 °C for transport perpendicular to the *c*-axis is about a factor of three greater than the diffusion coefficient reported by Pacaud et al. (1999) for transport along the *b*-axis, and extrapolation to lower temperatures yields a greater difference due to the lower activation energy of ~227 kJ/mol reported by Farver (1989). In addition, Farver (1989) reported a significant anisotropy,where the oxygen diffusion coefficients parallel to the *c*-axis are almost two orders of magnitude greater than those perpendicular to the *c*-axis. Hence, the oxygen diffusion coefficients parallel to the *c*-axis reported by Farver (1989) are significantly greater than those reported by Pacaud et al. (1999) for diffusion parallel to the *b*-axis. Ryerson and McKeegan (1994) suggested that the higher diffusivity and lower activation energy reported by Farver (1989) for hydrothermal experiments compared to their anhydrous experiments was due to a strong water effect on oxygen diffusion. Pacaud et al. (1999) suggested that the apparent enhanced diffusion along the *c*-axis reported by Farver (1989) may be a result of a shortcut of diffusion paths due to small amphibole lamellae developed along the (010) planes in the diopside crystals.

In order to resolve the outstanding questions regarding anisotropy of oxygen diffusion in diopsides and the effect of water on diffusion rates and activation energies, Ingrin et al. (2001) determined oxygen diffusion coefficients by nuclear reaction analysis of iron-free synthetic diopside single crystals along the three crystallographic directions, and in an iron-bearing natural diopside crystals along the *c*-direction. Their experiments were conducted at 1050-1370 °C and 0.1 MPa under controlled oxygen partial pressures of 10^{-3} to 10^{-12} atm.

The results of Ingrin et al.'s (2001) study indicate that oxygen diffusion along the *c*- and *a*-directions is one order of magnitude greater than along the *b*-direction, and diffusion along the *c*-direction in natural diopside is about a factor of two greater than in synthetic diopside. In addition, they indicate that oxygen diffusion along the *a*- and *c*-directions are slightly dependent

on the oxygen fugacity ($D_{Ox} \propto f_{O_2}^{0.04}$) while diffusion along the *b*-direction shows no dependence on f_{O_2}. They suggest the anisotropy is related to the oxygen diffusion path within the diopside, with preference for the under-bonded O2 oxygen site. They proposed a single law to describe oxygen diffusion along the fast directions in diopside at typical geological conditions close to the QFM buffer with the Arrhenius parameters $D_0 = 10^{-10}$ m^2/s and $E_a = 259\pm15$ kJ/mol (Fig. 5).

Hydrogen. To date, pyroxenes represent the most studied mineral with regard to hydrogen exchange/diffusion. Specifically, Skogby and Rossman (1989) and Skogby (1994) performed extensive hydrogen and deuterium exchange experiments in a range of pyroxene compositions, and pioneered the IR analysis of pyroxenes, but they did not quantify the diffusion kinetics. Ingrin et al. (1995) reported the first kinetics of hydrogen extraction in diopside single crystals through dehydration experiments conducted in air at 700-1000 °C. The hydrogen extraction was determined by the change in OH^- concentration as measured by FTIR analysis. Hydrogen extraction rates were determined along the [001], [100]*, and [010] directions and the results showed no measurable anisotropy. An Arrhenius law fit to the diffusion coefficients obtained for all orientations yielded an activation energy of 136±27 kJ/mol. The dehydration rates for diopside are 2 to 3 orders of magnitude less than the dehydration rates reported for olivine by Mackwell and Kohlstedt (1990).

Hercule and Ingrin (1999) investigated both the hydrogen uptake/extraction and hydrogen isotope exchange rates in natural diopside single crystals. The hydrogen uptake/extraction rates were determined by measuring the OH^- infrared absorption using FTIR analysis of samples annealed at 700-1000 °C and 0.01 and 0.1 MPa of hydrogen pressure. Their results indicate that the hydrogen uptake/extraction rate in diopside is independent of crystallographic orientation, pO_2 and pH_2. Their data yield an Arrhenius relation with activation energy of 126±24 kJ/mol (Fig. 5).

The hydrogen isotope exchange experiments were conducted at 600-900 °C and 0.1 MPa total pressure. The self-diffusion rates obtained from the H-^{2}H exchange in the same diopside samples yields an Arrhenius law for transport along the [001] and [100]* directions that is two orders of magnitude greater than the hydrogen uptake rate with an activation energy of 149±16 kJ/mol. The hydrogen self-diffusion rate along the [010] direction is one order of magnitude greater than the hydrogen uptake rate, with an activation energy of 143±33 kJ/mol.

Hercule and Ingrin (1999) noted that the results of their study, and the previous study by Ingrin et al. (1995), indicate that the hydrogen uptake/extraction in the diopside was not rate limited by the mobility of protons, but more likely by the mobility of electron holes connected with the iron oxidation-reduction process. In this case, the kinetics of hydrogen uptake in clinopyroxenes would increase with increasing Fe-content until it becomes rate-controlled by the hydrogen self-diffusion.

The hydrogen diffusion rates in diopside reported by Ingrin et al. (1995) and Hercule and Ingrin (1999) were measured by sequential dehydration/hydration experiments of H-^{2}H exchange experiments. Although measurements of bulk changes in H or ^{2}H concentration can provide accurate diffusivities when anisotropy is low, Carpenter-Woods et al. (2000) noted that more accurate determinations of diffusion coefficients are only possible when diffusion profiles are measured directly. As such, Carpenter-Woods et al. (2000) reported measurements of hydrogen diffusion profiles in natural diopside crystals.

The diopside samples employed by Carpenter-Woods et al. (2000) had a higher Fe-content (Fe/(Fe+Mg) = 0.69) compared to the diopside employed by Hercule and Ingrin (1999) (with Fe/(Fe+Mg) = 0.36). The hydroxyl concentration profile experiments included olivine to buffer the silica activity and a CO/CO_2 gas mixture to buffer the oxygen fugacity. The experiments were run at 700-850 °C and the hydrogen diffusivities were determined for the [100], [010], and [001]* directions by measuring the diffusion profiles. After the diffusion anneals, samples

were cut into slices to expose a central cross-section of the sample and the diffusion profiles were measured by collecting a series of FTIR spectra along traverses along the principal crystallographic directions – essentially typical step-scan analyses. They also performed several sequential dehydration/hydration experiments similar to those of Ingrin et al. (1995).

The chemical diffusion coefficients determined by Carpenter-Woods et al. (2000) from the hydroxyl concentration profiles and from the sequential dehydration experiments represent the process by which hydrogen is transported in diopside, and as such, it is assumed to involve the cooperative transport of protons and electronic defects (Skogby 1994; Ingrin et al. 1995). The chemical diffusion coefficient is a function of the concentration and diffusion coefficients of the hydrogen and electronic defect species; Carpenter-Woods et al. (2000) noted that in the case where electronic defects diffuse faster than protons, and are present in greater concentration than the hydrogen, the chemical diffusion coefficient is approximately equal to the hydrogen self-diffusion coefficient.

The hydrogen diffusion coefficients for transport parallel to [100] and [001]* yield activation energies of 181±38 kJ/mol and 153±32 kJ/mol, respectively, with no measurable differences in diffusivities or activation energies for these two directions. The diffusion rate parallel to [010], however, is about one order of magnitude less than those parallel to [100] or [001]*. In addition, all of the hydrogen diffusion coefficients reported by Carpenter-Woods et al. (2000) are greater than those reported by Ingrin et al. (1995) for the low Fe diopside, which showed no anisotropy. The results of Carpenter-Woods et al. (2000) are in good agreement with the ^{2}H-H exchange data of Hercule and Ingrin (1999) in activation energies, absolute diffusion coefficients, and anisotropy. As noted by Hercule and Ingrin (1999), one would expect that the measured hydrogen diffusion rate would increase with iron content until the rate limiting mechanism switched from transport of electronic species to hydrogen, at which point the hydrogen diffusion rate would become independent of the iron content. A comparison of the results of Hercule and Ingrin (1999) to Carpenter-Woods et al. (2000) suggests the switch from electronic species-limited to hydrogen self-diffusion-limited hydrogen transport in diopside occurs at an iron content somewhere between Fe/(Fe+Mg) = 0.36 and 0.69.

Citing the few hydrogen diffusion data available for natural orthopyroxenes, and the complete absence of hydrogen diffusion data for pure enstatite, Stalder and Skogby (2003) experimentally determined hydrogen diffusion rates in single crystals of a natural orthopyroxene ($\sim En_{90}Fs_{10}$) and a synthetic enstatite. The diffusion experiments involved stepwise dehydration in air or hydration in an H_2 atmosphere at 700 °C and 900 °C. The hydrogen uptake/extraction was determined by measuring the H_2O content of the sample before and after the diffusion experiments. Stalder and Skogby (2003) observed a small but significant anisotropy for hydrogen diffusion in the natural orthopyroxene with transport along [001] being fastest, followed by [100] and [010]. The hydrogen diffusion in the synthetic enstatite is about 2 orders of magnitude slower than in the natural orthopyroxene and is isotropic. The activation energy for hydrogen diffusion in the natural orthopyroxene is 213±47 kJ/mol and for the synthetic enstatite it is 295±55 kJ/mol (Fig. 5).

The hydrogen diffusion coefficients in natural orthopyroxene reported by Stalder and Skogby (2003) are of the same order of magnitude as the hydrogen [chemical] diffusion coefficients reported by Ingrin et al. (1995) for diopside. In addition, the hydrogen diffusion coefficients in the natural orthopyroxene are 2 orders of magnitude less than the hydrogen self-diffusion coefficients in diopside (Hercule and Ingrin 1999) and hydrogen diffusion in olivine (Mackwell and Kohlstedt 1990) and slightly less than hydrogen diffusion in pyrope garnets (Wang et al. 1996).

Recently, experimental studies reported by Stalder et al. (2007) on hydrogen diffusion in synthetic orthopyroxenes in the system $MgSiO_3$-$FeSiO_3$ confirm the assumption that hydrogen extraction is rate-limited by hydrogen self-diffusion if a threshold Fe-concentration of X_{Fe} ~

0.12 is exceeded (see Carpenter-Woods et al. 2000). In addition, the results of dehydration experiments using pure (Fe-free) synthetic diopside crystals recently reported by Sundvall et al. (2009) show no measureable anisotropy, and yield an activation energy of 312±55 kJ/mol for transport along [001]*. The diffusion rate in the pure synthetic diopside is about one order of magnitude less than for synthetic diopside with very low Fe-content, and several orders of magnitude less than for natural diopsides with appreciable Fe-contents (see Hercule and Ingrin 1999; Carpenter-Woods et al. 2000).

Amphiboles

Oxygen. The only experimental data on oxygen diffusion in amphiboles is from Farver and Giletti (1985) who determined oxygen diffusion rates in a range of amphibole compositions including hornblende, tremolite, and fluor-richterite. Their experiments were conducted at 650-800 °C under hydothermal conditions at 100 MPa water pressure. The isotope exchange profiles were measured using an ion microprobe. Analysis of oriented crystals of the hornblende indicate a measureable anisotropy, with the diffusion coefficient for transport parallel to *c* at least a factor of ten greater than parallel to *a*, and 20× greater than parallel to *b*. In addition, the *D* value at 800 °C shows a modest positive dependence on the water pressure (water fugacity), increasing by a factor of 2.7 for experiments run at 200 MPa compared to experiments run at 20 MPa. The oxygen diffusion coefficients for the three different amphibole compositions are similar within stated uncertainties, and *D* values at 800 °C, 100 MPa, for transport parallel to *c* range from 2.28×10^{-20} m^2/s (tremolite) to 5.03×10^{-20} m^2/s (fluor-richterite). Least squares linear fits to the diffusion coefficients measured at 100 MPa, for transport parallel to *c* yield similar activation energies for hornblende (172±25 kJ/mol) and tremolite (163±21 kJ/mol), with slightly higher activation energy for fluor-richterite (238±8 kJ/mol) (Fig. 6). Farver and Giletti (1985) suggested that the apparent difference in activation energy for the fluor-richterite was most likely due to the relatively small temperature range and uncertainties of the measurements relative to the total range in calculated *D* values.

Hydrogen. The hydrogen diffusion kinetics in amphiboles were reported by Graham et al. (1984) for a range of compositions including hornblende, tremolite, and actinolite. The primary goal of their study was to determine the equilibrium fractionation factors for amphibole-water pairs, but they also derived quantitative data on the kinetics of the isotope exchange between water and the amphiboles, as well as diffusion of hydrogen in the amphiboles. The experiments used powdered natural amphibole samples and were conducted at 350-800 °C and 200-800 MPa confining pressure. The diffusion rates were obtained from bulk exchange with waters of different hydrogen isotope composition. The hydrogen diffusion coefficients obtained were very similar for the hornblende and tremolite, and slightly higher for the actinolite, yielding Arrhenius relations with activation energies of 79-84 kJ/mol for hornblende, 71.5 kJ/mol for tremolite, and 99 kJ/mol for actinolite. Graham et al. (1984) noted that the activation energies were relatively low but comparable to other hydrous minerals.

The bulk exchange experiments of Graham et al. (1984) do not allow an assessment of whether the hydrogen diffusion in amphiboles is anisotropic, as is the case for oxygen diffusion (Farver and Giletti 1985). However, more recently, Ingrin and Blanchard (2000) determined hydrogen diffusion rates in kaersutite natural single crystals using sequential FTIR analysis. The experiments were run at 600-900 °C and 0.1 MPa pressure in a 90%Ar:10%$^2H_2$ atmosphere. The hydrogen diffusion coefficients are comparable to the actinolite data from Graham et al. (1984) and the Arrhenius relation yields an activation energy of 104±12 kJ/mol (Fig. 6). In addition, Ingrin and Blanchard's (2000) data clearly demonstrate that hydrogen diffusion in amphibole is anisotropic, with transport along the *c*-axis being about a factor of five faster than along the *b*-axis.

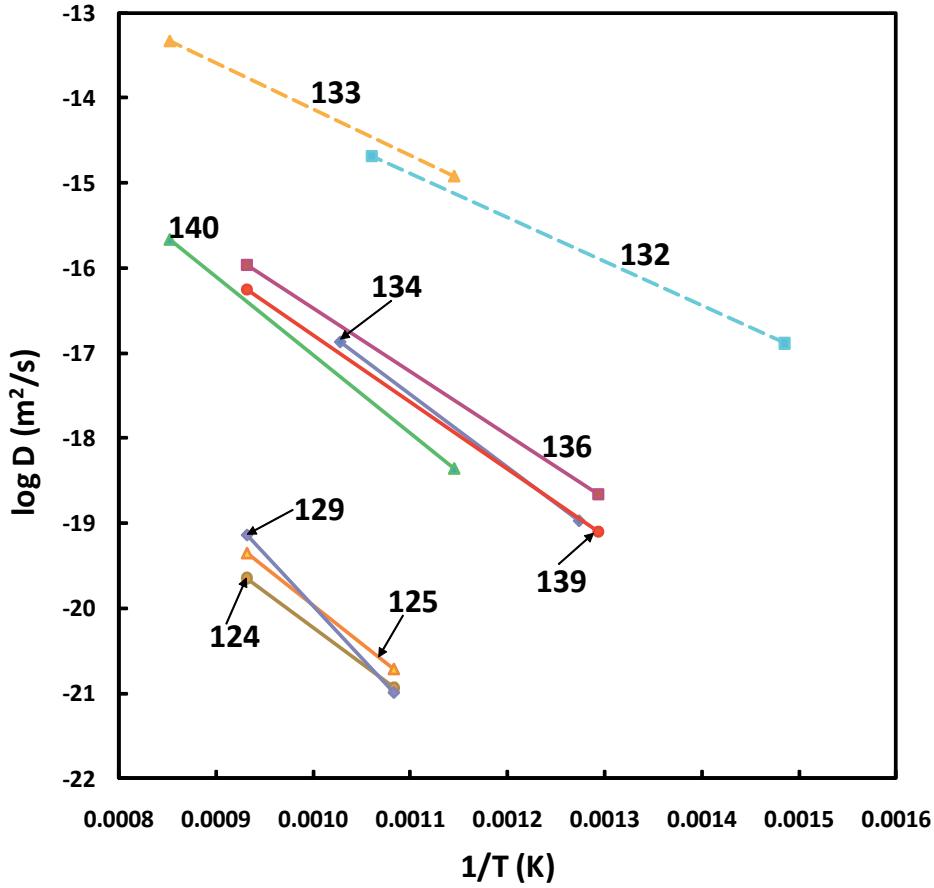

Figure 6. Arrhenius plot of select oxygen (solid) and hydrogen (dashed) diffusion coefficients and Arrhenius relations reported for amphiboles and micas. The numbers next to the points and lines correspond to the data source as presented in the Appendix. Sources: 124 = Farver and Giletti (1985); 125 = Farver and Giletti (1985); 129 = Farver and Giletti (1985); 132 = Graham et al. (1984); 133 = Ingrin and Blanchard (2000); 134 = Fortier and Giletti (1991); 136 = Fortier and Giletti (1991); 139 = Giletti and Anderson (1975); and 140 = Fortier and Giletti (1991).

Sheet silicates

Oxygen. The earliest experimental studies of oxygen diffusion in micas focused on natural phlogopites (annite 4%) by Giletti and Anderson (1975). These bulk exchange experiments were run under hydrothermal conditions at 500-800 °C and 200 MPa confining pressure using ^{18}O-enriched water. The diffusional transport was modeled as being anisotropic and dominated by transport parallel to the *c*-axis. A linear Arrhenius relation was obtained with the activation energy of 121±8 kJ/mol.

A much more extensive study of oxygen diffusion in a range of mica compositions was reported by Fortier and Giletti (1991). The samples included natural biotite, muscovite, and phlogopite micas. The experiments were conducted under hydrothermal conditions using both the bulk isotope exchange method and single crystal depth profiling methods. Most of the experiments were done using the bulk exchange at temperatures of 500-900 °C and 100 MPa confining pressure. The Arrhenius relations obtained for layer-parallel diffusive transport fit to an infinite cylinder model yielded activation energies of 142±8 kJ/mol for biotite, 163±21 kJ/mol for muscovite, and 176±13 kJ/mol for phlogopite, and the oxygen diffusion coefficients were similar (within a factor of five) for all three mica compositions over the temperature range of the experiments. The diffusion coefficient obtained from a single layer-parallel step profiling experiment was the same, within uncertainty, as the diffusion coefficients obtained

from the bulk exchange experiments. Experiments run at 700 °C and pressures of 20-200 MPa showed a slight dependence of the oxygen diffusion coefficient on water pressure in phlogopite. The combination of depth profiling and bulk exchange analysis allowed Fortier and Giletti (1991) to demonstrate that the dominant transport direction is layer parallel (perpendicular to *c*) and not parallel to the *c*-axis. They found that the rates perpendicular to the *c*-axis were 3 to 4 orders of magnitude greater than exchange parallel to *c* (Fig. 6). Fortier and Giletti (1991) noted, as with many other silicate minerals, that the oxygen diffusion rate in micas is dictated by the mineral structure much more so than the chemical composition.

Hydrogen. Hydrogen diffusion rates have been reported by Graham (1981) for bulk isotope exchange experiments with powdered natural samples of muscovite mica. The experiments were run under hydrothermal conditions at 450-750 °C and 200 or 400 MPa confining pressure. The activation energy obtained is 122 kJ/mol, similar to activation energies reported for hydrogen diffusion in other hydrous minerals. In addition, Graham (1981) calculated hydrogen diffusion coefficients for biotite mica from the data of Suzuoki and Epstein (1976) at 450 °C and 500 °C and found they are similar to the data for muscovite, suggesting there is no major compositional control on hydrogen diffusion in micas (Fig. 6).

As part of the same study, Graham (1981) also determined hydrogen diffusivities for epidote and zoisite by bulk isotope exchange at 200-650 °C and 200 or 400 MPa confining pressure and found the activation energies were relatively low and ranged from 67 to 132 kJ/mol. He found that at low temperatures, the hydrogen diffusion in epidote is almost four orders of magnitude faster than in muscovite, and two orders of magnitude faster than in zoisite.

Garnet

Oxygen. Two experimental studies of oxygen diffusion in garnets have been reported in the literature, but the data in both cases are somewhat questionable. The first reported oxygen diffusion data are for a natural grossular garnet run at 850 °C and 200 MPa confining pressure and at 1050 °C and 800 MPa confining pressure under hydrothermal conditions using ^{18}O-enriched water (Freer and Dennis 1982). The diffusion profiles were measured by depth profiling with an ion microprobe. However, plots of the inverse error function against penetration distance show two distinct linear regions. Freer and Dennis (1982) argued that the near surface region was probably the more reliable one to use to extract the lattice diffusion rates, and obtained oxygen diffusion coefficients of 4.8×10^{-21} m^2/s at 850 °C and 2.5×10^{-20} m^2/s at 1050 °C. They also noted that since the experiments were performed at different [water] pressure, the activation energy of ~101 kJ/mol obtained from a straight line fit to the two data points was likely to need later revision.

The other experimental study of oxygen diffusion in garnet is from Coughlan (1990) for a spess-almandine ($Sp_{0.286}An_{0.028}Py_{0.017}Al_{0.669}$) composition. The experiments were run at 800-1000 °C and 100 MPa under hydrothermal conditions using ^{18}O-enriched water as the tracer source. A linear least squares fit to the diffusion coefficients gives an apparent Arrhenius relation with activation energy of 301±46 kJ/mol (Fig. 7). However, Coughlan (1990) noted that the experiments at 1000 °C were time dependent, suggesting there may have been some influence of surface reactions on the isotope exchange profiles measured using the ion microprobe. The diffusion rates at 800 °C and 900 °C were too slow to do a time-dependency test, and Coughlan (1990) suggested that the reported Arrhenius relation likely represents an upper limit on the true oxygen diffusion rate in garnet.

Hydrogen. Wang et al. (1996) reported the results of dehydrogenation experiments using natural pyrope single crystals ($Py_{70}Alm_{16}Gr_{14}$) annealed in air or a continuous flow of N_2 gas at 0.1 MPa total pressure and 692-900 °C. They conducted two types of analyses, profiling experiments were conducted to examine the potential concentration dependence of diffusion of hydrous components, and mass-loss experiments were conducted to obtain diffusivities as

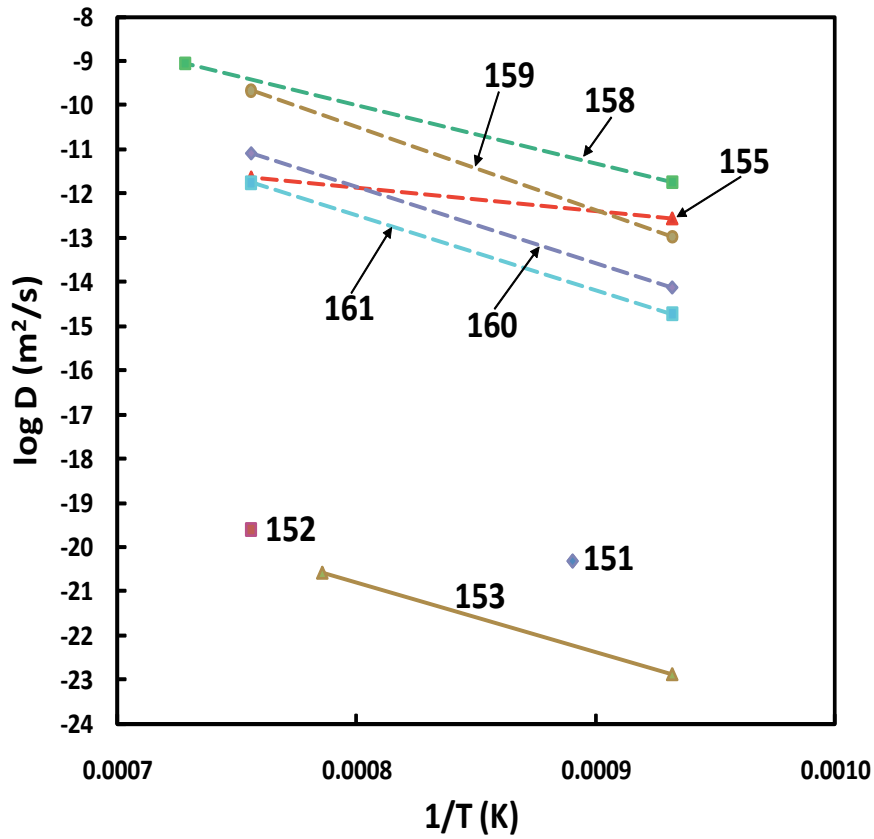

Figure 7. Arrhenius plot of select oxygen (solid) and hydrogen (dashed) diffusion coefficients and Arrhenius relations reported for garnets. The numbers next to the points and lines correspond to the data source as presented in the Appendix. Sources: 151 = Freer and Dennis (1982); 152 = Freer and Dennis (1982); 153 = Coughlan (1990); 155 = Kurka et al. (2005); 158 = Wang et al. (1996); 159 = Blanchard and Ingrin (2004a); 160 = Blanchard and Ingrin (2004a); and 161 = Kurka et al. (2005).

a function of temperature. They reported that the bulk extraction diffusion coefficients varied between the two samples they analyzed, but the activation energies were in good agreement with a weighted average of 253±13 kJ/mol.

Hydrogen extraction experiments on Dora Maira pyrope single crystals were conducted by Blanchard and Ingrin (2004a) at 800-1100 °C and 0.1 MPa in a 90%Ar:10%H_2 gas mixture under pO_2 = 0.21 atm and $pO_2 = 10^{-16}$ atm. Blanchard and Ingrin (2004a) reported that during the hydrogen extraction the two principal IR absorption bands for OH behaved independently, where the OHa triplet at 3651 cm^{-1} decreased 5× faster than the OHb band at 3602 cm^{-1}. They interpreted these results to reflect the presence of two distinct H defects, each defining its own Arrhenius relation slightly dependent on oxygen partial pressure. The resulting Arrhenius relations have the form: $D_{OHa} = 3.2(pO_2)^{0.119} \exp[-(277\pm22 \text{ kJ/mol})/RT]$, and $D_{OHb} = 79(pO_2)^{0.147} \exp[-(329\pm22 \text{ kJ/mol})/RT]$. The hydrogen extraction kinetics under reducing conditions ($pO_2 = 10^{-16}$ atm) for both absorption bands is about two orders of magnitude slower than in air (pO_2 = 0.21 atm). Also, this dependence of the hydrogen extraction on pO_2 ($(pO_2)^{1/8.5}$ and $(pO_2)^{1/7}$) for both H defects is in the range of the dependences measured for cation diffusion in garnets and olivine.

A comparison of Blanchard and Ingrin's (2004a) data to Wang et al.'s (1996) study shows that the hydrogen diffusion rates in Dora Maira pyrope for both H defects identified by Blanchard and Ingrin (2004) are slower than those in mantle pyrope reported by Wang et al. (1996), although they have comparable activation energies (Fig. 7). Further, the hydrogen

diffusion coefficients and activation energies in the Dora Maira pyrope reported by Blanchard and Ingrin (2004a) are very close to those reported by Kohlstedt and Mackwell (1998) for the diffusion of metal vacancies in olivine, and Blanchard and Ingrin (2004a) suggest it is very likely that the kinetics of dehydrogenation in pyrope are controlled by cation vacancies.

More recently, Kurka et al. (2005) reported the kinetics of hydrogen transport in grossular ($Gr_{83.2}$ $And_{14.3}$ $Py_{2.2}$) garnet. Their experiments were conducted at 800-1100 °C at 0.1 MPa in air and in gas mixtures of 90%Ar:10%$^2H_2$ and 90%Ar:10%:H_2. The diffusion rates were obtained from the sequential annealing experiments by monitoring with FTIR. The Arrhenius relation for deuterium diffusion yields the activation energy of 102±45 kJ/mol, and the Arrhenius relation for diffusion from hydrogen extraction in air yields the activation energy of 323±46 kJ/mol (Fig. 7). This activation energy compares well with the values reported by Blanchard and Ingrin (2004a) for the Dora Maira pyrope, but the diffusivity is slightly (less than an order of magnitude) slower for the grossular.

Zircons

Oxygen diffusion in natural, non-metamict zircon was determined under both dry and water-present conditions by Watson and Cherniak (1997). The dry experiments were run in air at 1100-1500 °C and 0.1 MPa with a fine powder of ^{18}O-enriched quartz as the tracer source. The wet experiments were conducted at 767-1160 °C and 7 to 1000 MPa confining pressure using ^{18}O-enriched quartz and water as the tracer source. The isotope concentration profiles for transport parallel and perpendicular to *c* were measured with nuclear reaction analysis (NRA), using the $^{18}O(p,\alpha)^{15}N$ reaction. There was no measurable anisotropy and for the dry experiments, the resulting oxygen diffusion coefficients define an Arrhenius relation with activation energy of 448.3 kJ/mol. Under wet conditions, there was little or no apparent dependence on pH_2O in the range 7-1000 MPa, and the diffusion coefficients obtained describe a single Arrhenius relation with activation energy of 210 kJ/mol (Fig. 8).

Titanite

Morishita et al. (1996) determined oxygen diffusion rates in natural titanite single crystals at 700-900 °C and 100 MPa under hydrothermal conditions. Transport parallel to the *a*, *b*, and *c*-axes were measured using SIMS. The oxygen diffusion parallel to the *c*-axis is described by an Arrhenius relation with activation energy of 254±28 kJ/mol (Fig. 8). The oxygen diffusion in titanite is isotropic within the reproducibility of the measurements.

Oxygen diffusion rates were determined by Zhang et al. (2006) in natural and synthetic single crystals of titanite under both dry and wet experimental conditions. The dry experiments were run at 700-1050 °C and 0.1 MPa using ^{18}O-enriched quartz powder and a fayalite-magnetite-quartz (FMQ) buffer assemblage. The hydrothermal experiments were run at 700-900 °C and 10-160 MPa confining pressure using ^{18}O-enriched water. The isotope exchange profiles were measured by NRA using the $^{18}O(p,\alpha)^{15}N$ reaction.

The isotope exchange profiles for natural crystals under both dry and wet experimental conditions showed two distinct regions, with a steep near-surface portion attributed to oxygen self-diffusion in the titanite lattice and a "tail" region attributed to diffusion along a fast path, such as pipe diffusion along static dislocations or some other planar defect (see Zhang et al. 2007 for details of the tail regions). Synthetic crystals that did not have euhedral morphologies showed similar behavior to the natural crystals, but the synthetic crystals with euhedral morphologies showed only lattice diffusion and no tailing.

Arrhenius relations obtained for the dry lattice diffusion yields an activation energy of 276±16 kJ/mol and for the wet (pH_2O = 100 MPa) lattice diffusion yields an activation energy of 180±39 kJ/mol, the lower activation energy for oxygen lattice diffusion in the wet experiments compared with the dry experiments, is similar to the behavior observed in many other silicate minerals (Fig. 8). In addition, the oxygen diffusion in titanite shows no apparent

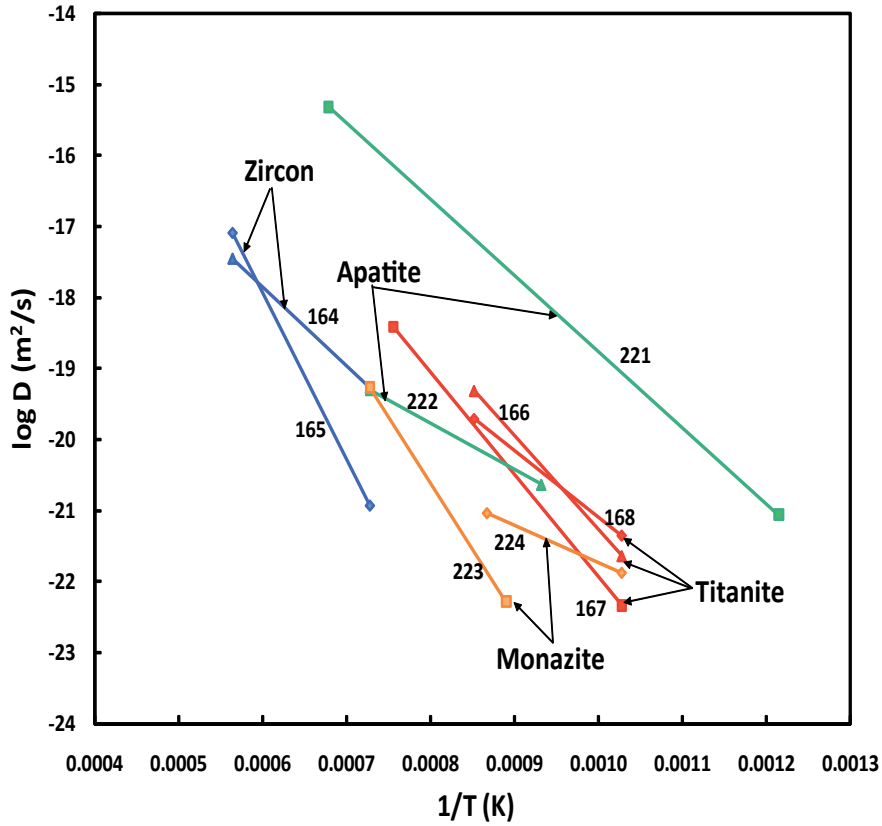

Figure 8. Arrhenius plot of select oxygen diffusion coefficients and Arrhenius relations reported for accessory minerals (zircon, titanite, apatite, monazite). The numbers next to the points and lines correspond to the data source as presented in the Appendix. Sources: 164 = Watson and Cherniak (1997); 165 = Watson and Cherniak (1997); 166 = Morishita et al. (1996); 167 = Zhang et al. (2006); 168 = Zhang et al. (2006); 221 = Farver and Giletti (1989); 222 = Farver and Giletti (1989); 223 = Cherniak et al. (2004)); and 224 = Cherniak et al. (2004).

dependence on water pressure in the range pH_2O = 10-160 MPa at 800 °C or pH_2O = 10-100 MPa at 880 °C. Also, as noted by Morishita et al. (1996), there is no evidence for anisotropy of oxygen diffusion in titanite. The absolute values of the oxygen diffusion coefficients obtained under wet conditions by Zhang et al. (2006) compare well with the values reported by Morishita et al. (1996) over the range of experimental conditions employed. However, Morishita et al. (1996) reported a significantly greater activation energy of ~254 kJ/mol for their wet diffusion experiments compared to ~180 kJ/mol reported by Zhang et al. (2006).

Melilite

Oxygen diffusion coefficients were measured in synthetic polycrystalline melilite by Hayashi and Muehlenbachs (1986) using a gas/solid bulk isotope exchange method. Two melilite compositions were investigated, $Ak_{50}Gh_{50}$ and $Ak_{75}Gh_{25}$, and the diffusion experiments were conducted at 700-1300 °C in flowing CO_2 gas. The oxygen diffusion coefficients and resulting Arrhenius relations fit to the data are similar for the two different melilite compositions, with Arrhenius parameters of D_0= 7.2×10^{-10} m^2/s and E_a = 164 kJ/mol for the $Ak_{75}Gh_{25}$ composition, and D_0 = 8.6×10^{-10} m^2/s and E_a = 140 kJ/mol for the $Ak_{50}Gh_{50}$ composition. Hayashi and Muehlenbachs (1986) noted that the measured oxygen diffusion rates in melilite are significantly greater than other minerals commonly found in Ca-Al rich inclusions of carbonaceous chondrite meteorites, and as such may provide a record of the isotopic composition of the last nebular gas to which they were exposed.

Diffusion of oxygen in synthetic single crystals of melilite endmembers gehlenite and akermanite were determined by Yurimoto et al. (1989). The samples were pre-annealed at 1200 °C in air for 10 hours, then annealed at 1000-1300 °C and 6.4 kPa in an ^{18}O-enriched CO_2 atmosphere. The lattice diffusion coefficients obtained along the different crystallographic axes in gehlenite and akermanite yielded Arrhenius relations with activation energies of 186±16 kJ/mol for transport parallel to the *c*-axis in gehlenite, 215±51 kJ/mol for transport parallel to the *c*-axis in akermanite, and 300±37 kJ/mol for transport parallel to the *a*-axis in akermanite. The oxygen lattice diffusion coefficients parallel to *c* are about one order of magnitude greater in akermanite than in gehlenite, and the lattice diffusion along the *a*-axis is about one order of magnitude greater than along the *c*-axis in akermanite over the temperature range of the experiments.

The oxygen diffusion rates in the endmember gehlenite and akermanite reported by Yurimoto et al. (1989) are three to four orders of magnitude less than the diffusion coefficients reported by Hayashi and Muehlenbachs (1986) for the intermediate composition melilites. Yurimoto et al. (1989) noted that Hayashi and Muehlenbachs (1986) used crushed melilite crystals, and crushed particles, in general, have irregular surfaces and a higher density layer of dislocations at the surface leading to an under estimation of surface area, and hence, an overestimation of the diffusion coefficient.

Ryerson and McKeegan (1994) determined oxygen diffusion rates in synthetic akermanite single crystals parallel to the *c*-axis in an ^{18}O-enriched CO-CO_2 gas composition that buffered the f_{O_2} at a value slightly above the Fe-FeO buffer. The experiments were conducted at 800-1300 °C and the oxygen diffusion coefficients obtained yield an Arrhenius law with the activation energy of 278±33 kJ/mol. The oxygen diffusion rates reported by Ryerson and McKeegan (1994) compare well with those reported by Yurimoto et al. (1989) even though their experiments were conducted at much higher f_{O_2}.

Tourmaline and beryl

Hydrogen/water. Hydrogen isotope exchange between natural schorlite-composition tourmaline and water was experimentally studied by Jibao and Yaqian (1997) at 450-800 °C and 15-25 MPa confining pressure. The experiments consisted of powdered tourmaline and ^{2}H-enriched water. The diffusion rates were calculated from the bulk isotope exchange with transport modeled using both a cylinder and plate geometry. The hydrogen diffusion coefficients obtained yield an Arrhenius relation with an activation energy of 128.0 kJ/mol for the cylinder model and 123.1 kJ/mol for the plate model, respectively. Jibao and Yaqian (1997) note that the similarity of the activation energies for both geometrical models suggests little or no anisotropy for hydrogen diffusion in tourmaline.

Hydrogen-deuterium exchange in elbaite-composition tourmaline natural single crystals has been studied by Desbois and Ingrin (2007) at 0.1 MPa and 700-800 °C. The isotope exchange was determined by micro-FTIR analysis. The stated purpose of their study was to investigate the anisotropy of hydrogen diffusion in tourmaline and the effect of composition. The results of Desbois and Ingrin (2007) indicate that hydrogen diffusion rates are two to three times faster along the *c*-direction than along directions parallel to the basal plane. The Arrhenius relation for transport along the *c*-direction has an activation energy of 106.3±36.8 kJ/mol, and along the *a* and [120] directions it has an activation energy of 66.8±19.6 kJ/mol. Diffusion within the basal plane is isotropic ($D_a = D_{[120]}$). In addition, Desbois and Ingrin (2007) found that the hydrogen diffusion rates in their elbaite-composition tourmaline are one order of magnitude greater than those reported for schorlite-composition tourmaline (Jibao and Yaqian 1997).

Diffusion rates for water molecules along channels in beryl single crystals have been reported by Fukuda et al. (2009). The experiments employed anhydrous synthetic beryl single crystals annealed under hydrothermal conditions at 500-700 °C and 50 to 150 MPa confining

pressure. The water transport profiles were determined by collecting polarized IR spectra parallel to the *c*-axis using a FTIR micro-spectrometer. For each sample, a series of spectra were collected from rim to core along the *c*-axis in 10 to 20 μm steps. The best fit of the water diffusion coefficients yields an Arrhenius relation with $D_0 = 2.5\times10^{-7}$ m^2/s and E_a = 133±12 kJ/mol. The diffusion coefficients for water transport through the beryl channels are about three orders of magnitude greater than those for ^{2}H-diffusion in tourmaline (Jibao and Yaqian 1997). Fukuda et al. (2009) state that the difference in the compactness of the crystal structure governs the diffusivity, and beryl channels are sufficiently large for H_2O diffusion. They note that the diffusivity of water molecules in beryl channels is similar to that along grain boundaries as determined in quartz aggregates (Farver and Yund 1991b).

Oxides

Rutile - oxygen. Oxygen diffusion rates in rutile were first reported by Haul and Dumbgen (1965) from bulk exchange experiments using synthetic TiO_2 powders annealed in O_2 gas. The experiments were run at 710-1300 °C and 0.1 MPa, and the diffusion coefficients yielded a single Arrhenius relation with activation energy of 251±6 kJ/mol. Haul and Dumbgen (1965) observed no dependence of oxygen diffusion on f_{O_2} over the range 10^{-1} to 1.3×10^{-7} MPa at 897 °C, and noted there was a slight anisotropy with diffusion perpendicular to the *c*-axis greater than parallel to the *c*-axis.

Oxygen diffusion in rutile has also been studied by Arita et al. (1979) who used SIMS depth profiling to determine oxygen tracer diffusion along the *c*-axis of single crystals of synthetic rutile at 877-1177 °C and 6 kPa in ^{18}O-enriched oxygen gas. Also, Derry et al. (1981) determined oxygen diffusion rates along the *c*-axis of single crystals of synthetic rutile annealed in a gas source at 900-1200 °C using the $^{18}O(p,\alpha)^{15}N$ nuclear reaction method.

The dry gaseous exchange experiments with synthetic near stoichiometric samples yield strikingly similar results for oxygen diffusion rates parallel to the *c*-axis in rutile (Fig. 9). This is noteworthy because the studies included bulk exchange and mass spectrometry (Haul and Dumbgen 1965), single crystals and depth profiling with SIMS (Arita et al. 1979) and single crystals analyzed using the $^{18}O(p,\alpha)^{15}N$ nuclear reaction method (Derry et al. 1981). These studies reported similar diffusion rates (within less than a factor of three) at common temperatures, and similar activation energies (251 to 282.6 kJ/mol).

Another noteworthy result of the oxygen diffusion studies in rutile is the effect of wet versus dry experimental conditions. Haul and Dumbgen (1965) reported diffusion rates for water-saturated experiments at 815 and 897 °C are slightly (less than a factor two) less than dry experiments. Oxygen diffusion coefficients were determined for synthetic and natural rutile single crystals under hydrothermal conditions with ^{18}O-enriched water at 100 MPa confining pressure and 600-1100 °C by Dennis and Freer (1993). The diffusion profiles for transport parallel to the *c*-axis were measured using SIMS. Their results indicate that between 700-1100 °C the natural and synthetic rutile samples define two linear Arrhenius relations with similar activation energies of 168.8 kJ/mol for the natural rutile and 172.5 kJ/mol for the synthetic rutile, but the pre-exponential factor for the synthetic rutile is about a factor of five less than for the natural sample.

A comparison of Dennis and Freer's (1993) results with the previous studies show a marked reduction in the oxygen diffusivity in rutile annealed wet at moderate pressure (100 MPa) at temperatures greater than 600 °C compared to the diffusivity under dry conditions at 0.1 MPa (Haul and Dumbgen 1965). This behavior is exactly opposite to what has been observed in most silicates and even other oxides (e.g., magnetite, Giletti and Hess 1988). However, the activation energy for the hydrothermal experiments is less than for the dry experiments and extrapolation to lower temperatures predicts the oxygen diffusion rate is greater for hydrothermal conditions at temperatures less than 600 °C. Dennis and Freer (1993)

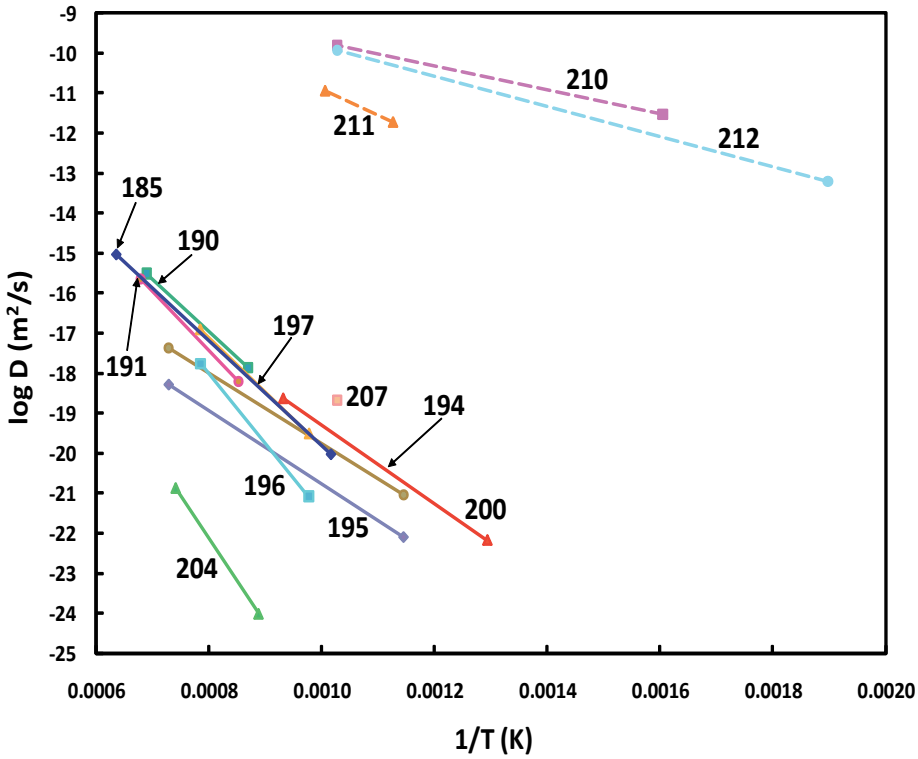

Figure 9. Arrhenius plot of select oxygen (solid) and hydrogen (dashed) diffusion coefficients and Arrhenius relations reported for oxides. The numbers next to the points and lines correspond to the data source as presented in the Appendix. Sources: 185 = Haul and Dumbgen (1965); 190 = Arita et al. (1979); 191 = Derry et al. (1981); 194 = Dennis and Freer (1993); 195 = Dennis and Freer (1993); 196 = Moore et al. (1998); 197 = Moore et al. (1998); 200 = Giletti and Hess (1988); 204 = Reddy and Cooper (1983); 207 = Sabioni et al. (1993); 210 = Johnson et al. (1975); 211 = Johnson et al. (1975); and 212 = Cathcart et al. (1979).

interpreted their results to indicate that oxygen transport in rutile under hydrous conditions occurs through a defect model in which substitutional hydroxyl ions on oxygen sites are the dominant positive defect.

An extensive study of oxygen diffusion in rutile was presented by Moore et al. (1998), who used synthetic and natural single crystals. Most of the experiments were run under hydrothermal conditions using ^{18}O-enriched water. In addition, two experiments were run dry at 780 °C and 807 °C and 0.1 MPa using ^{18}O-enriched Al_2O_3 powder. The hydrothermal experiments were run at 700-1000 °C and 33 to 1000 MPa confining pressure. The isotope concentration profiles for transport parallel and perpendicular to the *c*-axis were determined by NRA using the $^{18}O(p,\alpha)^{15}N$ reaction. In addition, for most of the experiments the samples were pre-annealed dry at 0.1 MPa, and then wet-reduced to Ni-NiO conditions during the beginning of the hydrothermal experiments.

The results of Moore et al. (1998) show that oxygen diffusion in rutile is faster parallel to the *c*-axis than perpendicular to *c*, by about a half an order of magnitude. There is no measurable effect of confining pressure between 0.1 to 100 MPa or from 600 to 1000 MPa, but between 100 to 600 MPa the D-values decrease by about one order of magnitude. Also, the oxygen fugacity does not in itself influence the oxygen diffusion rates in rutile.

The most striking result of the Moore et al. (1998) study was the effect of the presence of water during the reduction at the start of the experiments. The experiments using rutile that had been reduced in the presence of water yielded ^{18}O profiles with tails. The tails were attributed

to a second, rapid diffusion mechanism. Moore et al. (1998) were able to demonstrate that two D-values were extractable from the ^{18}O profiles, one from the near-surface region and one from the tail region. The diffusion coefficients from the near-surface region of the diffusion profiles corresponds to the slower diffusion mechanism and yields an Arrhenius relation with activation energy of 330±15 kJ/mol. This slower diffusion mechanism for the water-reduced rutile is dominantly controlled by migration of Ti^{3+} interstitials, with subordinate contribution from O vacancy migration. The diffusion coefficients determined from the tail regions of the composite profiles represent the faster diffusion mechanism, with the activation energy of 258±22 kJ/mol (Fig. 9). The faster diffusion for the non- and dry-reduced rutile corresponds to the migration of O vacancies.

A comparison of the oxygen diffusion rates reported by Haul and Dumbgen (1965) and Derry et al. (1981) for synthetic rutile under dry conditions with transport parallel to the *c*-axis to Moore et al.'s (1998) data show them to be essentially identical to the Arrhenius relation for the faster diffusion mechanism. In a practical sense, as noted by Moore et al. (1998), it is useful to note that because few geologic settings are truly dry, the slower oxygen diffusion law is the appropriate one to use for most geological applications.

Rutile - hydrogen. Diffusion of tritium in single crystals of synthetic rutile has been studied by Caskey (1974) at 155–300 °C in a tritium gas source. The diffusion coefficients were determined from microdensitometer traces of autoradiographs produced by the β-decay of the tritium. Caskey (1974) found that the tritium diffusion was anisotropic with *D* values along the *c*-axis about two orders of magnitude greater than along the *a*-axis. Linear fits to the diffusion coefficients yields the Arrhenius parameters $D_0 = 7.5\times10^{-10}$ m^2/s and $E_a = 38$ kJ/mol for transport along the *c*-axis, and $D_0 = 2.7\times10^{-10}$ m^2/s and $E_a = 55$ kJ/mol along the *a*-axis.

Hydrogen and deuterium diffusion rates in synthetic rutile single crystals have been reported by Johnson et al. (1975). Their experiments were conducted at 350-721 °C in H_2O or $^2H_2O/O_2$ gas, and the H and ^2H concentrations were measure using IR. They also noted a significant anisotropy, with rates parallel to the *c*-axis an order of magnitude or more greater than parallel to the *a*-axis over the temperature range of their experiments, and there is a factor of two lower activation energy (57 vs. 124 kJ/mol) parallel to the *c*-axis compared to parallel to the *a*-axis.

Cathcart et al. (1979) determined tritium diffusion rates in synthetic rutile crystals along the *a*- and *c*-directions. The samples were annealed in a tritium gas source at 254-700 °C (parallel to *c* experiments) and 500-910 °C (parallel to *a* experiments). The experiments were run at a total gas pressure of 400 Pa with various metal-metal oxide compounds that kept the samples at near equilibrium stoichiometric conditions. The tritium concentration profiles were measured by serial sectioning and liquid-scintillation counting of the tritium β-decay emissions (Gruzin method). Cathcart et al. (1979) reported two species, O^3H^- ions and $^3H_2$ molecules, are involved in tritium (hydrogen) migration in rutile, with $^3H^+$ ions associated with the O^3H^- ions diffusing four orders of magnitude faster than the $^3H_2$ molecules, along the *a*-axis.

The absolute values of hydrogen diffusion rates in rutile reported in the three studies noted above (Caskey 1974; Johnson et al. 1975; Cathcart et al. 1979) are in good agreement at temperatures where the measurements overlap, but the relatively large range in activation energies, 38-72 kJ/mol for transport along the *c*-direction and 55-124 kJ/mol for transport along the *a*-direction, yields large deviations in *D*-values when extrapolated to lower temperatures. In addition, all three show strong anisotropy for hydrogen diffusion in rutile.

The strong anisotropy, including the difference in activation energies for different transport directions for hydrogen diffusion in rutile, has been linked to the different migration paths as dictated by the crystal structure. Specifically, the diffusion path in the *c*-direction is a helix as protons migrate from one oxygen ion to another along the large open channels between

the TiO_6 octahedra. Whereas, along the *a*-direction proton migration requires a combination of rotations on hydroxyls with proton jumping from one channel to another (see Ingrin and Blanchard 2006).

Magnetite. Oxygen diffusion rates were determined in magnetite by bulk isotope exchange with ^{18}O-enriched water vapor by Castle and Surman (1969). The experiments were run at 300-500 °C and 0.1 MPa, and the ^{18}O exchange was monitored by continuously measuring the $\delta^{18}O$ of the water vapor by feeding it directly into a mass spectrometer. The data define an Arrhenius relation with relatively low activation energy of 71 kJ/mol. In addition, Castle and Surman (1969) reported a modest dependence of oxygen diffusion on oxygen fugacity in their experiments at 500 °C, expressed by the relation $D = 2.9\times10^{-22}$ m^2/s $(pH_2/pH_2O)^{0.27}$.

Oxygen diffusion rates were determined in magnetite single crystals by exchange with ^{18}O-enriched water by Giletti and Hess (1988). The experiments, run at 550-800 °C and 100 MPa water pressure, yield an Arrhenius relation with activation energy of 203±16 kJ/mol (Fig. 9). Experiments conducted at 800 °C and 10-200 MPa show no measurable dependence of oxygen diffusivity on water pressure in magnetite. In addition, experiments buffered at Ni-NiO and Fe_2O_3-Fe_3O_4 conditions showed no apparent dependence of oxygen diffusion rates on oxygen fugacity.

In comparison of their results to the data of Castle and Surman (1969), Giletti and Hess (1988) note that while the two data sets are not incompatible, one set would clearly not predict the other. The most prominent difference is the respective activation energies of ~203 kJ/mol for Giletti and Hess (1988) and 71 kJ/mol for Castle and Surman (1969). Giletti and Hess (1988) suggested that possibly two different mechanisms for oxygen diffusion were operative at the different experimental conditions of the two studies, with an intrinsic mechanism at temperatures above ~460 °C and an extrinsic mechanism at temperatures below ~460 °C, although 460 °C is a very low temperature for a transition between an extrinsic and a pure intrinsic mechanism.

Carbonates

Calcite and dolomite. Oxygen diffusion rates in carbonate minerals were first reported by Anderson (1969). Bulk isotope exchange experiments were conducted by annealing powdered natural calcite in ^{18}O-enriched CO_2 gas at 650-850 °C and <0.1 MPa. The progress of the diffusion exchange was monitored by the change in isotope composition of the gas. A least squares linear fit to the oxygen diffusion coefficients yielded the activation energy of ~422 kJ/mol. Anderson (1969) noted that preliminary CO_2-calcite exchange experiments at 750-850 °C and 50-80 MPa CO_2 pressure resulted in oxygen diffusion coefficients 10-30× greater than in the <0.1 MPa experiments. He also noted diffusion coefficients in pre-annealed material are systematically lower than in "as-is" material.

In a follow-up companion study, Anderson (1972) measured oxygen diffusion rates in natural powdered dolomite by isotope bulk exchange with CO_2 at 645-785 °C and 12-93.5 MPa. He found that the oxygen diffusion coefficients were about two orders of magnitude greater in dolomite than calcite under similar experimental conditions, and when plotted on an Arrhenius plot the oxygen diffusion rates in dolomite yield an activation energy of ~486 kJ/mol. In addition, several runs were made with calcite at elevated CO_2 pressures, and the oxygen diffusion coefficients obtained under high pressure (~100 MPa) were an order of magnitude greater than at low pressure (<0.1 MPa), confirming the preliminary results reported by Anderson (1969).

Oxygen diffusion rates were determined in two calcite single crystals with different Mn contents by Kronenberg et al. (1984). The experiments were run at 500-800 °C in a CO_2-H_2O atmosphere (pCO_2 = 0.1 to 0.5 MPa, pH_2O = 0.002 to 2.4 MPa) enriched in ^{18}O and ^{13}C. The isotope composition gradients were measured with SIMS for transport parallel and perpendicular to the *c*-axis. Kronenberg et al. (1984) reported that oxygen diffusion in calcite

is nearly isotropic, with oxygen diffusion slightly faster perpendicular to the *c*-axis. They also reported that oxygen diffusion is enhanced by the presence of H_2O with *D*-values obtained from their experiments at pH_2O = 0.1 MPa being one to two orders of magnitude greater than the *D*-values reported for experiments at dry conditions (Anderson 1969). Also, for their experiments conducted at H_2O pressures of 0.002 to 0.74 MPa at 700 °C, a nearly linear increase in diffusion coefficients was found.

Perhaps the most striking result of the Kronenberg et al. (1984) study was that carbon diffusion coefficients showed an excellent fit to the Arrhenius relation over the entire temperature range of their experiments, but the oxygen diffusion coefficients did not fit a single Arrhenius relation. At temperatures of 650-800 °C the oxygen diffusion data fit an Arrhenius relation only approximately, with activation energies of ~380±42 and ~343±38 kJ/mol for the Mn-poor (100 ppm Mn) and Mn-rich (1180 ppm Mn) calcite samples, respectively (Fig. 10). They also noted the apparent *D*-values at 600 °C for oxygen in the Mn-rich sample were 100× greater than the *D*-values measured at 650 °C. Also, samples that were first pre-annealed at 700 °C and then run at 600 °C yield *D*-values nearly two orders of magnitude less than the samples that were not pre-annealed. Kronenberg et al. (1984) interpreted this behavior to be due to a permanent reduction by defect annihilation between 600-650 °C of point defects initially present in the starting material.

In a follow-up study, Farver (1994) measured oxygen diffusion rates in the same starting materials as employed by Kronenberg et al. (1984), but over a much broader range in water fugacity and pre-annealing conditions for the Mn-rich sample. Farver (1994) ran experiments at 400-800 °C and 10-350 MPa confining pressure under hydrothermal conditions. The ^{18}O

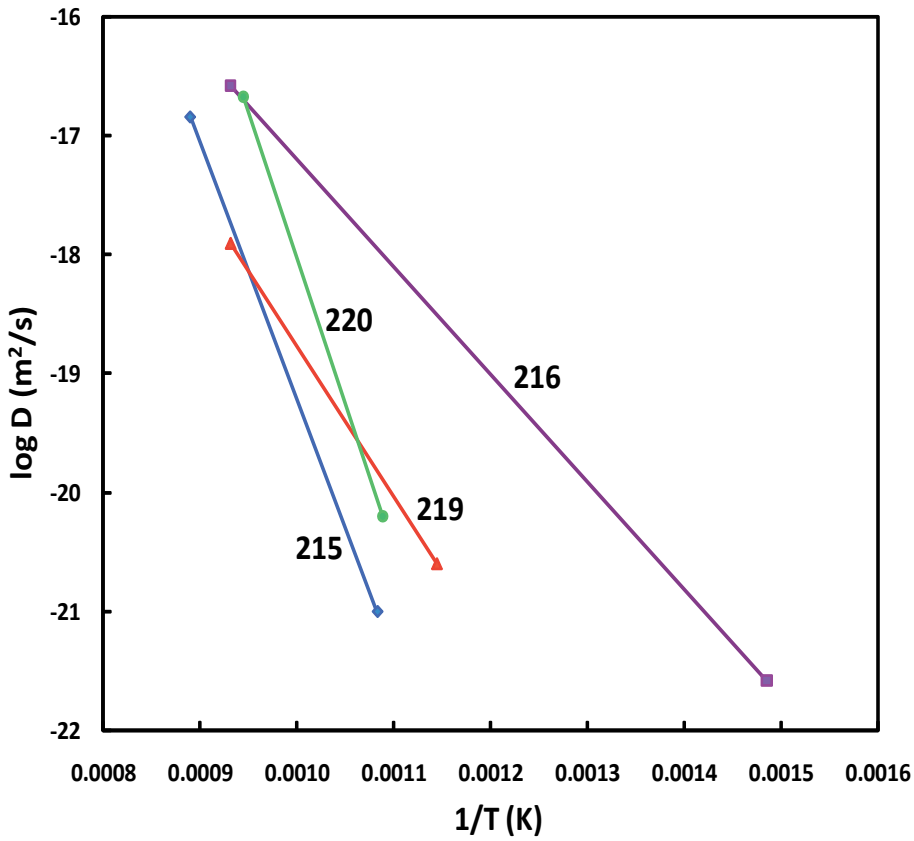

Figure 10. Arrhenius plot of select oxygen diffusion coefficients and Arrhenius relations reported for carbonates. Numbers next to the lines correspond to the data source as presented in the Appendix. Sources: 215 = Anderson (1969); 216 = Farver (1994); 219 = Labotka et al. (2000); and 220 = Anderson (1972).

diffusion profiles were measured using SIMS. At 100 MPa confining pressure, the Arrhenius relation obtained for oxygen diffusion in calcite has an activation energy of 173±6 kJ/mol, and no measurable anisotropy was observed. By using a combination of oxide buffers (e.g, Fe-FeO, Mn_2O_3-Mn_3O_4) and addition of CO_2 (as $Ag_2C_2O_4$) to "dilute" the water, experiments were run at a range of oxygen fugacities of 4 to 240 MPa at 700 °C. The oxygen diffusion coefficients increased linearly (slope = 0.9) with the increasing water fugacity of the experiments, consistent with the nearly linear dependence reported over the pH_2O range of 0.002 to 0.74 MPa by Kronenberg et al. (1984).

Finally, consistent with the results of Kronenberg et al. (1984), the Mn-rich and Mn-poor calcite samples yielded essentially the same oxygen diffusion coefficients at 600-800 °C but at 550 °C, the Mn-rich sample showed a dramatic increase in its apparent *D*-value compared to the Mn-poor sample. Farver (1994) showed that the apparent *D*-value obtained at 550 °C for the Mn-rich sample was time dependent (decreasing with longer diffusion anneal times), and following Kronenberg et al.'s (1984) observation, Farver (1994) observed that pre-annealing the Mn-rich sample caused a significant decrease in the apparent *D*-value to within a factor of four of the value obtained for the Mn-poor sample. In combination with Kronenberg et al.'s (1984) results, Farver (1994) proposed that pre-annealing of the Mn-rich sample caused a permanent reduction in some defect important for oxygen transport in calcite but not related to an equilibrium defect.

The diffusivity of oxygen in calcite in a pure CO_2 atmosphere at 100 MPa was determined by Labotka et al. (2000). Their experiments were done at 600-800 °C using calcite single crystals that were pre-annealed to reduce the effects of any nonequilibrium defects on the diffusion rates. The oxygen diffusion coefficients fit an Arrhenius relation with activation energy of 242±39 kJ/mol (Fig. 10). This is significantly less than the activation energy reported by Anderson (1969) for the dry CO_2-calcite bulk isotope exchange experiments at <0.1 MPa. Labotka et al. (2000) suggested that the difference may be due to the higher pCO_2 of their experiments.

As noted by Farver (1994) and Labotka et al. (2000), one of the most interesting outcomes of the diffusion studies of calcite is when the oxygen and carbon diffusion kinetics are combined. The results of the carbon and oxygen diffusion studies indicate that fluid composition could have a dramatic effect on the relative rates of carbon and oxygen diffusion in calcite. For CO_2-rich fluids, the oxygen and carbon diffusion rates are similar, but with increasing water content in the fluid, the oxygen diffusion rates become orders of magnitude greater than the carbon. This change in relative diffusion rates of oxygen and carbon as a function of fluid composition could have profound effects on the oxygen and carbon isotope systematics of calcite. As shown by Farver (1994), at 500 °C over geologically reasonable time scales, the amount of diffusional exchange for a 1 mm grain of calcite can be below detection limits for carbon and oxygen under "dry" conditions, but under "wet" conditions, while the carbon diffusional exchange remains below detection limits, the oxygen isotopes could be completely equilibrated with the fluid.

Phosphates

Experimental studies of oxygen diffusion in phosphates are limited to apatite (Farver and Giletti 1989) and monazite (Cherniak et al. 2004). Farver and Giletti (1989) determined oxygen diffusion in single crystals of Durango apatite at 550-1200 °C under hydrothermal conditions at 100 MPa. They observed a large anisotropy, with the diffusion coefficient for transport parallel to *c* about three orders of magnitude greater than that perpendicular to *c* at 800 °C and 100 MPa. A straight line fit to the diffusion coefficients for transport parallel to *c* yielded the activation energy of 205±12 kJ/mol (Fig. 8). They also reported a modest increase of a factor of three in the *D* values for transport parallel to *c* at 800 °C going from 20 to 200 MPa water pressure. In some of their experiments they simultaneously determined

the strontium diffusion rates, and cite the difference in diffusion profile lengths for the two different isotope tracers, ^{18}O and ^{86}Sr, as strong evidence of a diffusion mechanism and not a dissolution-reprecipitation process.

The Cherniak et al. (2004) study employed natural single crystals of monazite from Hiddenite, NC (the so-called "eBay monazite") that were pre-annealed under buffered conditions to equilibrate point defects at conditions of the subsequent diffusion experiments. They determined the oxygen diffusion rates under both dry and wet conditions. The dry experiments were conducted at 850-1100 °C and 0.1 MPa using an ^{18}O-enriched $CePO_4$ powder, with oxygen fugacity buffered at Ni-NiO. The wet experiments were run at 700-880 °C and 100 MPa using ^{18}O-enriched water. The oxygen isotope concentration profiles were measured using NRA and the reaction $^{18}O(p,\alpha)^{15}N$. Most of the experiments measured diffusion normal to the (100) growth face, but experiments were also run to measure diffusion normal to the (111), (101), and (110) faces, and they observed no apparent anisotropy. Hydrothermal experiments at 800 °C run at water pressures of 10 to 160 MPa showed a weak (< factor of 2) dependence of diffusivity on water pressure. Cherniak et al. (2004) found that the oxygen diffusion under wet conditions has a significantly lower activation energy (100±20 kJ/mol) than under dry conditions (356±26 kJ/mol), as has been reported in many other minerals (Fig. 8). The difference in activation energies leads to a large difference in diffusion coefficients at lower temperatures, hence large differences in predicted oxygen closure temperatures depending upon whether an aqueous fluid is present.

DISCUSSION

In this section a brief overview of the influence of various parameters on the kinetics of oxygen and hydrogen diffusion in minerals will be presented. The general trends observed for the different minerals are highlighted and specific deviations from the trends noted.

Effect of temperature

Provided the diffusion mechanism does not change with temperature (e.g., extrinsic to intrinsic mechanism), the temperature dependence of the diffusion coefficient, D, can be described by the Arrhenius relationship:

$$D = D_0 \exp\left[\frac{-E_a}{RT}\right]$$

where D_0 is the pre-exponential factor (m^2/s), E_a is the activation energy (kJ/mol), R is the gas constant, and T is the absolute temperature (K). All of the diffusion data presented in the Appendix appear to exhibit Arrhenian temperature dependence where a plot of log D against $1/T$ yields a straight line over the temperature range of the experiments. The activation energy and pre-exponential factor are both independent of temperature but are strongly dependent on the identity and form of the diffusing species, and the structure and composition of the mineral. To a first order, D_0 is dependent on the jump distance and frequency, defect structure, and geometry of the crystal (see Manning 1968). The activation energy is dependent on the energy required to form defects and to cause the atoms to jump from different lattice sites. Examples of the temperature dependence of oxygen and hydrogen diffusion in an assortment of minerals are shown in Figures 11a and 11b.

There are several general observations that can be made with regard to the temperature dependence of diffusion in different minerals, for different species, and under different experimental conditions. First, oxygen and hydrogen diffusivities vary greatly for different minerals, presumably due to differences in mineral structures and nature of the various defects. For example, at 800 °C and 100 MPa confining pressure oxygen diffusion coefficients from

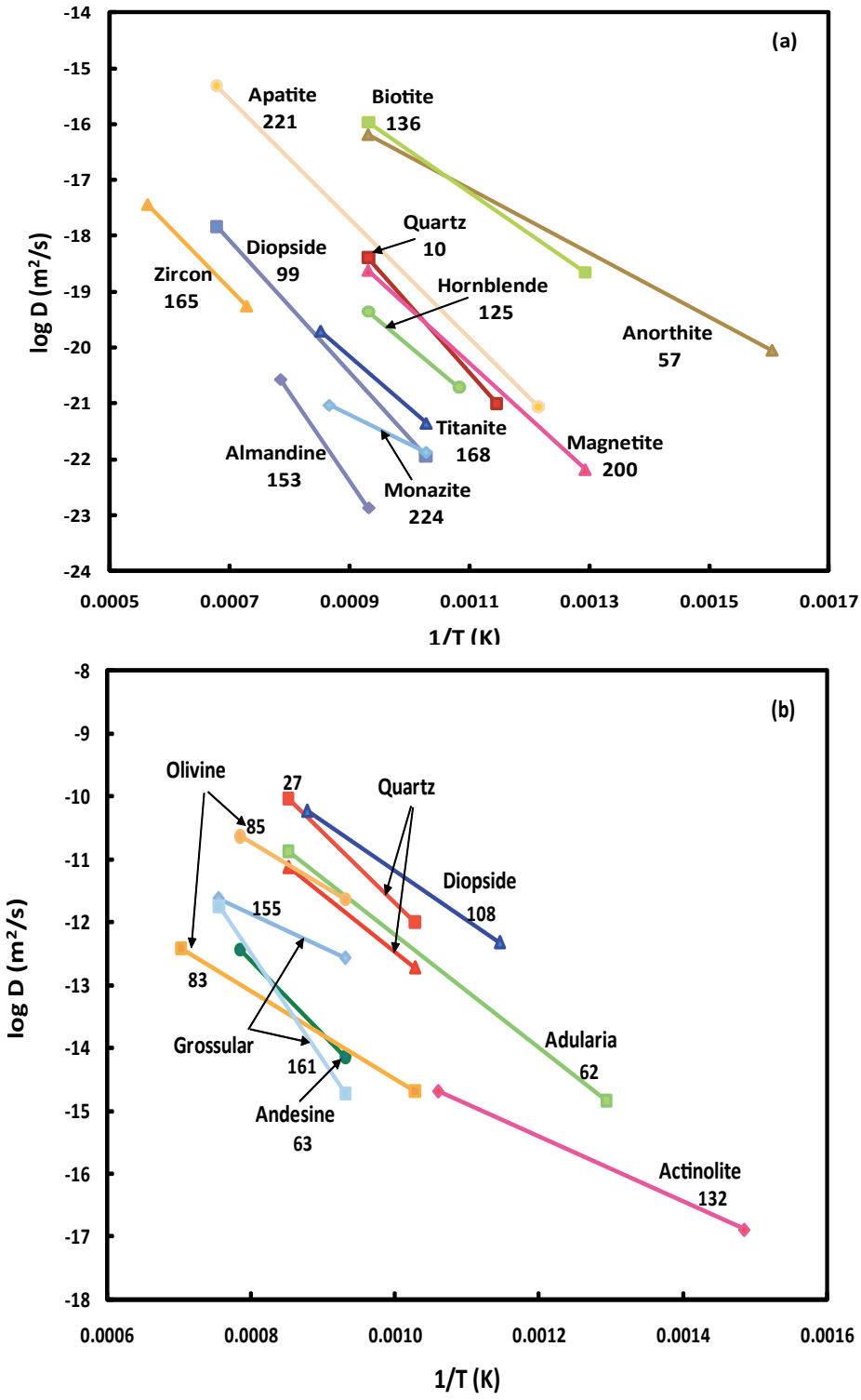

Figure 11. Arrhenius plots of select oxygen diffusion (a) and hydrogen diffusion (b) Arrhenius relations reported for different minerals showing the strong influence of mineral structure on diffusion. The numbers next to the lines correspond to the data source as presented in the Appendix. Sources: (a) 10 = Giletti and Yund (1984); 57 = Giletti et al. (1978); 99 = Farver (1989); 125 = Farver and Giletti (1985); 136 = Fortier and Giletti (1991); 153 = Couglan (1990); 165 = Watson and Cherniak (1997); 168 = Zhang et al. (2006); 200 = Giletti and Hess (1988); 223 = Cherniak et al. (2004); 221 = Farver and Giletti (1989); and 224 = Cherniak et al. (2004) (b) 26 = Kats et al. (1962); 27 = Kronenberg et al. (1986); 62 = Kronenberg et al. (1996); 63 = Johnson (2003); 83 = Ingrin and Blanchard (2006); 85 = Mackwell and Kohlstedt (1990); 108 = Hercule and Ingrin (1999); 132 = Graham et al. (1984); 155 = Kurka et al. (2005); and 161 = Kurka et al. (2005).

hydrothermal experiments show a range of 6 orders of magnitude for different silicate minerals, and the range is even greater when extrapolated to lower temperatures due to the differences in activation energies (Fig. 11a). Second, a comparison between the different diffusing species in hydrous minerals show that hydrogen diffusion rates are faster than oxygen (Fig. 11b), and the diffusion rates measured using single crystals are often much slower than those measured using bulk experiments with powdered samples. Third, for oxygen diffusion, anhydrous ('dry') systems generally yield higher activation energies and slower diffusivities than hydrothermal ('wet') systems at the same temperature (Fig. 12). Some of these general observations are explored further below.

Effect of mineral structure

In silicates, at least, there is a very strong first-order control of oxygen diffusivity exerted by the mineral structure. The structural control is much greater than any compositional influence, as witnessed by the narrow range in oxygen diffusion coefficients reported for different feldspars (e.g., Giletti et al. 1978, Fig. 3), different amphiboles (e.g., Farver and Giletti 1985, Fig. 6), or different micas (e.g., Fortier and Giletti 1991, Fig. 6) compared to the drastic difference in the oxygen diffusion rates for feldspars compared to amphiboles compared to micas (Fig. 11a).

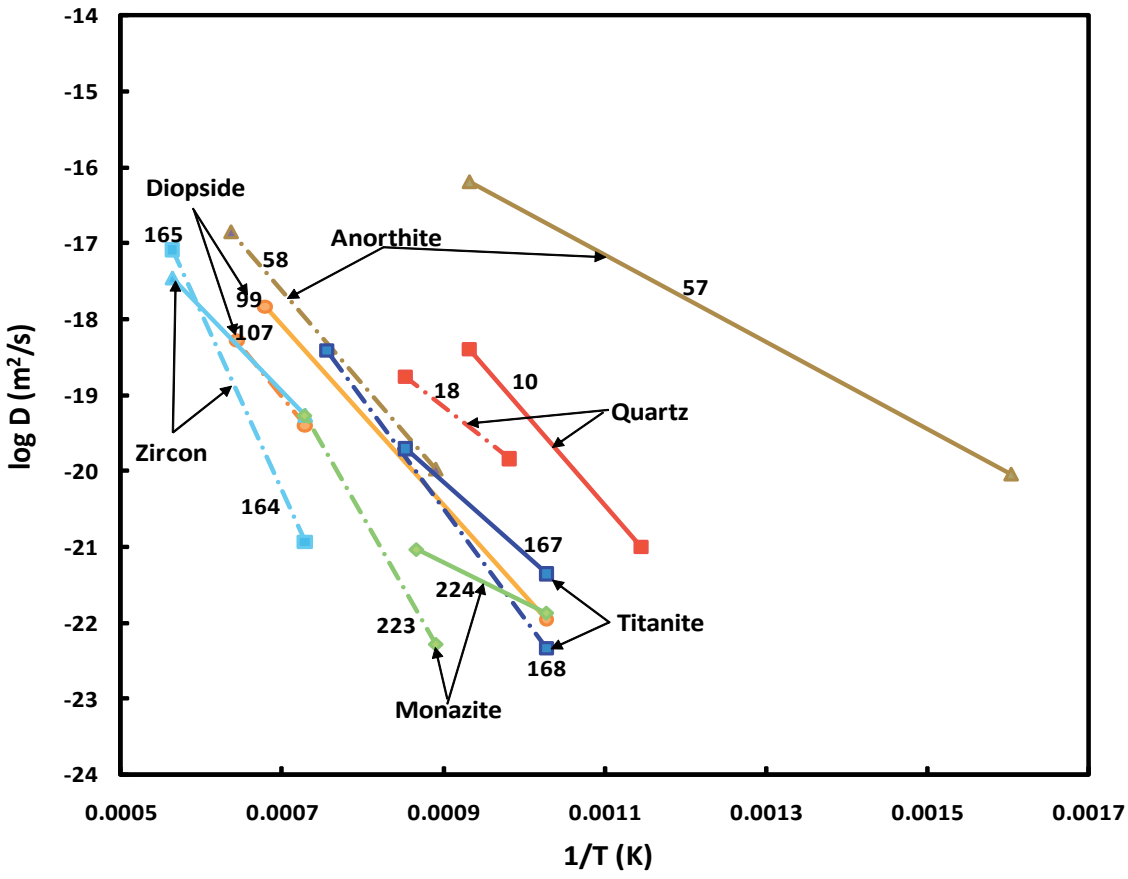

Figure 12. Arrhenius plot of select oxygen diffusion Arrhenius relations reported for different minerals under "wet" (solid lines) and "dry" (dashed lines) experimental conditions. The numbers next to the lines correspond to the data source as presented in the Appendix. Sources: 10 = Giletti and Yund (1984); 18 = Sharp et al. (1991); 57 = Giletti et al. (1978); 58 = Elphick et al. (1988); 107 = Ingrin et al. (2001); 99 = Farver (1989); 164 = Watson and Cherniak (1997); 165 = Watson and Cherniak (1997); 167 = Zhang et al. (2006); 168 = Zhang et al. (2006); 223 = Cherniak et al. (2004); and 224 = Cherniak et al. (2004).

Empirical methods

The apparent first order dependence of oxygen volume diffusion on mineral structure has led several workers to propose empirical models to predict oxygen diffusion kinetics in minerals. Dowty (1980) proposed that the amount of open space in a mineral should play an important role in diffusion rates through the structure, and Connolly and Muehlenbachs (1988) noted that the relatively high activation energy for oxygen diffusion in diopside was consistent with its high packing density. More recently, Fortier and Giletti (1989), Muehlenbachs and Connolly (1991), and Zheng and Fu (1998) have built upon Dowty's idea by developing empirical models relating the total ionic or anionic porosity with diffusivity, or with the Arrhenius parameters E_a and D_0. The total ionic porosity as defined by Fortier and Giletti (1989) is simply the total volume of the unit cell minus the volume of the anions and cations within the unit cell. Muehlenbachs and Connolly (1991) and Zheng and Fu (1998) choose to ignore the contribution of the cations and used the anionic porosity rather than total ionic porosity. Fortier and Giletti (1989) plotted hydrothermal oxygen diffusivities in silicates at a given temperature and pressure as a function of the total ionic porosity and found good correlations for all minerals plotted except the micas. In similar fashion, Muehlenbachs and Connolly (1991) found reasonably good correlations between anionic porosity and E_a and log D_0 for oxygen diffusivities in dry systems.

While these ionic porosity–diffusivity relations may provide a useful first-order prediction of oxygen diffusion in other minerals, they are strictly empirical and do not account for the complexity of oxygen diffusion, especially with regard to hydrothermal diffusion and the potential role of different oxygen-bearing transport species as outlined above. An important consideration in applications of these empirical models is the inherent assumption that the same transport mechanism and species are dominant in the different minerals at the experimental/geological conditions at which the diffusion rates are to be predicted. Indeed, oxygen diffusion rates for nonsilicates including magnetite, apatite, and calcite deviate greatly from the values predicted using their ionic porosities (Fig. 13) and recent results of oxygen diffusion measurements in monazite (Cherniak et al. 2004) and titanite (Zhang et al. 2006) under both dry and hydrothermal conditions also show significant deviations from the values predicted from the empirical ionic porosity models.

Anisotropy

The use of crystallographically oriented single crystals has allowed an analysis of diffusion rates along different crystallographic directions for various diffusing species in minerals of widely different crystal structures. Significant anisotropies have been observed for both oxygen and hydrogen diffusion in several silicate and nonsilicate minerals. One of the earliest reported cases of anisotropic oxygen diffusion was in quartz (Giletti and Yund 1984) who reported nearly a factor of 100 greater D-values for diffusion parallel to the c-axis compared to perpendicular to the c-axis (Fig. 1). The most pronounced anisotropies for oxygen diffusion have been reported for sheet silicate micas (Fig. 6) with D-values parallel to the layers about 1000× greater than perpendicular to the layers (Fortier and Giletti 1989). The chain silicates diopside and hornblende also show significant anisotropies with D-values 100× and 10× greater along the c-axis, respectively (Farver 1989; Farver and Giletti 1985). Recently, Ingrin et al. (2001) reported that the oxygen diffusion rate in a synthetic diopside along the c- and a-directions is one order of magnitude greater than along the b-direction, and questioned whether the 100× greater value reported by Farver (1989) in the natural diopside was enhanced by the presence of amphibole lamellae. In either case, oxygen diffusion in diopside is anisotropic, and Ingrin et al. (2001) suggested it is due to oxygen diffusion paths within the crystallographic structure that prefer the under-bonded O2 oxygen site. In nonsilicates, fluorapatite shows the greatest anisotropy, with oxygen diffusion rates 1000× faster along the c-axis (Farver and Giletti 1989).

For hydrogen diffusion, the first reported anisotropy was in rutile (Johnson et al. 1975) where the D-value parallel to the c-axis is a factor of ~20× greater than parallel to the a-axis

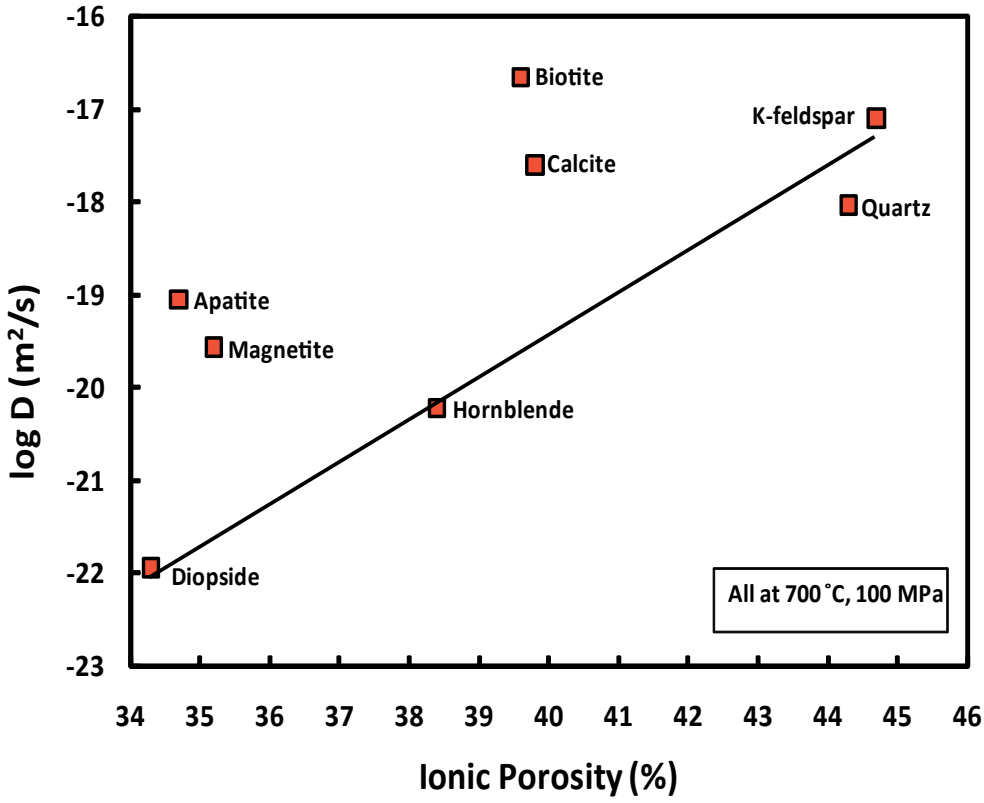

Figure 13. Select published oxygen diffusion coefficients as a function of total ionic porosity. Data are from hydrothermal experiments at 700 °C and 100 MPa confining pressure (after Farver 1994). The straight line is the relationship calculated for silicates (except mica) from Fortier and Giletti (1989). Sources: K-feldspar = Giletti et al. (1978); Quartz = Giletti and Yund (1984); Hornblende = Farver and Giletti (1985); Magnetite = Giletti and Hess (1988); Diopside = Farver (1989); Apatite = Farver and Giletti (1989); Biotite = Fortier and Giletti (1991); and Calcite = Farver (1994).

at 700 °C, and a factor of ~100× greater at 500 °C. Although a strong anisotropy has been reported for oxygen diffusion in quartz (Giletti and Yund 1984), no resolvable anisotropy has been observed for hydrogen (Kats et al. 1962; Kronenberg et al. 1986). However, the number of data points is very limited and the uncertainties are relatively large making it difficult to discern if some degree of anisotropy may be present for H diffusion in quartz.

The most detailed hydrogen diffusion studies have been for diopside, and Hercule and Ingrin (1999) reported *D*-values along the *c*-axis are about a factor of 30× greater than along the *b*-axis, but with similar activation energies. For hydrous minerals, Ingrin and Blanchard (2000) observed hydrogen diffusion parallel to the *c*-axis in the amphibole kaersutite was a factor 5× greater than parallel to the *b*-axis. Hence, in these chain silicates, strong anisotropies for both oxygen and hydrogen have been determined, with the fastest diffusion along the *c*-axis, which corresponds to the long axis of the silicate chain.

Diffusional anisotropy is a function of both the mineral structures and of the diffusion mechanism. This is illustrated well by hydrogen diffusion in Fe-free and Fe-bearing diopsides (Ingrin et al. 1995; Hercule and Ingrin 1999; Carpenter-Woods et al. 2000). These workers have shown that in diopside the hydrogen self-diffusion (H-^{2}H exchange) which is governed by transport of protons, is anisotropic and transport parallel to the [001] and [100]* directions are one order of magnitude faster than parallel to the [010] direction. However, hydrogen chemical diffusion (H uptake/extraction) rates, which are governed by electron hole defects associated with iron oxidation/reduction, are isotropic.

Pressure dependence

The pressure dependence of volume diffusion is typically described by the Arrhenius relation:

$$D_{(P,T)} = D_{(0.1\,\mathrm{MPa},T)} \exp\left[\frac{-PV^*}{RT}\right]$$

where V^* is the activation volume (cm^3/mol) that represents the pressure dependence of the diffusion coefficient. The slope of a plot of D against P provides the magnitude and sign of V^* for a specific species in a specific mineral. In general, it is expected that the diffusion rate will decrease with increasing confining pressure. This has been observed for cations in garnet and olivine (e.g., Freer 1993; Chakraborty et al. 1994). However, the magnitude of V^* appears to be small (1-3 cm^3/mol) and the change in D values over the pressure range of most of the H and O diffusion experiments reported is often within the estimated uncertainties of the data, and as such, it is typically impossible to determine a meaningful value for V^*. The exceptions include the anhydrous calcite-CO_2 experiments of Labotka et al. (2000) that were run at 800 °C and 0.1 to 200 MPa confining pressures, and the quartz-CO_2 experiments of Sharp et al. (1991) run at 900 °C and 10 to 720 MPa confining pressures. Labotka et al. (2000) found nearly constant D-values for oxygen, although there was nearly a 2.5 orders of magnitude decrease in D-values for carbon going from 0.1 to 200 MPa pressure. Similarly, Sharp et al. (1991) reported nearly constant D-values for oxygen from 10 to 345 MPa pressure, and a slight increase at 720 MPa that was interpreted to be most likely due to a small amount of water present in the sample assemblage of that experiment. In the case of hydrogen there have been no systematic experimental studies to address the effect of confining pressure on volume diffusion.

Effect of water

The most controversial consideration of oxygen diffusion rates centers around the effect of water. The intent of this section is not to resolve this issue but to report the various observations and proposed interpretations.

Presence of water. It has been noted for some time that the presence of water can dramatically affect oxygen volume diffusion kinetics in minerals. Several minerals, including the silicates quartz (Giletti and Yund 1984; Sharp et al. 1991), feldspars (Giletti et al. 1978; Ryerson et al. 1989; Derdau et al. 1998), diopside (Farver 1989; Elphick and Graham 1990; Ryerson and McKeegan 1994), olivine (Chakraborty and Costa 2004), zircon (Watson and Cherniak 1997), titanite (Zhang et al. 2006) and the nonsilicates calcite (Farver 1994; Labotka et al. 2000) and monazite (Cherniak et al. 2004) exhibit a pronounced difference in oxygen diffusion under dry versus wet conditions. The effect is almost always that there are significantly greater oxygen diffusion rates and lower activation energies under wet versus dry conditions. The one exception of note is rutile, where it appears that dry diffusion rates are faster than wet, due to rutile's complicated defect structure (see Moore et al. 1998). However, the activation energy for the wet rutile experiments is less than for the dry, and extrapolation to lower temperatures predicts the oxygen diffusion rate is greater for wet conditions at temperatures less than 600 °C. The "wet versus dry" effect appears to be limited to oxygen, and volume diffusion of cations appears to be largely insensitive to the presence or absence of water, as well as the amount (f_{H_2O}) of water (see Cherniak and Watson 2001; Cherniak and Watson 2007; Cherniak 2010).

There is general agreement that wet oxygen diffusion is atomistically more complex than dry oxygen diffusion. Under water-absent conditions, oxygen atoms would diffuse as lattice oxygen, most likely via a vacancy mechanism. It has been suggested that speciation plays a significant role in the elevated oxygen diffusion rates observed under hydrothermal conditions. Specifically, it has been suggested that under hydrothermal conditions, oxygen can diffuse as a neutral water molecule that is similar in size to an O^{-2} ion, and hence may migrate more easily

through the ionic structure of minerals. Zhang et al. (1991) developed the theoretical basis for this argument and also for further testing this hypothesis. Supporting arguments put forth by both McConnell (1995) and Doremus (1998b) also indicate that molecular water plays a major role in oxygen diffusion in quartz. In addition, the presence of water-related species such as OH^- or H^+ (H_3O^+) in the lattice under hydrothermal conditions can affect structural bonds, possibly resulting in a decrease in the activation energy relative to dry conditions.

Amount (fugacity) of water. While the presence or absence of water clearly plays an important role in oxygen and hydrogen diffusion in many minerals, there are seemingly contradictory observations as to the exact nature of that role. For example, the early studies of oxygen diffusion in quartz by Giletti and Yund (1984) indicated an increased diffusion rate with increased pH_2O, while a similar study published in the same volume of JGR by Dennis (1984), reported no apparent correlation between the oxygen diffusion rate and pH_2O of the experiment. Likewise, Yund and Anderson (1978) reported a strong positive dependence of oxygen diffusion in adularia on water pressure (f_{H_2O}) while Freer and Dennis (1982) reported no dependence of oxygen diffusion in albite on water pressure. Studies of oxygen diffusion in amphiboles (Farver and Giletti 1985), micas (Fortier and Giletti 1991), and calcite (Farver 1994) under hydrothermal conditions show an apparent positive correlation between D_{Ox} and pH_2O (or f_{H_2O}). Rigorously buffered experiments on quartz (Farver and Yund 1991a) and adularia (Farver and Yund 1990) show that oxygen diffusion rates are strongly correlated with f_{H_2O} and not with a_{H+}, f_{O_2}, or f_{H_2} (Fig. 5). However, the studies of Elphick and Graham (1988) and Graham and Elphick (1991) indicated that oxygen diffusion in feldspars was enhanced by high a_{H+} (the so-called fast proton transients) due to their ability to move rapidly through the structure.

Zhang et al. (1991) derived an expression for the "apparent" diffusivity of total oxygen, $D^*_{\Sigma O}$, in a crystal as a function of water species of the form:

$$D^*_{\Sigma O} \approx D_{O,\,dry} + D_{H_2O}[H_2O] + D_{OH}[OH]$$

where $[H_2O]$ and $[OH]$ are the respective mole fractions of these species on a single oxygen basis. The value of $D^*_{\Sigma O}$ is directly dependent on which species is most dominant. The Zhang et al. (1991) model provides a strong theoretical reason for why ^{18}O transport in crystals is dominated by diffusion of water molecules even at low (ppm) water contents. In their model, when H_2O is the dominant oxygen-bearing transport species, $D^*_{\Sigma O}$ will be linearly proportional to f_{H_2O} at low water content. This is consistent with the nearly linear dependence of D on log f_{H_2O} reported for quartz [$D_{ox} \propto (f_{H_2O})^{0.78}$] and adularia feldspar [$D_{ox} \propto (f_{H_2O})^{1.18}$] (Farver and Yund 1990, 1991a). Also, when OH is the dominant oxygen-bearing transport species, $D^*_{\Sigma O}$ is linearly related to $(f_{H_2O})^{1/2}$. The hydrothermal oxygen diffusion data as a function of f_{H_2O} for OH-bearing amphiboles [$D_{ox} \propto (f_{H_2O})^{0.43}$] (Farver and Giletti 1985) and apatite (Farver and Giletti 1989) are consistent with OH being the dominant diffusing species.

Hydrogen chemical diffusion and the role of defects

The hydrogen uptake and extraction experiments yield chemical interdiffusion coefficients, and as such the nature of the reaction can greatly influence the apparent or effective diffusion rates. The hydrogen uptake experiments in olivine reported by Mackwell and Kohlstedt (1990), and their follow-up studies in olivine and synthetic forsterite (Kohlstedt and Mackwell 1998; Demouchy and Mackwell 2003) provide an excellent example of the influence of a specific reaction of the hydrogen D-values. Based on their experimental results, these authors proposed two different mechanisms for hydrogen chemical diffusion in their samples. The first involves a relatively rapid redox exchange reaction with polarons localized on iron atoms. In this case, the flux of protons is charge compensated by a counter-flux of polarons, and the measured rapid hydrogen uptake is related to the diffusivity of the polarons. The second mechanism involves a much slower exchange reaction that is rate limited by the mobility of metal vacancy point defects.

Hydrogen uptake/extraction and exchange experiments on natural diopside crystals with different iron contents (Ingrin et al. 1995; Hercule 1996; Hercule and Ingrin 1999) show the effective diffusivity of hydrogen in a low Fe content sample (X_{Fe} = 0.036) is isotropic and is much smaller than the hydrogen diffusivities. However, the effective diffusivity of hydrogen extraction increases with increasing Fe content and at X_{Fe} = 0.07 and 0.126, the extraction diffusivities approach the hydrogen diffusivities (see Hercule and Ingrin 1999 for details). These studies demonstrate the important role of point defects, especially those related to iron, in natural samples compared to synthetic materials.

ACKNOWLEGMENTS

The author wishes to thank the co-editors, Youxue Zhang and Daniele Cherniak, for the invitation to participate in this short course volume, and especially for their patience and encouragement. Jannick Ingrin and the co-editors are thanked for their thorough reviews. Finally, I would like to thank Bruno Giletti and Dick Yund, two true pioneers of the study of diffusion in minerals, who have been exceptional mentors, colleagues, and friends.

REFERENCES

Amami B, Addou M, Millot F, Sabioni A, Monty C (1999) Self-diffusion in α-Fe_2O_3 natural single crystals. Ionics 5:358-370

Anderson TF (1969) Self-diffusion of carbon and oxygen in calcite by isotope exchange with carbon dioxide. J Geophys Res 74:3918-3932

Anderson TF (1972) Self-diffusion of carbon and oxygen in dolomite. J Geophys Res 77:857-861

Anderson TF, Kasper RB (1975) Oxygen diffusion in albite under hydrothermal conditions. EOS Trans Am Geophys Union 56:459

Ando K, Oishi Y (1983) Effect of ratio of surface area to volume on oxygen self-diffusion coefficients determined for crushed MgO-Al_2O_3 spinels. J Am Ceram Soc 66:C131-C132

Ando K, Kurokawa H, Oishi Y, Takei H (1981) Self-diffusion coefficient of oxygen in single-crystal forsterite. J Am Ceram Soc 64:C-30

Arita M, Hosoya M, Kobayashi M, Someno M (1979) Depth profile measurement by secondary ion mass spectrometry for determining the tracer diffusivity of oxygen in rutile. J Am Ceram Soc 62:443-446

Bagshaw AN, Hyde BG (1976) Oxygen tracer diffusion in the magneli phases Ti_nO_{2n-1}. J Phys Chem Solids 37:835-838

Beran A (1986) A model of water allocation in alkali feldspar, derived from infrared-spectroscopy investigations. Phys Chem Miner 13:306-310

Blanchard M, Ingrin J (2004a) Hydrogen diffusion in Dora Maira pyrope. Phys Chem Miner 31:593-605

Blanchard M, Ingrin J (2004b) Kinetics of deuteration in pyrope. Eur J Mineral 16:567-576

Brady JB (1995) Diffusion data for silicate minerals, glasses, and liquids. *In*: Handbook of Physical Constants. Vol 2. Arhens TH (ed) Am Geophysical Union, p 269-290

Brady JB, Cherniak DJ (2010) Diffusion in minerals: an overview of published experimental diffusion data. Rev Mineral Geochem 72:899-920

Carpenter-Woods S, Mackwell SJ, Dyar D (2000) Hydrogen in diopside: Diffusion profiles. Am Mineral 85:480-487

Caskey GR Jr (1974) Diffusion of tritium in rutile (TiO_2). Mater Sci Eng 14:109-114

Castle JE, Surman PL (1967) The self-diffusion of oxygen in magnetite. Techniques for sampling and isotopic analysis of micro-quantities of water. J Phys Chem 71:4255-4259

Castle JE, Surman PL (1969) The self-diffusion of oxygen in magnetite. The effect of anion vacancy concentration and cation distribution. J Phys Chem 73:632-634

Cathcart JV, Perkins RA, Bates JB, Manley LC (1979) Tritium diffusion in rutile (TiO_2). J Appl Phys 50:4110-4119

Chacko T, Cole DR, Horita J (2001) Equilibrium oxygen, hydrogen and carbon isotope fractionation factors applicable to geologic systems. Rev Mineral Geochem 43:1-81

Chakraborty S (2010) Diffusion coefficients in olivine, wadsleyite and ringwoodite. Rev Mineral Geochem 72:603-639

Chakraborty S, Farver JR, Yund RA, Rubie DC (1994) Mg tracer diffusion in synthetic forsterite and San Carlos olivine as a function of P, T and f_{O_2}. Phys Chem Miner 21:489-500

Cherniak DJ (2010) Cation diffusion in feldspars. Rev Mineral Geochem 72:691-734
Cherniak DJ, Watson EB (2001) Pb diffusion in zircon. Chem Geol 172:5-24
Cherniak DJ, Watson EB (2007) Ti diffusion in zircon. Chem Geol 242:473-481
Cherniak DJ, Hervig R, Koepke J, Zhang Y, Zhao D (2010) Analytical methods in diffusion studies. Rev Mineral Geochem 72:107-169
Cherniak DJ, Zhang XY, Nakamura M, Watson EB (2004) Oxygen diffusion in monazite. Earth Planet Sci Lett 226:161-174
Chou I-M (1987) Oxygen buffer and hydrogen sensor techniques at elevated pressures and temperatures. *In*: Hydrothermal Experimental Techniques. Ulmer GC, Barnes HL (eds) J Wiley & Sons. p 61-99
Choudhury A, Palmer DW, Amsel G, Curien H, Baruch P (1965) Study of oxygen diffusion in quartz by using the nuclear reaction $O^{18}(p,\alpha)N^{15}$. Solid State Comm 3:119-122
Clayton RN, Mayeda TK (1963) The use of bromine pentafluoride in the extraction of oxygen from oxides and silicates for isotopic analysis. Geochim Cosmochim Acta 27:43-52
Cole DR, Chakraborty S (2001) Rates and mechanism of isotope exchange. Rev Mineral Geochem 43:82-223
Condit RH, Weed HC, Piwinskii AJ (1985) A technique for observing diffusion along grain boundary regions in synthetic forsterite. *In*: Point Defects in Minerals. Schock RN (ed) Geophys Monogr 31, Mineral Phys 1:97-105
Connolly C, Muehlenbachs K (1988) Contrasting oxygen diffusion in nepheline, diopside and other silicates and their relevance to isotopic systematics in meteorites. Geochim Cosmochim Acta 52: 1585-1591
Costa F, Chakraborty S (2008) The effect of water on Si and O diffusion rates in olivine and implications for transport properties and processes in the upper mantle. Phys Earth Planet Int 166:11-29
Coughlan RAN (1990) Studies in diffusional transport: Grain boundary transport of oxygen in feldspars, strontium and REE's in garnet, and thermal histories of granitic intrusions in south-central Maine using oxygen isotopes. PhD dissertation. Brown University, Providence, Rhode Island
Crank J (1975) The Mathematics of Diffusion. Oxford University Press
Demouchy S, Mackwell SJ (2003) Water diffusion in synthetic iron-free forsterite. Phys Chem Miner 30: 486-494
Dennis PF (1984) Oxygen self-diffusion in quartz under hydrothermal conditions. J Geophys Res 89:4047-4057
Dennis PF, Freer R (1993) Oxygen self-diffusion in rutile under hydrothermal conditions. J Mater Sci 28:4804-4810
Derdau D, Freer R, Wright K (1998) Oxygen diffusion in anhydrous sanidine feldspar. Contrib Mineral Petrol 133:199-204
Derry DJ, Lees DG, Calbert JM (1981) A study of oxygen self-diffusion in the *c*-direction of rutile using a nuclear technique. J Phys Chem Solids 42:57-64
Dersch O, Rauch F (1999) Water uptake of quartz investigated by means of ion-beam analysis. Fres J Anal Chem 365:114-116.
Dersch O, Zouine A, Rauch F, Ericson JE (1997) Investigation of water diffusion into quartz using ion beam analysis techniques. Fres J Anal Chem 358:217-219
Desbois G, Ingrin J (2007) Anisotropy of hydrogen diffusion in tourmaline. Geochim Cosmochim Acta 71:5233-5243
Dobson DP, Dohmen R, Wiedenbeck M (2008) Self-diffusion of oxygen and silicon in $MgSiO_3$ perovskite. Earth Planet Sci Lett 270:125-129
Dohmen R, Chakraborty S, Becker H-W (2002) Si and O diffusion in olivine and implications for characterizing plastic flow in the mantle. Geophys Res Lett doi:10.1029/2002GL015480
Doremus RH (1998a) Comment on "Stationary and mobile hydrogen defects in potassium feldspar". Geochim Cosmochim Acta 62:377-378
Doremus RH (1998b) Diffusion of water and oxygen in quartz: Reaction-diffusion model. Earth Planet Sci Lett 163:43-51
Dowty E (1980) Crystal-chemical factors affecting the mobility of ions in minerals. Am Mineral 65:174-182
Elphick SC, Graham CM (1988) The effect of hydrogen on oxygen diffusion in quartz: Evidence for fast proton transients? Nature 335:243-245
Elphick SC, Graham CM (1990) Hydrothermal oxygen diffusion in diopside at 1 kb, 900-1200 °C, a comparison with oxygen diffusion in forsterite, and constraints on oxygen isotope disequilibrium in peridotite nodules. Terr Abstracts 7:22
Elphick SC, Dennis PF, Graham CM (1986) An experimental study of the diffusion of oxygen in quartz and albite using an overgrowth technique. Contrib Mineral Petrol 92:322-330
Elphick SC, Graham CM, Dennis PF (1988) An ion microprobe study of anhydrous oxygen diffusion in anorthite: A comparison with hydrothermal data and some geological implications. Contrib Mineral Petrol 100:490-495
Ewald AH (1985) The effect of pressure on oxygen isotope exchange in silicates. Chem Geol 49:179-185

Farver JR (1989) Oxygen self-diffusion in diopside with applications to cooling rate determinations. Earth Planet Sci Lett 92:322-330
Farver JR (1994) Oxygen self-diffusion in calcite: Dependence on temperature and water fugacity. Earth Planet Sci Lett 121:575-587
Farver JR, Giletti BJ (1985) Oxygen diffusion in amphiboles. Geochim Cosmochim Acta 49:1403-1411
Farver JR, Giletti BJ (1989) Oxygen and strontium diffusion kinetics in apatite and potential applications to thermal history determinations. Geochim Cosmochim Acta 53:1621-1631
Farver JR, Yund RA (1990) The effect of hydrogen, oxygen, and water fugacity on oxygen diffusion in alkali feldspar. Geochim Cosmochim Acta 54:2953-2964
Farver JR, Yund RA (1991a) Oxygen diffusion in quartz: Dependence on temperature and water fugacity. Chem Geol 90:55-70
Farver JR, Yund RA (1991b) Measurement of oxygen grain boundary diffusion in natural, fine grained, quartz aggregates. Geochim Cosmochim Acta 55:1597-1607
Farver JR, Yund RA (1999) Oxygen bulk diffusion measurements and TEM characterization of a natural ultramylonite: Implications for fluid transport in mica-bearing rocks. J Metamorphic Geol 17:669-683
Foland KA (1974) Alkali diffusion in orthoclase. *In*: Geochemical Transport and Kinetics. Hofmann AW, Giletti BJ, Yoder HS, Yund RA (eds) Carnegie Inst of Washington p 77-98
Fortier SM, Giletti BJ (1989) An empirical model for predicting diffusion coefficients in silicate minerals. Science 245:1481-1484
Fortier SM, Giletti BJ (1991) Volume self-diffusion of oxygen in biotite, muscovite, and phlogopite micas. Geochim Cosmochim Acta 55:1319-1330
Frantz JD, Eugster HP (1973) Acid-base buffers: Use of Ag + AgCl in the experimental control of solution equilibria at elevated pressures and temperatures. Am J Sci 273:268-286
Freer R (1981) Diffusion in silicate minerals and glasses: A data digest and guide to the literature. Contrib Mineral Petrol 76:440-454
Freer R (1993) Diffusion in silicate minerals. Defect & Diffusion Forum 101-102:1-17
Freer R, Dennis PF (1982) Oxygen diffusion studies. I. A preliminary ion microprobe investigation of oxygen diffusion in some rock-forming minerals. Mineral Mag 45:179-192
Freer R, Wright K, Kroll H, Gottlicher J (1997) Oxygen diffusion in sanidine feldspar and a critical appraisal of oxygen isotope-mass-effect measurements in non-cubic materials. Phil Mag A 75:485-503
Fukuda J, Shinoda K, Nakashima S, Miyoshi N, Aikawa N (2009) Polarized infrared spectroscopic study of diffusion of water molecules along structure channels in beryl. Am Mineral 94:981-985
Gerard O, Jaoul O (1989) Oxygen diffusion in San Carlos olivine. J Geophys Res 94:4119-4128
Giletti BJ, Anderson TF (1975) Studies in diffusion-II. Oxygen in phlogopite mica. Earth Planet Sci Lett 28:225-233
Giletti BJ, Hess KC (1988) Oxygen diffusion in magnetite. Earth Planet Sci Lett 89:115-122
Giletti BJ, Yund RA (1984) Oxygen diffusion in quartz. J Geophys Res 89:4039-4046
Giletti BJ, Semet MP, Yund RA (1978) Studies in diffusion-III. Oxygen in feldspars: An ion microprobe determination. Geochim Cosmochim Acta 42:45-57
Giletti BJ, Hickey JH, Tullis TE (1979) Oxygen diffusion in olivine under hydrous conditions. EOS Trans Am Geophys Union 60:370
Graham CM (1981) Experimental hydrogen isotope studies III: Diffusion of hydrogen in hydrous minerals, and stable isotope exchange in metamorphic rocks. Contrib Mineral Petrol 76:216-228
Graham CM, Elphick SC (1991) Some experimental constraints on the role of hydrogen in oxygen and hydrogen diffusion and Al-Si interdiffusion in silicates. *In:* Diffusion, Atomic Ordering, and Mass Transport – Selected Topics in Geochemistry. Ganguly J (ed) Adv Phys Geochem 8:248-285
Graham CM, Harmon RS, Sheppard SMF (1984) Experimental hydrogen isotope studies: Hydrogen isotope exchange between amphibole and water. Am Mineral 69:128-138
Graham CM, Viglino JA, Harmon RS (1987) Experimental study of hydrogen-isotope exchange between aluminous chlorite and water and of hydrogen diffusion in chlorite. Am Mineral 72:566-579
Griggs D (1967) Hydrolytic weakening of quartz and other silicates. Geophys J 14:19-31
Gruenwald TB, Gordon G (1971) Oxygen diffusion in single crystals of titanium dioxide. J Inorg Chem 33:1151-1155
Guillaumou N, Dumas P, Ingrin J, Carr GL, Williams JP (1999) Microanalysis of fluids in minerals in the micron scale range by synchrotron infrared microspectrometry. Internet J Vibrational Spec 3:1-11
Hallwig D, Schachtner R, Sockel HG (1982) Diffusion of magnesium, silicon and oxygen in Mg_2SiO_4 and formation of the compound in the solid state. *In*: Reactivity in Solids. Dyrek K, Habor J, Nowotry J (eds) Proc Intl Symp (9th), p 166-169
Hart EW (1957) On the role of dislocations in bulk diffusion. Acta Metall 5:597
Haul RAW, Dumbgen G (1962) Investigation of oxygen diffusion in TiO_2, quartz and quartz glass by isotope exchange. Z Electrochm 66:636-641

Haul RAW, Dumbgen G (1965) Oxygen self-diffusion in rutile crystals. J Phys Chem Solids 26:1-10
Hayashi T, Muehlenbachs K (1986) Rapid oxygen diffusion in melilite and its relevance to meteorites. Geochim Cosmochim Acta 50:585-591
Hercule S (1996) Cinetique et solubilite d l'hydrogene dans le diopside monocrystallin. PhD Dissertation, University Paris XI, Orsay, France
Hercule S, Ingrin J (1999) Hydrogen in diopside: Diffusion, kinetics of extraction-incorporation, and solubility. Am Mineral 84:1577-1587
Houlier B, Jaoul O, Abel F, Liebermann RC (1988) Oxygen and silicon self-diffusion in natural olivine at T=1300 °C. Phys Earth Planet Interiors 50:240-250
Huebner JS (1971) Buffering techniques for hydrostatic systems at elevated pressures. *In*: Research Techniques for High Pressure and High Temperature. Ulmer GC (ed) Springer-Verlag, New York p 123-178
Ingrin J, Blanchard M (2000) Hydrogen mobility in single crystal kaersutite. EMPG VIII, J Conf Abstr 5:52
Ingrin J, Blanchard M (2006) Diffusion of hydrogen in minerals. Rev Mineral Geochem 62:291-320
Ingrin J, Hercule S, Charton T (1995) Diffusion of hydrogen in diopside: Results of dehydrogenation experiments. J Geophys Res 100:15489-15499
Ingrin J, Pacaud L, Jaoul O (2001) Anisotropy of oxygen diffusion in diopside. Earth Planet Sci Lett 92:347-361
Jaoul O, Houlier B, Abel F (1983) Study of ^{18}O diffusion in magnesium orthosilicate by nuclear microanalysis. J Geophys Res 88:613-624
Jaoul O, Froidevaux C, Durham WB, Michaut M (1980) Oxygen self-diffusion in forsterite: Implications for the high temperature creep mechanism. Earth Planet Sci Lett 47:613-624
Jibao G, Yaqian Q (1997) Hydrogen isotope fractionation and hydrogen diffusion in the tourmaline-water system. Geochim Cosmochim Acta 21:4679-4688
Johnson EA (2003) Hydrogen in nominally anhydrous crustal minerals. PhD Dissertation, California Institute of Technology, Pasadena, USA
Johnson OW, Paek S-H, DeFord JW (1975) Diffusion of H and D in TiO_2: Suppression of internal fields by isotope exchange. J Appl Phys 46:1026-1033
Kats A, Haven Y, Stevels JM (1962) Hydroxyl groups in α-quartz. Phys Chem Glasses 3:69-76
Kohlstedt DL, Mackwell SJ (1998) Diffusion of hydrogen and intrinsic point defects in olivine. Z Phys Chem 207:147-162
Kronenberg AK (1994) Hydrogen speciation and chemical weakening of quartz. Rev Mineral Geochem 29:123-176
Kronenberg AK, Yund RA, Giletti BJ (1984) Carbon and oxygen diffusion in calcite: Effects on Mn content and P_{H2O}. Phys Chem Miner 11:101-112
Kronenberg AK, Kirby SH, Aines RD, Rossman GR (1986) Solubility and diffusional uptake of hydrogen in quartz at high water pressures: Implications for hydrolytic weakening. J Geophys Res 91:12723-12744
Kronenberg AK, Yund RA, Rossman GR (1996) Stationary and mobile hydrogen defects in potassium feldspar. Geochim Cosmochim Acta 60:4075-4094
Kronenberg AK, Yund RA, Rossman GR (1998) Reply to the comment by Robert H. Doremus on "Stationary and mobile hydrogen defects in potassium feldspar". Geochim Cosmochim Acta 62:379-382
Kurka A (2005) Hydrogen in Ca-rich garnets: Diffusion and stability of OH-defects. PhD Dissertation, University Paul Sabatier, Toulouse, France
Kurka A, Blanchard M, Ingrin J (2005) Kinetics of hydrogen extraction and deuteration in grossular. Mineral Mag 69:359-371
Labotka TC, Cole DR, Riciputi LR (2000) Diffusion of C and O in calcite at 100 MPa. Am Mineral 85:488-494
Lanford WA (1992) Analysis for hydrogen by nuclear reaction and energy recoil detection. Nucl Inst Meth Phys Res B66:65-82
Lanford WA (1995) Nuclear reactions for hydrogen analysis. *In*: Handbook of Modern Ion Beam Materials Analysis. Tesmer JR, Nastasi MA (eds) Materials Research Society p 193-204
Libowitzky E, Beran A (2006) The structure of hydrous species in nominally anhydrous minerals: Information from polarized IR spectroscopy. Rev Mineral Geochem 62:29-52
Lin T-H, Yund RA (1972) Potassium and sodium self-diffusion in alkali feldspar. Contrib Mineral Petrol 34:177-184
Mackwell SJ, Kohlstedt DL (1990) Diffusion of hydrogen in olivine: Implications for water in the mantle. J Geophys Res 95:5079-5088
Manning JR (1968) Diffusion Kinetics for Atoms in Crystals. Van Nostrand, Princeton, New Jersey, 257 p
Marion S, Meyer H-W, Carpenter M, Norby T (2001) H_2O-D_2O exchange in lawsonite. Am Mineral 86:1166-1169
Matthews A, Palin JM, Epstein S, Stolper EM (1994) Experimental study of $^{18}O/^{16}O$ partitioning between crystalline albite, albitic glass, and CO_2 gas. Geochim Cosmochim Acta 58:5255-5266

McConnell JDC (1995) The role of water in oxygen isotope exchange in quartz. Earth Planet Sci Lett 136:97-107

Merigoux H (1968) Etude de la mobilite d l'oxygen dans the feldspaths alcalins. Bull Soc fr Mineral Crystallogr 91:51-64

Millot F, Niu Y (1997) Diffusion of O^{18} in Fe_3O_4: an experimental approach to study the behavior of minority defects in oxides. J Phys Chem Solids 58:63-72

Millot F, Lorin JC, Klossa B, Niu Y, Tarento JR (1997) Oxygen self-diffusion in Fe_3O_4: An experimental example of interactions between defects. Ber Bunsenges Phys Chem 101:1351-1354

Moore DK, Cherniak DJ, Watson EB (1998) Oxygen diffusion in rutile from 750 to 1000 °C and 0.1 to 1000 MPa. Am Mineral 83:700-711

Morishita Y, Giletti BJ, Farver JR (1996) Volume self-diffusion of oxygen in titanite. Geochem J 30:71-79

Muehlenbachs K, Connolly C (1991) Oxygen diffusion in leucite: Structural controls. *In*: Stable Isotope Geochemistry: A Tribute to Samuel Epstein. Taylor HP, O'Neil JR, Kaplan IR (eds) The Geochemical Society, Spec Publ 3:27-34

Muehlenbachs K, Kushiro I (1974) Oxygen isotopic exchange and equilibrium of silicates with CO_2 or O_2. Carnegie Inst Wash Yearb 73:232-236

Niu Y, Millot F (1999) Oxygen self-diffusion and interactions between defects in Fe_3O_4. Acta Metallurgica Simica 12:137-142

Oishi Y, Kingery WD (1960) Self-diffusion of oxygen in single crystal and polycrystalline aluminum oxide. J Chem Phys 33:480-486

Pacaud L, Ingrin J, Jaoul O (1999) High-temperature diffusion of oxygen in synthetic diopside measured by nuclear reaction analysis. Miner Mag 63:673-686

Peterson NL (1975) Diffusion in Solids – Recent Developments. Academic Press, New York, p 115-170

Prot D, Monteу C (1996) Self-diffusion in α-Al_2O_3 II. Oxygen diffusion in "undoped" single crystals. Phil Mag A 73:899-917

Reddy KPR, Cooper AR (1982) Oxygen diffusion in sapphire. J Am Ceram Soc 65:634-638

Reddy KPR, Cooper AR (1983) Oxygen diffusion in MgO and α-Fe_2O_3. J Am Ceram Soc 66:664-666

Reddy KPR, Oh SM, Major LD Jr., Cooper AR (1980) Oxygen diffusion in forsterite. J Geophys Res 85:322-326

Reed DJ, Wuensch BJ, Bowen HK (1978) Research in Materials. Annual Report MIT

Robin R, Cooper AR, Heuer AH (1973) Applications of a non-destructive single-spectrum proton activation energy to study oxygen diffusion in zinc oxide. J Appl Phys 44:3770-3777

Rosenbaum JM (1994) Stable isotope fractionation between carbon dioxide and calcite at 900 °C. Geochim Cosmochim Acta 58:3747-3753

Rossman GR (2006) Analytical methods for measuring water in nominally anhydrous minerals. Rev Mineral Geochem 62:1-28

Ryerson FJ (1987) Diffusion measurements: Experimental methods. *In*: Methods of Experimental Geophysics. Sammis CG, Henyey T (eds) Vol 24 Academic Press p 89-129

Ryerson FJ, Durham WB, Cherniak DJ, Lanford WA (1989) Oxygen diffusion in olivine: Effect of oxygen fugacity and implications for creep. J Geophys Res 94:4105-4118

Ryerson FJ, McKeegan KD (1994) Determination of oxygen self-diffusion in akermanite, anorthite, diopside, and spinel: Implications for oxygen isotopic anomalies and the thermal histories of Ca-Al rich inclusions. Geochim Cosmochim Acta 58:3713-3734

Sabioni ACS, Freire FL, Barros Leite CV (1993) Study of oxygen self-diffusion in oxides by ion beam techniques: Comparison between nuclear reaction analysis and SIMS. Nucl Inst Meth Phys Res B73:85-89

Schachtner R, Sockel HG (1977) Study of diffusion in quartz by activation analysis. *In*: Reactivity of Solids. Wood J, Lindquist IO, Helgeson C, Vannerburg NG (eds) Proc International Symp (8^{th}) p 605-609

Shaffer EW, Sang SL, Cooper AR, Heuer AH (1974) Diffusion of tritiated water in β-quartz. *In*: Geochemical Kinetics and Transport. Hofmann AW, Giletti BJ, Yoder H, Yund RA (eds) Carnegie Inst Wash Publ 634:131-138

Sharp ZD (1991) Determination of oxygen diffusion rates in magnetite from natural isotopic variations. Geology 19:653-656

Sharp ZD, Jenkin GRT (1994) An empirical estimate of the diffusion rate of oxygen in diopside. J Metamorphic Geol 12:89-97

Sharp ZD, Giletti BJ, Yoder HS (1991) Oxygen diffusion rates in quartz exchanged with CO_2. Earth Planet Sci Lett 107:339-348

Sherwood JN (1981) The Plastically Crystalline State. Wiley, London p 39-83

Skogby H (1994) OH incorporation in synthetic clinopyroxene. Am Mineral 79:240-249

Skogby H, Rossman G (1989) OH^- in pyroxene: An experimental study of incorporation mechanisms and stability. Am Mineral 74:1059-1069

Stalder R, Skogby H (2003) Hydrogen diffusion in natural and synthetic orthopyroxene. Phys Chem Miner 30:12-19

Stalder R, Purwin H, Skogby H (2007) Influence of Fe on hydrogen diffusivity in orthopyroxene. Eur J Mineral 19:899-903

Suman KD, Cole DR, Riciputi LR, Chacko T, Horita J (2000) Experimental determination of hydrogen diffusion rates in hydrous minerals using the ion microprobe. J Conf Abstr 5(2):340

Sundvall R, Skogby H, Stalder R (2009) Hydrogen diffusion in synthetic Fe-free diopside. Eur J Mineral 21:963-970

Suzuoki T, Epstein S (1976) Hydrogen isotope fractionation between OH-bearing minerals and water. Geochim Cosmochim Acta 40:1229-1240

Valley JW, Graham CM, Harte B, Eiler JM, Kinny PD (1998) Ion microprobe analysis of oxygen, carbon, and hydrogen isotopic ratios. *In*: Rev Econ Geol McKibben MA, Shanks WC, Ridley WI (eds) 7:73-98

Van Orman JA, Crispin KL (2010) Diffusion in oxides. Rev Mineral Geochem 72:757-825

Vennemann TW, O'Neil JR, Deloule E, Chaussidon M (1996) Mechanism of hydrogen exchange between hydrous minerals and molecular hydrogen: Ion microprobe study of D/H exchange and calculations of hydrogen self-diffusion rates. Goldschmidt. J Conf Abstr 1(1):648

Walker AM, Wright K, Slater B (2003) A computational study of oxygen diffusion in olivine. Phys Chem Miner 30:536-545

Wang L, Zhang Y, Essene E (1996) Diffusion of the hydrous component in pyrope. Am Mineral 81:706-718

Watson EB, Dohmen R (2010) Experimental methods in diffusion studies. Rev Mineral Geochem 72:447-507

Watson EB, Cherniak DJ (1997) Oxygen diffusion in zircon. Earth Planet Sci Lett 148:527-544

Wright K, Freer R, Catlow CRA (1996) Water-related defects and oxygen diffusion in albite: A computer simulation study. Contrib Mineral Petrol 125:161-166

Yaqian Q, Jibao G (1993) Study of hydrogen isotope equilibrium and kinetic fractionation in the ilvaite water system. Geochim Cosmochim Acta 57:3073-3082

Yund RA, Anderson TF (1974) Oxygen isotope exchange between potassium feldspar and KCl solutions. *In*: Geochemical Transport and Kinetics. Hofmann AW, Giletti BJ, Yoder HS, Yund RA (eds) Carnegie Inst Wash Publ 634:99-105

Yund RA, Anderson TF (1978) The effect of fluid pressure on oxygen isotope exchange between feldspar and water. Geochim Cosmochim Acta 42:235-239

Yund RA, Smith BM, Tullis J (1981) Dislocation assisted diffusion of oxygen in albite. Phys Chem Miner 7:185-189

Yurimoto H, Morioka M, Nagasawa H (1989) Diffusion in single crystals of melilite: I. Oxygen. Geochim Cosmochim Acta 53:2387-2394

Yurimoto H, Morioka M, Nagasawa H (1992) Oxygen self-diffusion along high diffusivity paths in forsterite. Geochem J 26:181-188

Zhang XY, Cherniak DJ, Watson EB (2006) Oxygen diffusion in titanite: Lattice diffusion and fast-path diffusion in single crystals. Chem Geol 235:105-123

Zhang XY, Watson EB, Cherniak DJ (2007) Oxygen self-diffusion "fast-paths" in titanite single crystals and a general method for deconvolving self-diffusion profiles with "tails". Geochim Cosmchim Acta 71:1563-1573

Zhang Y (2008) Geochemical Kinetics. Princeton University Press, Princeton, NJ, 656 pp

Zhang Y (2010) Diffusion in minerals and melts: theoretical background. Rev Mineral Geochem 72:5-59

Zhang Y, Ni H (2010) Diffusion of H, C, and O components in silicate melts. Rev Mineral Geochem 72:171-225

Zhang Y, Stolper EM, Wasserburg GJ (1991) Diffusion of a multi-species component and its role in oxygen and water transport in silicates. Earth Planet Sci Lett 103:228-240

Zheng Y-F, Fu B (1998) Estimation of oxygen diffusivity from anion porosity in minerals. Geochem J 32:71-89

APPENDIX

Published experimental hydrogen and oxygen volume diffusion data for minerals.

No.	Sample Material	Temperature Range (°C)	Pressure Range (MPa)	Diffusing Species/ Form	E_a (kJ/mol) or D (m^2/s)
	QUARTZ				
	Oxygen Self-Diffusion				
1	α-Quartz, natural powder	1010-1220	<0.1	$^{18}O/O_2$	230
2	β-Quartz, natural single Xal	667	82	$^{18}O/H_2O$	D = 4.1 E−16 m^2/s
3	β-Quartz, natural single Xal	667	82	$^{18}O/H_2O$	D = 8.4 E−18 m^2/s
4	β-Quartz, natural single Xal	870-1180	2.1	$^{18}O/O_2$	195
5	β-Tridymite, natural single Xal	1070-1280	2.1	$^{18}O/O_2$	195
6	α-Quartz, natural single Xal	500-550	100	$^{18}O/H_2O$	284 ±92
7	α-Quartz, natural single Xal	500-550	100	$^{18}O/H_2O$	238 ±12
8	β-Quartz, natural single Xal	600-800	100	$^{18}O/H_2O$	142 ±4
9	β-Quartz, natural single Xal	600-800	100	$^{18}O/H_2O$	155 ±8
10	β-Quartz, natural single Xal	600-800	100	$^{18}O/H_2O$	234 ±8
11	β-Quartz, synthetic single Xal	600-800	100	$^{18}O/H_2O$	205 ±12
12	β-Quartz, natural single Xal	700	25-350	$^{18}O/H_2O$	D = 3.1 E−19 to 3.6 E−18
13	β-Quartz, natural single Xal	700-850	100	$^{18}O/H_2O$	138 ±19
14	β-Quartz, natural single Xal	700-850	100	$^{18}O/H_2O$	204 ±2
15	β-Quartz, natural single Xal	600-825	100	$^{18}O/H_2O$	98 ±7
16	β-Quartz, natural single Xal	700	100	$^{18}O/H_2O$	D = 1.7 E−18 m^2/s
17	β-Quartz, natural single Xal	800	100	$^{18}O/H_2$, Ar	D = 2.5 E−18 m^2/s
18	β-Quartz, natural single Xal	745-900	10	$^{18}O/CO_2$	159 ±13
19	β-Quartz, natural single Xal	900	345	$^{18}O/CO_2$	D = 2.24 E−19
20	β-Quartz, natural single Xal	900	727	$^{18}O/CO_2$	D = 8.13 E−19
21	β-Quartz, natural single Xal	835	10	^{18}O /CO_2, H_2O	D = 1.32 E−19
22	α-Quartz, natural single Xal	450-590	100	$^{18}O/H_2O$	243 ±17
23	β-Quartz, natural single Xal	600	150-350	$^{18}O/H_2O$	log D = 0.565 (log f_{H_2O})−24.04
24	β-Quartz, natural single Xal	700	5-350	$^{18}O/H_2O$	log D = 0.783 (log f_{H_2O})−23.3
	Hydrogen Self-Diffusion				
25	α-Quartz, natural single Xal	400-620	2.5	$^{2}H/H_2O$,$^{2}H_2O$	79.5
26	β-Quartz, natural single Xal	700-900	2.5	$^{2}H/H_2O$,$^{2}H_2O$	175.5
27	β-Quartz, natural single Xals	700-900	1100	$^{2}H/^{2}H_2O$	215 ±92
28	β-Quartz, natural single Xals	800-900	1100	$^{2}H/^{2}H_2O$	156
	Hydrogen Chemical Diffusion				
29	β-Quartz, natural single Xal	720-850	0.06	$^{3}H/^{3}H_2O$	100 ±9
30	β-Quartz, natural single Xal	700-900	890-1540	H/H_2O	200 ±20
31	β-Quartz, natural single Xal	800	890	H/H_2O	D = 2 E−11 m^2/s
	FELDSPARS, FELDSPATHOIDS				
	Oxygen Self-Diffusion				
32	Albite, powder synthetic Xal	440-805	25-60	$^{18}O/H_2O$	154.8
33	Albite, powder natural Xal	600-800	200	$^{18}O/H_2O$	154.8 ±8
34	Albite, natural single Xal	350-805	100	$^{18}O/H_2O$	87.5
35	Albite, natural single Xal	807	200	$^{18}O/H_2O$	D = 2.11 E−17 m^2/s
36	Albite, natural single Xal	807	200	$^{18}O/H_2O$	D = 1.74 E−17 m^2/s
37	Albite, natural single Xal	807	200	$^{18}O/H_2O$	D = 2.42 E−17 m^2/s
38	Albite, powder natural Xal	450-750	200	$^{18}O/H_2O$	139.8 ±3
39	Albite, powder deformed natural Xal	450-750	200	$^{18}O/H_2O$	129.5 ±5
40	Albite, natural single Xal	600	100	$^{18}O/H_2O$	D = 4.2 E−19 m^2/s
41	Albite, natural single Xal	650	100-1500	$^{18}O/H_2O$	log D = 0.732 (logf_{H_2O})−19.145
42	Albite, powder natural Xal	750-950	0.1	$^{18}O/H_2O$	90
43	Microcline, powder natural Xal	400-700	200	^{18}O/2M KCl	123.9 ±4
44	Sanidine, natural single Xal	550-850	100	^{18}O, $^{17}O/H_2O$	109.7 ±4

D_0 (m^2/s)	pO_2, f_{H_2O}	Orientation	Analytical Method	Reference	Notes
3.70 E−13	O_2	bulk	BE-MS	Haul & Dumbgen (1962)	
		para *c*	$^{18}O(p,\alpha)^{15}N$	Choudhury et al. (1965)	
		perp *c*	$^{18}O(p,\alpha)^{15}N$	Choudhury et al. (1965)	
1.10 E−14	in O_2 gas	para & perp *c*	$^{18}O(p,n)^{18}F$	Schachtner & Sockel (1977)	
1.10 E−13	in O_2 gas	para & perp *c*	$^{18}O(p,n)^{18}F$	Schachtner & Sockel (1977)	
1.90 E−2	UB/NNO	para *c*	SIMS	Giletti & Yund (1984)	
8.00 E−6	UB/NNO	perp (10-11)	SIMS	Giletti & Yund (1984)	
4.00 E−11	UB/NNO	para *c*	SIMS	Giletti & Yund (1984)	
9.00 E−11	UB/NNO	perp (10-11)	SIMS	Giletti & Yund (1984)	
1.00 E−7	UB/NNO	perp *c*	SIMS	Giletti & Yund (1984)	
2.00 E−10	UB/NNO	perp *c*	SIMS	Giletti & Yund (1984)	
	UB/NNO	perp *c*	SIMS	Giletti & Yund (1984)	
2.09 E−15	NNO	para *c*	SIMS	Dennis (1984)	
1.40 E−14	NNO	perp (10-10)	SIMS	Dennis (1984)	
3.4 E−13	NNO	para *c*	SIMS	Elphick et al. (1986)	overgrowth
	NNO	para *c*	SIMS	Elphick & Graham (1988)	
	1:1 H_2/Ar gas	para *c*	SIMS	Elphick & Graham (1988)	
2.10 E−12	CO_2	para *c*	SIMS	Sharp et al. (1991)	
	CO_2	para *c*	SIMS	Sharp et al. (1991)	
	CO_2	para *c*	SIMS	Sharp et al. (1991)	
	X CO_2 = 0.85	para *c*	SIMS	Sharp et al. (1991)	
2.90 E−5	UB/NNO	para *c*	SIMS	Farver & Yund (1991)	
	multiple buffers	para *c*	SIMS	Farver & Yund (1991)	
	multiple buffers	para *c*	SIMS	Farver & Yund (1991)	
5.00 E−9	UB	para *c*	IR	Kats et al. (1962)	
5 E−4	UB	para *c*	IR	Kats et al. (1962)	
3.5 E−1	UB	para *c*	bulk IR	Kronenberg et al. (1986)	
3.5 E−4	UB	perp *c*	bulk IR	Kronenberg et al. (1986)	
4.26 E−11	UB	para *c*	liquid scintillation	Shaffer et al. (1974)	
1.4 E−1	UB	para *c*	bulk IR	Kronenberg et al. (1986)	
	UB	perp *c*	bulk IR	Kronenberg et al. (1986)	
4.50 E−9		bulk, sphere	BE-MS	Merigoux (1968)	
2.50 E−9		bulk, sphere	BE-MS	Anderson & Kasper (1975)	
1.69 E−13	UB/NNO	perp (001)	SIMS	Giletti et al. (1978)	
	UB/NNO	perp (-111)	SIMS	Giletti et al. (1978)	
	UB/NNO	perp (130)	SIMS	Giletti et al. (1978)	
	UB/NNO	perp (010)	SIMS	Giletti et al. (1978)	
9.80 E−10	UB	bulk, sphere	BE-MS	Yund et al. (1981)	
7.60 E−10	UB	bulk, sphere	BE-MS	Yund et al. (1981)	
	UB	perp (001)	SIMS	Freer & Dennis (1982)	
	multiple buffers	perp (001)	SIMS	Farver & Yund (1990)	
2.00E−20	CO_2	bulk, sphere	BE-MS	Matthews et al. (1994)	
2.80 E−10	UB/NNO	bulk, sphere	BE-MS	Yund & Anderson (1974)	
3.95 E−12		perp (001)	SIMS	Freer et al. (1997)	

No.	Sample Material	Temperature Range (°C)	Pressure Range (MPa)	Diffusing Species/ Form	E_a (kJ/mol) or D (m^2/s)
45	Sanidine, natural single Xal	869-1053	0.1	$^{18}O/O_2$	245 ±15
46	Adularia, powder synthetic Xal	520-800	32.5-60	$^{18}O/H_2O$	133.9
47	Adularia, powder natural Xal	400-700	200	^{18}O/2M KCl	123.9 ±5
48	Adularia, powder natural Xal	712-843	0.1	$^{18}O/CO_2$	D = 1 E−20 m^2/s
49	Adularia, powder natural Xal	1107	0.1	^{18}O	D = 1 E−19 m^2/s
50	Adularia, powder natural Xal	650	25-400	$^{18}O/H_2O$	$\log D = 0.604(\log f_{H_2O})-19.16$
51	Adularia, natural single Xal	350-700	100	$^{18}O/H_2O$	107.1
52	Adularia, natural single Xal	650	5 to 11	$^{18}O/H_2O$	$\log D = 1.18(\log f_{H_2O})-19.20$
53	Adularia, natural single Xal	650	25-1500	$^{18}O/H_2O$	$\log D = (0.516(\log f_{H_2O})-18.48$
54	Oligoclase, natural single Xal	550, 800	100	$^{18}O/H_2O$	D = 2.2E−19, 1.8E−17
55	Labradorite, natural single Xal	550, 700	100	$^{18}O/H_2O$	D = 4.4E−19, 8.3E−18
56	Anorthite, powder synthetic Xal	1280-1480	0.1	$^{18}O/CO,CO_2$	344
57	Anorthite, natural single Xal	350-800	100	$^{18}O/H_2O$	109.6
58	Anorthite, natural single Xal	850-1298	0.1	$^{18}O/O_2$	236 ±8
59	Anorthite, natural single Xal	1008-1295	0.1	$^{18}O/CO,CO_2$	162 ±36
60	Nepheline, powder natural Xal	1000-1300	0.1	$^{18}O/O_2$	104.6 ±10
61	Leucite, powder natural Xals	1000-1300	0.1	$^{18}O/CO_2$	58.6 ±12.5
	Hydrogen Chemical Diffusion				
62	Adularia ($Ab_9Or_{90}Cs_1$), natural single Xals	500-900	0.1	H extraction	172 ±15
63	Andesine ($Ab_{66}An_{30}Or_3$), natural single Xals	800-1000	0.1	H extraction	224 ±33
	OLIVINE				
	Oxygen Self-Diffusion				
64	Forsterite, powder natural Xals	1280	0.1	$^{18}O/O_2$	D = 1.1 E−18 m^2/s
65	Forsterite, natural single Xals	1000	400	$^{18}O/H_2O$	D = 2.0 E−20 m^2/s
66	Forsterite, natural single Xals	1275-1560	0.1	$^{18}O/O_2$	324.3
67	Forsterite, natural single Xals	1275-1628	0.1	$^{18}O/O_2$	364.4
68	Forsterite, natural single Xals	1425-1628	0.1	$^{18}O/O_2$	379.9
69	Forsterite, natural single Xals	1150-1600	0.1	^{18}O/Ar, H_2O	328.4
70	Forsterite, synthetic single Xals	1472-1734	0.02	$^{18}O/O_2$	416
71	Forsterite, synthetic single Xals	1000-1500	0.02	$^{18}O/O_2$	377.8
72	Forsterite, synthetic single Xals	1300-1600	0.1	$^{18}O/H_2$, H_2O	292.9
73	Forsterite, synthetic single Xals	1325	0.1	$^{18}O/O_2$	D = 1.8E−15 m^2/s
74	Forsterite, natural single Xals	1300	0.1	$^{18}O/H_2$, H_2O	D = 2.56 E−19 m^2/s
75	Forsterite, natural single Xals	1300	0.1	$^{18}O/H_2$, H_2O	D = 6.26 E−19 m^2/s
76	Forsterite (0.90), natural single Xals	1300	0.1	$^{18}O/H_2$, H_2O	D = 4.31 E−18 m^2/s
77	Forsterite (0.90), natural single Xals	1090-1500	0.1	$^{18}O/H_2$, H_2O	318 ±17
78	Forsterite (0.92), natural single Xals	1198-1401	0.1	$^{18}O/CO,CO_2$	266 ±11
79	Forsterite, synthetic single Xals	1100	0.1	$^{18}O/CO_2$	D = 2.76 E−21 m^2/s
80	Forsterite, synthetic single Xals	1200	0.1	$^{18}O/CO_2$	D = 8.15E−21 m^2/s
81	Olivine (Fo_{93}) natural single Xals	1100-1500	0.1	^{18}O thin film	338 ±14
82	Olivine (Fo_{93}) natural single Xals	1200-1350	2 GPa	^{18}O thin film	437 ±17
	Hydrogen Self-Diffusion				
83	Forsterite (0.25 wt% Fe), natural single Xal	700-1150	0.1	$^2H/^2H_2$	134 ±7
	Hydrogen Chemical Diffusion				
84	Olivine ($Mg_{0.91}Fe_{0.09}Ni_{0.003})_2SiO_4$, natural single Xals	800-1000	300	H/H_2O	130 ±30

D_0 (m^2/s)	pO_2, f_{H_2O}	Orientation	Analytical Method	Reference	Notes
8.40 E−11	O_2	perp (001)	SIMS	Derdau et al. (1998)	
9.00 E−11		bulk, sphere	BE-MS	Merigoux (1968)	
5.3 E−11	UB/NNO	bulk, sphere	BE-MS	Yund & Anderson (1974)	
	CO_2	bulk, sphere	BE-MS	Yund & Anderson (1974)	
	air	bulk, sphere	BE-MS	Yund & Anderson (1974)	
		bulk, sphere	BE-MS	Yund & Anderson (1978)	
4.51 E−12	UB/NNO	perp (001)	SIMS	Giletti et al. (1978)	
		perp (001)	SIMS	Farver & Yund (1990)	
	multiple buffers	perp (001)	SIMS	Farver & Yund (1990)	
	UB/NNO	perp (001)	SIMS	Giletti et al. (1978)	
	UB/NNO	perp (001)	SIMS	Giletti et al. (1978)	
1.59E−09	CO_2, O_2	bulk, sphere	BE-MS	Muehlenbachs & Kushiro (1974)	
1.39E−11	UB/NNO	perp (001)	SIMS	Giletti et al. (1978)	
1.00E−09	O_2	perp (001)	SIMS	Elphick et al. (1988)	
8.40 E−13	CO−CO_2 (QFM)	para (010)	SIMS	Ryerson & McKeegan (1994)	
5.90 E−13	CO_2	bulk, sphere	BE-MS	Connolly & Muehlenbachs (1988)	
1.30 E−15	CO_2	bulk, sphere	BE-MS	Connolly & Muehlenbachs (1988)	
6.16 E−4	0.021	para [001]*	seq IR	Kronenberg et al. (1996)	
5.75 E−4	UB	para [010]*, perp [010]*	seq polarized IR	Johnson (2003)	
	O_2	bulk, sphere	BE-MS	Muehlenbachs & Kushiro (1974)	
	UB	perp (110)	SIMS	Giletti et al. (1979)	
9.30 E−9	O_2	para (100)	$^{18}O(p,\alpha)^{15}N$	Reddy et al. (1980)	
1.86 E−7	O_2	para (010)	$^{18}O(p,\alpha)^{15}N$	Reddy et al. (1980)	
1.38 E−6	O_2	para (001)	$^{18}O(p,\alpha)^{15}N$	Reddy et al. (1980)	
1.46 E−8	log pO_2 = −9.2, −4.4	isotropic	SIMS, $^{18}O(p,\alpha)^{15}N$	Jaoul et al. (1980)	
2.85 E−6	O_2	sphere	BE-MS	Ando et al. (1981)	
5.90 E−8	pO_2 = 0.02		SIMS	Hallwig et al. (1982)	
2.30 E−10	log pO_2 = −11 to −4	isotropic	$^{18}O(p,\alpha)^{15}N$	Jaoul et al. (1983)	
	O_2		$^{18}O(p,n)^{17}F$	Condit et al. (1985)	
	log pO_2 = −8.3 to −7	para (100)	$^{18}O(p,\alpha)^{15}N$	Houlier et al. (1988)	
	log $pO2$ = −8.3	para (010)	$^{18}O(p,\alpha)^{15}N$	Houlier et al. (1988)	
	log pO_2 = −9.5	para (001)	$^{18}O(p,\alpha)^{15}N$	Houlier et al. (1988)	
0.34 log (pO_2) −6.784	log pO_2 = −12 to −7	para (001)	$^{18}O(p,\alpha)^{15}N$	Gerard & Jaoul (1989)	
0.21 log (pO_2) −9.585	NNO, IW	para (100, 010)	$^{18}O(p,\alpha)^{15}N$	Ryerson et al. (1989)	
		para *c*	SIMS	Yurimoto et al. (1992)	
		para *c*	SIMS	Yurimoto et al. (1992)	
4.6 E−9	log pO_2 = −10	para *c*	SIMS	Dohmen et al. (2002)	
1.43 E−4	f_{H_2O}~0.93 GPa	para *c*	SIMS	Costa and Chakraborty (2008)	
3.2 E−8	E−23 to E−13	para *c*	seq IR	Ingrin & Blanchard (2006)	
6 E−5	Fe/FeO, NNO, E−19 to E−11	para *a*	IR profile	Mackwell & Kohlstedt (1990)	

No.	Sample Material	Temperature Range (°C)	Pressure Range (MPa)	Diffusing Species/ Form	E_a (kJ/mol) or D (m^2/s)
85	Olivine $(Mg_{0.91}Fe_{0.09}Ni_{0.003})_2SiO_4$, natural single Xals	800-1000	300	H/H_2O	130 ±30
86	Olivine $(Mg_{0.91}Fe_{0.09}Ni_{0.003})_2SiO_4$, natural single Xals	800-1000	300	H/H_2O	110 ±50
87	Olivine $(Mg_{0.91}Fe_{0.09}Ni_{0.003})_2SiO_4$, natural single Xals	800-1000	300	H/H_2O	145 ±30
88	Olivine $(Mg_{0.91}Fe_{0.09}Ni_{0.003})_2SiO_4$, natural single Xals	800-1000	300	H/H_2O	180 ±50
89	Olivine $(Mg_{0.91}Fe_{0.09}Ni_{0.003})_2SiO_4$, natural single Xals	900-1000	200	H/H_2O	260 ±20 (assumed)
90	Olivine $(Mg_{0.91}Fe_{0.09}Ni_{0.003})_2SiO_4$, natural single Xals	900-1000	200	H/H_2O	260 ±20 (assumed)
91	Olivine $(Mg_{0.91}Fe_{0.09}Ni_{0.003})_2SiO_4$, natural single Xals	900-1000	200	H/H_2O	260 ±20 (assumed)
92	Forsterite, synthetic single Xals	900-1110	1500 and 200	H/H_2O	210 ±33
93	Forsterite, synthetic single Xals	1000-1110	1500 and 200	H/H_2O	205 ±31
94	Forsterite, synthetic single Xals	1000-1100	1500 and 200	H/H_2O	225 ±40
	PYROXENES				
	Oxygen Self-Diffusion				
95	Enstatite, powder synthetic Xals	1280	0.1	$^{18}O/O_2$	D = 6.0 E−16 m^2/s
96	Diopside, powder synthetic Xals	1280	0.1	$^{18}O/O_2$	D = 1.8 E−16 m^2/s
97	Diopside, powder synthetic Xals	1280	0.1	$^{18}O/CO_2$	D = 2.9 E−16 m^2/s
98	Diopside, powder synthetic Xals	1150-1350	0.1	$^{18}O/CO_2$	404.6
99	Diopside, natural single crystal	700-1200	100	$^{18}O/H_2O$	225.9 ±21
100	Diopside, natural single crystal	1000-1200	100	$^{18}O/H_2O$	225.9
101	Diopside, natural single crystal	900-1200	100	$^{18}O/H_2O$	351 ±21
102	Diopside, natural single crystal	1104-1251	0.1	$^{18}O/O_2$	457 ±26
103	Diopside, powder natural Xals	800	700-800	$^{18}O/CaCO_3$	D = 5.6 E−24 m^2/s
104	Diopside, synthetic single Xals	1200-1370	1E−3 to 1E−14	$^{18}O/H_2O$	310 ±30
105	Diopside, synthetic single Xals	1050-1370	1E−4 to 1E−13	$^{18}O/H_2O$	259 ±15
106	Diopside, synthetic single Xals	1250-1350	1E−10 to 1.6E−13	$^{18}O/H_2O$	323 ±27
107	Dioside, natural single Xals	1100-1280	4 E−3 to 1.2 E−11	$^{18}O/H_2O$	255 ±33
	Hydrogen Self-Diffusion				
108	Diopside, (Fe/Fe+Mg)=0.036, natural single Xal	600-866	0.1	$^2H/^2H_2$	149 ±16
109	Diopside, (Fe/Fe+Mg)=0.036, natural single Xal	700-900	0.1	$^2H/^2H_2$	143 ±33
	Hydrogen Chemical Diffusion				
110	Diopside (Fe/(Fe+Mg)=0.07), natural single Xals	700-850	0.1	H extraction	181 ±38
111	Diopside (Fe/(Fe+Mg)=0.07), natural single Xals	700-850	0.1	H extraction	153 ±32
112	Diopside (Fe/(Fe+Mg)=0.036), natural single Xals	700-1000	0.1	H extraction	126 ±24
113	Diopside (Fe/(Fe+Mg)=0.036), natural single Xals	700-1000	0.1-0.1	H/H_2	126 ±24
114	Diopside (Fe/(Fe+Mg)= 0.05, natural single Xals	600-900	0.1	H extraction	107 ±30

D_0 (m^2/s)	pO_2, f_{H_2O}	Orientation	Analytical Method	Reference	Notes
5 E−6	Fe/FeO, NNO, E−19 to E−11	para *c*	IR profile	Mackwell & Kohlstedt (1990)	
2.6 E−7	Fe/FeO, E−19 to E−13	para *c*	IR profile	Kohlstedt & Mackwell (1998)	
3 E−4	Fe/FeO, E−19 to E−13	para *a*	IR profile	Kohlstedt & Mackwell (1998)	
6.2 E−4	Fe/FeO, E−19 to E−13	para *b*	IR profile	Kohlstedt & Mackwell (1998)	
	NNO, E−13 to E−11	para *c*	IR profile	Kohlstedt & Mackwell (1998)	cation vacancies
	NNO, E−13 to E−11	para *a*	IR profile	Kohlstedt & Mackwell (1998)	cation vacancies
	NNO, E−13 to E−11	para *b*	IR profile	Kohlstedt & Mackwell (1998)	cation vacancies
5 E−4	NNO, E−13 to E−10	para *c*	IR profile	Demouchy & Mackwell (2003)	
8 E−5	NNO, E−13 to E−10	para *b*	IR profile	Demouchy & Mackwell (2003)	
1.6 E−4	NNO, E−13 to E−10	para *a*	IR profile	Demouchy & Mackwell (2003)	
	O_2	bulk, sphere	BE-MS	Muehlenbachs & Kushiro (1974)	
	O_2	bulk, sphere	BE-MS	Muehlenbachs & Kushiro (1974)	
	CO_2	bulk, sphere	BE-MS	Muehlenbachs & Kushiro (1974)	
6.3 E−4	CO_2	bulk, sphere	BE-MS	Connolly & Muehlenbachs (1988)	
1.50 E−10	UB	para *c*	SIMS	Farver (1989)	
2.80 E−12	UB	perp *c*	SIMS	Farver (1989)	
9.00 E−7		para *c*	SIMS	Elphick & Graham (1990)	
4.3 E−4	NNO	para *c*	SIMS	Ryerson & McKeegan (1994)	
		bulk, sphere	BE-MS	Sharp & Jenkin (1994)	empirical
6.31 E−10		para *b*	$^{18}O(p,\alpha)^{15}N$	Pacaud et al. (1999)	
1 E −10	~QFM	para *a*, *c*	$^{18}O(p,\alpha)^{15}N$	Ingrin et al. (2001)	a, *c* data combined
1.6 E−9	~QFM	para *b*	$^{18}O(p,\alpha)^{15}N$	Ingrin et al. (2001)	
2 E−10	~QFM	para *c*	$^{18}O(p,\alpha)^{15}N$	Ingrin et al. (2001)	
4 E−4	E−26 to E−19	para *c* and *a**	seq IR	Hercule & Ingrin (1999)	
1 E−5	E−23 to E−18	para *b*	seq IR	Hercule & Ingrin (1999)	
8 E−3	E−15, olivine	para *a*	seq IR	Carpenter-Woods et al. (2000)	
4 E−4	E−15, olivine	para *c**	seq IR	Carpenter-Woods et al. (2000)	
2 E−7	0.021	para *a**, *b*, *c*	seq IR	Ingrin et al. (1995)	Combined with data from Hercule & Ingrin (1999)?
2 E−7	E−17 to E−21	para *a**, *b*, *c*	seq IR	Hercule & Ingrin (1999)	Combined with data from Ingrin et al. (1995)?
2.3 E−7	0.021	para *c*	seq IR	Hercule (1996)	

No.	Sample Material	Temperature Range (°C)	Pressure Range (MPa)	Diffusing Species/ Form	E_a (kJ/mol) or D (m^2/s)
115	Diopside (Fe/(Fe+Mg)=0.126, natural single Xals	700-900	0.1	H extraction	109
116	Diopside (Fe/(Fe+Mg)=0.036, natural single Xals	1200	0.1	H/H_2	D = 5 E−13 m^2/s
117	Enstatite, synthetic single Xals	700-900	0.1	H extraction	295 ±55
118	Enstatite ($En_{90}Fs_{70}$), natural single Xals	700	0.1	H extraction	D = 2.5 E−14 m^2/s
119	Enstatite ($En_{90}Fs_{70}$), natural single Xals	700	0.1	H extraction	D = 6.3 E−14 m^2/s
120	Enstatite ($En_{90}Fs_{70}$), natural single Xals	700	0.1	H extraction	D = 6.3 E−15 m^2/s
121	Enstatite-Ferrosilite synthetic single Xals	600-900	0.1	H extraction	193 ±20
122	Diopside, synthetic single Xals	800-1000	0.1	H extraction	331 ±50
123	Diopside, synthetic single Xals	800-1000	0.1	H extraction	312 ±55
	AMPHIBOLES				
	Oxygen Self-Diffusion				
124	Tremolite, natural single Xals	650-800	100	$^{18}O/H_2O$	163.2 ±21
125	Hornblende, natural single Xals	650-800	100	$^{18}O/H_2O$	171.6 ±25
126	Hornblende, natural single Xals	800	100	$^{18}O/H_2O$	D = 4.05 E−21 m^2/s
127	Hornblende, natural single Xals	800	100	$^{18}O/H_2O$	D = 2.1 E−21 m^2/s
128	Hornblende, natural single Xals	800	20-200	$^{18}O/H_2O$	$\log D = 0.434(\log f_{H_2O})-20.08$
129	Richterite, natural single Xals	650-800	100	$^{18}O/H_2O$	238.5 ±8
	Hydrogen Self-Diffusion				
130	Hornblende, powdered natural sample	350-550	200 - 800	$^2H/H_2O$,^2H_2O	79−84
131	Tremolite, powdered natural Xals	350-800	200-400	$^2H/H_2O$,^2H_2O	71.5
132	Actinolite, powdered natural Xals	400-670	200	$^2H/H_2O$,^2H_2O	99
133	Kaersutite, natural single Xal	600-900	0.1	$^2H/^2H_2$	104 ±12
	SHEET SILICATES				
	Oxygen Self-Diffusion				
134	Muscovite, powder natural Xals	512-700	100	$^{18}O/H_2O$	163.2 ±21
135	Muscovite, powder natural Xals	600, 700	100	$^{18}O/H_2O$	D = 7.73 E−23 m^2/s, D = 1.6 E−21 m^2/s
136	Biotite, powder natural Xals	500-800	100	$^{18}O/H_2O$	142.3 ±8
137	Biotite, powder natural Xals	600, 700	100	$^{18}O/H_2O$	D = 2.5 E−22 m^2/s, D = 2.1 E−21 m^2/s
138	Phlogopite, powder natural Xals	500-800	200	$^{18}O/H_2O$	121.3 ±8
139	Phlogopite, powder natural Xals	500-800	200	$^{18}O/H_2O$	150.6 ±8
140	Phlogopite, powder natural Xals	600-900	100	$^{18}O/H_2O$	175.5 ±13
141	Phlogopite, powder natural Xals	800, 900	100	$^{18}O/H_2O$	D = 7.7 E−22 m^2/s, D = 8.3 E−21 m^2/s
142	Phlogopite, powder natural Xals	700	20-200	$^{18}O/H_2O$	D = 5.25 E−18
	Hydrogen Self-Diffusion				
143	Muscovite, powdered natural Xals	450-750	200 or 400	$^2H/H_2O$,^2H_2O	121
144	Zoisite ($Ca_2Fe_{0.1}Al_{2.9}Si_3O_{12}OH$), powdered natural Xals	350-650	200 or 400	$^2H/H_2O$,^2H_2O	100−103
145	Epidote ($Ca_2Fe_{0.9}Al_{2.1}Si_3O_{12}OH$), powdered natural Xals	450-650	200 or 400	$^2H/H_2O$,^2H_2O	52−58
146	Epidote ($Ca_2Fe_{0.9}Al_{2.1}Si_3O_{12}OH$), powdered natural Xals	250-350	200 or 400	$^2H/H_2O$,^2H_2O	128
147	Epidote ($Ca_2FeAl_2Si_3O_{12}OH$), natural single Xals	200-600	200	$^2H/^2H_2O$	67
148	Lawsonite ($CaAl_2Si_3O_{12}(OH_2)H_2O$), powdered natural Xals	375-425	0.1	$^2H/^2H_2O$	80 ±70
149	Chlorite, powdered natural Xals	500-700	200 or 500	$^2H/H_2O$,^2H_2O	166−172
150	Ilvaite, powdered natural Xals	350-650	5 to 20	$^2H/H_2O$,^2H_2O	115−119

D_0 (m^2/s)	pO_2, f_{H_2O}	Orientation	Analytical Method	Reference	Notes
2 E−6	0.021	para [212]	seq IR	Hercule (1996)	
	0.021		IR profile	Guilhaumou et al. (1999)	cation vacancies
1.4	0.021	para *a* and *b*	seq IR	Stalder & Skogby (2003)	
	0.021	para *a*	seq IR	Stalder & Skogby (2003)	
	0.021	para *b*	seq IR	Stalder & Skogby (2003)	
	0.021	para *c*	seq IR	Stalder & Skogby (2003)	
2.03 E−5		para [100]	seq IR	Stalder et al. (2007)	Fe-doped samples
8		para [010]	seq IR	Sundvall et al. (2009)	
3		para [100]*	seq IR	Sundvall et al. (2009)	
2.00 E−12	UB/NNO	para *c*	SIMS	Farver & Giletti (1985)	
1.00 E−11	UB/NNO	para *c*	SIMS	Farver & Giletti (1985)	
	UB/NNO	para *a*	SIMS	Farver & Giletti (1985)	
	UB/NNO	para *b*	SIMS	Farver & Giletti (1985)	
	UB/NNO	para *c*	SIMS	Farver & Giletti (1985)	
3.00 E−8	UB/NNO	para *c*	SIMS	Farver & Giletti (1985)	
2 E−5 to 2.5 E−12	UB	bulk, 1D-2D model	BE-MS	Graham et al. (1984)	
2 E−11 to 8 E−13	UB	bulk, 1D-2D model	BE-MS	Graham et al. (1984)	
6.3 E−10	UB	bulk, 2D	BE-MS	Graham et al. (1984)	
2 E−9	E−26 to E−18	para *b*	seq IR	Ingrin & Blanchard (2000)	
7.74 E−9	UB/NNO	bulk, cylinder perp c	BE-MS	Fortier & Giletti (1991)	
	UB/NNO	para *c*	SIMS	Fortier & Giletti (1991)	
9.10 E−10	UB/NNO	bulk, cylinder perp *c*	BE-MS	Fortier & Giletti (1991)	
	UB/NNO	para *c*	SIMS	Fortier & Giletti (1991)	
1.03 E−13		bulk, plate para *c*	BE-MS	Giletti & Anderson (1975)	
1.20 E−9		bulk, cylinder perp *c*	BE-MS	Giletti & Anderson (1975)	
1.40 E−8	UB/NNO	bulk, cylinder perp *c*	BE-MS	Fortier & Giletti (1991)	
	UB/NNO	para *c*	SIMS	Fortier & Giletti (1991)	
	UB/NNO	bulk, cylinder perp *c*	BE-MS	Fortier & Giletti (1991)	
1 E−8 to 1 E−11	UB	bulk, 1D-2D model	BE-MS	Graham (1981)	
1.6 E−8 to 4 E−9	UB	bulk, 1D-2D model	BE-MS	Graham (1981)	capsule leak?
1 E−9 to 3 E−10	UB	bulk, 1D-2D model	BE-MS	Graham (1981)	capsule leak?
1 E−4 to 1 E−3	UB	bulk, 1D-2D model	BE-MS	Graham (1981)	capsule leak?
2.5 E−14	UB	para *b*	SIMS	Suman et al. (2000)	
1.0 E−9	UB	bulk	thermogravimetry	Marion et al. (2001)	
6.3 E−6 to 5 E−8	UB	bulk, 1D-2D model	BE-MS	Graham et al. (1987)	
1E−7 to 4 E−8	UB	bulk, 1D-2D model	BE-MS	Yaqian & Jibao (1993)	

No.	Sample Material	Temperature Range (°C)	Pressure Range (MPa)	Diffusing Species/ Form	E_a (kJ/mol) or D (m^2/s)
	GARNET				
	Oxygen Self-Diffusion				
151	Grossular, natural single Xals	850	200	$^{18}O/H_2O$	D = 4.8 E−21 m^2/s
152	Grossular, natural single Xals	1050	800	$^{18}O/H_2O$	D =2.5 E−20 m^2/s
153	Almandine, natural single Xals	800-1000	100	$^{18}O/H_2O$	301±46
	Hydrogen Self-Diffusion				
154	Pyrope ($Gr_3Alm_{15}Py_{81}$), natural single Xal	700-950	0.1	$^2H/^2H_2$	140 ±38
155	Grossular ($Gr_{84}And_{14}Py_2$), natural single Xal	800-1050	0.1	$^2H/^2H_2$	102 ±45
156	Grossular ($Gr_{73}And_{23}Py_2$), natural single Xal	700-950	0.1	$^2H/^2H_2$	185 ±28
157	Andradite (Gr_1And_{99}), natural single Xal	800-900	0.1	$^2H/^2H_2$	70
	Hydrogen Chemical Diffusion				
158	Pyropes ($Py_{67-72}Alm_{14-21}Gr_{10-14}$) natural single Xals	800-1100	0.1	H extraction	253 ±13
159	Pyrope ($Gr_3Alm_{15}Py_{81}$) natural single Xals	800-1050	0.1	H extraction	277 ±22
160	Pyrope ($Gr_3Alm_{15}Py_{81}$) natural single Xals	800-1050	0.1	H extraction	329 ±21
161	Grossular ($Gr_{84}And_{14}Py_2$), natural single Xal	800-1050	0.1	H extraction	323 ±46
162	Grossular ($Gr_{73}And_{23}Py_2$), natural single Xal	700-950	0.1	H extraction	180 ±10
163	Andradite (Gr_1And_{99}), natural single Xal	700-950	0.1	H extraction	271 ±35
	OTHER SILICATES				
	Oxygen Self-Diffusion				
164	Zircon, natural single Xals	1100-1500	0.1	$^{18}O/Si^{18}O_2$	448.3
165	Zircon, natural single Xals	1100-1500	7 to 70	$^{18}O/H_2O$, SiO_2	210.2
166	Titanite, natural single Xals	700-900	100	$^{18}O/H_2O$	254 ±28
167	Titanite, synthetic single Xals	700-1050	0.1	$^{18}O/Si^{18}O_2$	276 ±16
168	Titanite, synthetic single Xals	700-900	10-160	$^{18}O/H_2O$	180 ±39
169	Perovskite, synthetic single Xals	1400-1800	25 GPa	$^{18}O/^{29}Si^{18}O_2$	501 ±80
170	$Ak_{0.5}Gh_{0.5}$, powdered natural Xals	700-1300	0.1	$^{18}O/CO_2$	140.2
171	$Ak_{0.75}Gh_{0.25}$, powdered natural Xals	700-1300	0.1	$^{18}O/CO_2$	133.5
172	Akermanite, synthetic single Xals	800-1303	0.1	$^{18}O/CO,CO_2$	278 ±33
173	Akermanite, synthetic single Xals	1000-1300	0.0064	$^{18}O/CO_2$	215 ±51
174	Akermanite, synthetic single Xals	1000-1300	0.0064	$^{18}O/CO_2$	300 ±37
175	Gehlenite, synthetic single Xals	1000-1300	0.0064	$^{18}O/CO_2$	186 ±16
	Hydrogen/Water DIffusion				
176	Tourmaline (14.27% FeO, 1.93% MgO, 31.34%Al_2O_3) powdered natural Xal	450-800	15-25	$^2H/H_2O,^2H_2O$	123−128
177	Tourmaline (elbaite), natural single Xals	700-800	0.1	$^2H/Ar,^2H_2$	106.3 ±36.8
178	Tourmaline (elbaite), natural single Xals	700-800	0.1	$^2H/Ar,^2H_2$	66.8 ±19.6
179	Beryl, synthetic single Xals	500-700	50-150	H_2O/H_2O	133 ±12
	OXIDES				
	Oxygen Self-Diffusion				
180	Corundum, synthetic single Xals	1580-1840	0.1	$^{18}O/O_2$	788 ±29
181	Corundum, powdered synthetic Xals	1650-1780	0.02	$^{18}O/O_2$	635 ±105
182	Corundum, powdered synthetic Xals	1400-1650	0.02	$^{18}O/O_2$	241
183	Corundum, synthetic single Xals	1000-1100	0.2-0.5	$^{18}O/O_2$	636
184	Sapphire, synthetic single Xals	1477-1677	0.1	$^{18}O/O_2$	615 ±42
185	Rutile, powdered synthetic Xals	710-1300	0.1	$^{18}O/O_2$	251

D_0 (m^2/s)	pO_2, f_{H_2O}	Orientation	Analytical Method	Reference	Notes
			SIMS	Freer & Dennis (1982)	
			SIMS	Freer & Dennis (1982)	
5.99 E−9		isotropic	SIMS	Coughlan (1990)	
1.6 E−6	E−23 to E−18		seq IR	Blanchard and Ingrin (2004)	
2.5 E−08	E−21 to E−16		seq IR	Kurka et al. (2005)	
1.6 E−4	E−23 to E−18		seq IR	Kurka (2005)	
1.3 E−9	E−21 to E−19		seq IR	Kurka (2005)	
1.2 to 6.3	UB		seq IR	Wang et al. (1996)	
3.16	0.021		seq IR	Blanchard & Ingrin (2004)	
79	E−21 to E−16		seq IR	Blanchard & Ingrin (2004)	
10	0.021		seq IR	Kurka et al. (2005)	
2 E−4	0.021		seq IR	Kurka (2005)	
0	0.021		seq IR	Kurka (2005)	
1.33 E−4		para *c*, perp *c*	$^{18}O(p,\alpha)^{15}N$	Watson & Cherniak (1997)	
5.50 E−12		para *c*, perp *c*	$^{18}O(p,\alpha)^{15}N$	Watson & Cherniak (1997)	
1 E−8	UB/NNO	para *a*, *b*, *c*	SIMS	Morishita et al. (1996)	
3.03 E−8	FMQ	perp (001)	$^{18}O(p,\alpha)^{15}N$	Zhang et al. (2006)	"lattice diffusion"
2.05 E−12		perp (001), (100), (110)	$^{18}O(p,\alpha)^{15}N$	Zhang et al. (2006)	"lattice diffusion"
9.16 E−4			SIMS	Dobson et al. (2008)	multianvil, NaCl cell
8.60 E−10		bulk, sphere	BE-MS	Hayashi & Muehlenbachs (1986)	
7.20 E−10		bulk, sphere	BE-MS	Hayashi & Muehlenbachs (1986)	
4.70 E−11	NNO, IW	para *c*	SIMS	Ryerson & McKeegan (1994)	
9.41 E−10		para *c*	SIMS	Yurimoto et al. (1989)	
6.96 E−6		para *a*	SIMS	Yurimoto et al. (1989)	
4.36 E−12		para *c*	SIMS	Yurimoto et al. (1989)	
2.5 E−10 to 1E−10	UB	bulk, 1D-2D model	BE-MS	Jibao & Yaqian (1997)	
1.58 E−10		para *c*	FTIR	Desbois & Ingrin (2007)	
6.31 E−13		perp *c*	FTIR	Desbois & Ingrin (2007)	
2.5 E−7		perp *c* (channels)	FTIR	Fukuda et al. (2009)	H_2O diffusion
1.56 E−10			SIMS	Reed et al. (1978)	
1.90 E−7			BE-MS	Oishi & Kingery (1960)	
1.90 E−12			BE-MS	Oishi & Kingery (1960)	
2.06 E−2		para *c*	SIMS	Prot & Monty (1996)	
2.66 E−2		perp (10-12)	$^{18}O(p,\alpha)^{15}N$	Reddy & Copper (1982)	
2.00 E−7		bulk	BE-MS	Haul & Dumbgen (1965)	

No.	Sample Material	Temperature Range (°C)	Pressure Range (MPa)	Diffusing Species/ Form	E_a (kJ/mol) or D (m^2/s)
186	Rutile, synthetic single Xals	806	0.1	$^{18}O/O_2$	D = 3.2 E−20 m^2/s
187	Rutile, synthetic single Xals	806	0.1	$^{18}O/O_2$	D = 1.75 E−19 m^2/s
188	Rutile, powdered synthetic Xals	1000	0.1	$^{18}O/O_2$	D = 2.15 E−20 m^2/s
189	Rutile, powdered synthetic Xals	966	0.1	$^{18}O/O_2$	D = 6.78 E−21 m^2/s
190	Rutile, synthetic single Xals	877-1177	0.006	$^{18}O/O_2$	251
191	Rutile, synthetic single Xals	900-1200	0.0049-0.02	$^{18}O/O_2$	282.6
192	Rutile, natural single Xal	600	100	$^{18}O/H_2O$	D = 1.7 E−20 m^2/s
193	Rutile, natural single Xal	1050	100	$^{18}O/H_2O$	D = 3.2 E−19 m^2/s
194	Rutile, natural single Xal	600-1100	100	$^{18}O/H_2O$	168.8
195	Rutile, synthetic single Xals	600-1100	100	$^{18}O/H_2O$	175.2
196	Rutile, synthetic single Xals	750-1000	100	$^{18}O/H_2O$	330 ±15
197	Rutile, synthetic single Xals	750-1000	0.1-100	$^{18}O/H_2O$	258 ±22
198	Magnetite, powdered synthetic Xals	302-550	<0.1	$^{18}O/H_2O$	71.1 ±7
199	Magnetite, powdered synthetic Xals	302-550	1 E−5 to 3.8	$^{18}O/H_2$, H_2O	$\log D = -3.715(1000/T) - 0.27\log(pH_2/pH_2O) - 16.74$
200	Magnetite, natural single Xals	500-800	100	$^{18}O/H_2O$	188.3
201	Magnetite, natural single Xals	500-655	low	$^{18}O/CaCO_3$	211 ±20
202	Magnetite, synthetic single & powdered Xals	1150	PO_2 = 1 E−10 to 1 E−4	$^{18}O/H_2$, H_2O	$\log D = -18.82 - 0.5(\log pO_2)$
203	Magnetite, synthetic single & powdered Xals	800	PO_2 = 1 E−17 to 1 E−9	$^{18}O/H_2$, H_2O	$\log D = -25.39 - 0.5(\log pO_2)$
204	Hematite, synthetic & natural single Xals	852-1077	0.1	$^{18}O/O_2$	405 ±25
205	Hematite, natural single Xals	890-1227	aO_2 = 4.5 E−4 to 6.5 E−1	$^{18}O/O_2$	$\log D = 4.431 - 0.26\log(aO_2) - 28.312(1000/T)$
206	Wustite, synthetic single Xals	700	PO_2 = 1.22 E−21	$^{18}O/H_2$, H_2O	D = 3.2 E−19 m^2/s
207	Wustite, synthetic single Xals	700	PO_2 = 2.82 E−21	$^{18}O/H_2$, H_2O	D = 2.1 E−19 m^2/s
	Hydrogen Self-Diffusion				
208	Rutile, synthetic single Xals	155-300	0.15-0.19	$^3H/^3H_2$	38
209	Rutile, synthetic single Xals	155-300	0.15-0.19	$^3H/^3H_2$	55
210	Rutile, synthetic single Xals	350-700	7 E−3	$^2H/H_2$	57
211	Rutile, synthetic single Xals	614-721	7 E−3	$^2H/H_2$	124
212	Rutile, synthetic single Xals	254-700	4 E−4	$^3H/^3H_2O$	72
213	Rutile, synthetic single Xals	500-910	4 E−4	$^3H/^3H_2O$	107
214	Rutile, synthetic single Xals	651-902	4 E−4	$^3H/^3H_2O$	187
	CARBONATES AND PHOSPHATES				
	Oxygen Self-Diffusion				
215	Calcite, powdered synthetic Xals	650-850	<0.1	$^{18}O/CO_2$	411.9
216	Calcite, natural single Xals	400-800	100	$^{18}O/H_2O$	173 ±6
217	Calcite, natural single Xals	700	log f_{H_2O} 0.6 to 2.38	$^{18}O/H_2O$	$\log D = 0.835\log f_{H_2O} - 23.03$
218	Calcite, powdered natural Xals	900	1250	$^{18}O/CO_2$	D = 9 E−17 m^2/s
219	Calcite, natural single Xals	600-800	100	$^{18}O/CO_2$	242 ±39
220	Dolomite, powdered natural Xals	645-785	12-93.5	$^{18}O/CO_2$	485.96
221	Fluorapatite, natural single Xals	550-1200	100	$^{18}O/H_2O$	205 ±12.5
222	Fluorapatite, natural single Xals	800-1100	100	$^{18}O/H_2O$	125.5 ±33
223	Monazite, natural single Xals	850-1100	0.1	$^{18}O/CeP^{18}O_4$	356 ±26
224	Monazite, natural single Xals	700-880	100	$^{18}O/H_2O$	100 ±20
225	Monazite, natural single Xals	800	10-160	$^{18}O/H_2O$	$\log D = (1.75 \text{ E}{-3})pH_2O - 21.481$

D_0 (m^2/s)	pO_2, f_{H_2O}	Orientation	Analytical Method	Reference	Notes
		para *c*	$^{18}O(p,\alpha)^{15}N$	Gruenwald & Gordon (1971)	
		perp *c*	$^{18}O(p,\alpha)^{15}N$	Gruenwald & Gordon (1971)	
		bulk, sphere	BE-MS	Bagshaw & Hyde (1976)	
		bulk, sphere	BE-MS	Bagshaw & Hyde (1976)	
3.40 E−7		para *c*	SIMS	Arita et al. (1979)	
2.40 E−6		para *c*	$^{18}O(p,\alpha)^{15}N$	Derry et al. (1981)	
		para *c*	SIMS	Freer & Dennis (1982)	
		para *c*	SIMS	Freer & Dennis (1982)	
1.14 E−11		para *c*	SIMS	Dennis & Freer (1993)	
2.41 E−12		para *c*	SIMS	Dennis & Freer (1993)	
5.90 E−5		para *c*	$^{18}O(p,\alpha)^{15}N$	Moore et al. (1998)	Ti reduced by H_2O
4.70 E−7		para *c*	$^{18}O(p,\alpha)^{15}N$	Moore et al. (1998)	
3.2 E−18			BE-MS	Castle & Surman (1967)	
			BE-MS	Castle & Surman (1969)	
3.50 E−10			SIMS	Giletti & Hess (1988)	
4.30 E−13		sphere model	empirical	Sharp (1991)	
		perp (111)	SIMS	Millot & Niu (1997)	
		perp (111)	SIMS	Niu & Millot (1999), Millot et al. (1997)	
6.3 E−6		para (0001), para (10-12)	$^{18}O(p,\alpha)^{15}N$	Reddy & Copper (1983)	
			SIMS	Amami et al. (1999)	
			$^{18}O(p,\alpha)^{15}N$	Sabioni et al. (1993)	
			$^{18}O(p,\alpha)^{15}N$	Sabioni et al. (1993)	
7.50 E−10		para *c*	autoradiography	Caskey (1974)	
2.70 E−10		perp *c*	autoradiography	Caskey (1974)	
1.80 E−7	3 E−3 to 7 E−3	para *c*	seq IR	Johnson et al. (1975)	
3.80 E−5	3 E−3 to 7 E−3	perp *c*	seq IR	Johnson et al. (1975)	
8.50 E−7	E−39 to E−17	para *c*	SS	Cathcart et al. (1979)	
1.77 E−6	E−30 to E−6	perp *c*	SS	Cathcart et al. (1979)	"fast" O^3H^- species
8.90 E−6	E−30 to E−6	perp *c*	SS	Cathcart et al. (1979)	"slow" $^3H_2$ species
2.05 E+2		bulk, plate	BE-MS	Anderson (1969)	
7.00 E−9	UB/NNO	isotropic	SIMS	Farver (1994)	
	multiple buffers	isotropic	SIMS	Farver (1994)	
		bulk, plate	BE-MS	Rosenbaum (1994)	
7.50 E−7		para *c*	SIMS	Labotka et al. (2000)	
2.81 E+7	UB	bulk, plate	BE-MS	Anderson (1972)	
9.00 E−9	UB	para *c*	SIMS	Farver & Giletti (1989)	
3.00 E−15		perp C	SIMS	Farver & Giletti (1989)	
1.9 E−6	NNO	perp (100), (101), (110), (111)	$^{18}O(p,\alpha)^{15}N$	Cherniak et al. (2004)	
3.1 E−17			$^{18}O(p,\alpha)^{15}N$	Cherniak et al. (2004)	
			$^{18}O(p,\alpha)^{15}N$	Cherniak et al. (2004)	